Application of the Linear Driving Force Approximation to the Study of Mass Transfer in Ion-Exhange Chromatography

Hansen, Ernst

Publication date:
2000

Document Version
Publisher's PDF, also known as Version of record

Application of the Linear Driving Force Approximation to the study of Mass Transfer in Ion-exchange Chromatography

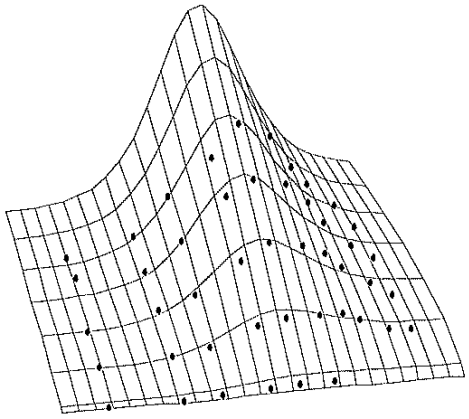

Ernst Hansen

Engineering Research Centre IVC-SEP
Department of Chemical Engineering
The Technical University of Denmark, DTU
Lyngby, Denmark

Application of the Linear Driving Force Approximation to the study of Mass Transfer in Ion-exchange Chromatography

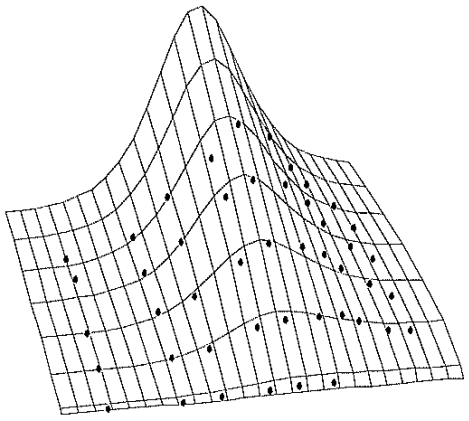

Ernst Hansen

Engineering Research Centre IVC-SEP
Department of Chemical Engineering
The Technical University of Denmark, DTU
Lyngby, Denmark

Preface

This thesis is submitted in partial fulfillment of the requirements for admission to candidacy for the degree of doctor of philosophy, Ph.D.

It is with deep gratitude that I acknowledge the contribution of my advisor Jørgen Mollerup to the scientific work constituting this thesis. The combination of his patience and fundamental theoretical insight and my curiosity have resulted in an excellent collaboration.

I thank Steffen Kidal for his expert assistance in the experimental work and for the joyful times spent at the department.

Ernst Hansen, February 2000

In case of inconsistency between map and terrain, the terrain applies.

Abstract

Mass transfer in ion-exchange resins have been investigated by application of the linear driving force approximation. The general model includes external mass transfer from the mobile phase to the particle surface, denoted film diffusion, and parallel diffusion in the particle comprising pore diffusion and diffusion in the adsorbed phase, denoted solid diffusion. The experimental and theoretical studies are divided into *linear* and *non-linear* mass transfer.

The study of non-linear mass transfer comprises frontal analysis of BSA on various resins and additional studies of Lysozyme and Aprotinin, all at strong non-linear adsorbing conditions. The results show that mass transfer is generally predominated by film diffusion and that pore diffusion can be neglected. A correlation of the Sherwood numbers for the external mass transfer coefficient with the Reynolds numbers of the various resins coluld be determined for BSA. The correlation reveals an unexpected strong Reynolds number dependence of the Sherwood number and this is supported by the additonal data for Lysozyme and Aprotinin.

In the study of linear mass transfer the plate height (HETP) was determined from pulse injections at linear isocratic conditions. The experimental data were correlated by use of the van Deemter equation including an over-all mass transfer coefficient described by the parallel diffusion model. The plate height for Tyrosine and Aprotinin was determined on three resin types comprising porous, macroporous, and gel-filled particles, at conditions ranging from weak to strong retention. The results show that pore diffusion predominates at weak retention, solid diffusion predominates at stronger retention, while the plate height at very strong retention primarily consists of the contributions from film diffusion and axial disperison. A correlation of experimental data for BSA (Jensen, 1999) obtained at four different pH shows that the plate height and thus the mass transfer coefficients do not depend directly on the salt concentration and pH, but only on the resulting retention.

The Sherwood number correlation obtained by frontal analysis do not apply to the plate height results which show an apparent weak velocity dependence of the external mass transfer coefficient.

The mass transfer at linear and non-linear adsorbing conditions in three types of ion-exchange resins have been described satisfactory by application of a general model for parallel diffusion.

Resumé

Anvendelse af filmmodeller til studiet af massetransport i ionbytningskromatografi.

Massetransporten i kromatografiske ionbytterkolonner er blevet undersøgt ved brug af filmmodeller, hvor gradienterne givet ved diffusion approksimeres med en lineær drivende kraft, og de enkelte transportbidrag er givet ved produktet af et stofovergangstal og den tilhørende drivende kraft. Den gennemgående model indeholder en ekstern transport fra mobilfasen til partiklens overflade, kaldet filmdiffusion, samt parallel transport i partiklen, bestående af porediffusion og diffusion i den adsorberede fase, kaldet fastfase diffusion. De eksperimentelle og teoretiske studier er opdelt i *lineær* og *ikke-lineær* massetransport.

Studiet af ikke-lineær masstransport omhandler frontalanalyse af BSA på forskellige matricetyper samt supplerende studier af Lysozym og Aprotinin, alle ved stærkt bindende ikke-lineære betingelser. Resultaterne viser at massetransporten hovedsaligt domineres af den eksterne transportmodstand, og at porediffusion kan negligeres ved disse betingelser. En samlet korrelation af Sherwoodtallet for de eksterne stofovergangstal med Reynoldstallet på de forskellige matricerer blev bestemt for BSA. Korrelationen viser en overraskende kraftig Reynoldstalafhængihed af Sherwoodtallet, og dette understøttes af de supplerende forsøg med Lysozym og Aprotinin.

I studiet af lineær massetransport blev højden af en overføringsenhed, eller et teoretisk trin (HETP), bestemt fra pulsinjektioner under lineære isokratiske betingelser. De eksperimentelle data blev korreleret ved brug af van Deemter ligningen, hvor det totale stofovergangstal er givet ved modellen for paralleldiffusion. Trinhøjden for Tyrosin og Aprotinin blev bestemt på tre typer af matricer indholdende henholdsvis porøse, makroporøse og gelfyldte partikler, ved betingelser varierende fra ikke-bindende til stærkt bindende. Resultaterne viser at porediffusion er dominernde under svagt bindende betingelser, fastfasediffusion er dominererende ved stærkere bindingsbetingelser, mens pladehøjden for meget stærkt bindende betingelser primært udgøres af bidraget fra filmdiffusion og aksial disperison. En korrelation af data for BSA (Jensen, 1999) opnået ved fire forskellige pH viser at trinhøjden og dermed stofovergangstallene ikke afhænger direkte af saltkoncentrationen og pH, men kun af den resulterende retention.

Korrelationen af Sherwoodtallet med Reynoldstallet opnået ved frontalanalyse stemmer ikke overens med resultaterne af pulsfosøgene, der udviser en tilsydenladende svag hastihedsafhængighed af det eksterne stofovergangstal.

Massetransporten ved såvel lineære som ikke-lineære betingelser i tre typer af ionbyttermatricer er blevet beskrevet tilfredstillende ved anvendelse af en generel model for paralleldiffusion.

Contents

Symbols

A	linear equilibrium ratio, q/c_p	
B	lumped equilibrium parameter	M^v
b	Langmuir parameter	L/g
c	mobile phase concentration	g/L
c_0	mobile phase concentration at the interface	g/L
c_F	feed concentration	g/L
c_p	pore phase concentration	g/L
c_s	counter ion concentration	M
D	diffusion coefficient in free solution	cm^2/s
D_a	axial dispersion coefficient, $\lambda v d_p$	cm^2/s
D_p	pore diffusion coefficient	cm^2/s
d_p	particle diameter	cm
D_q	solid diffusion coefficient	cm^2/s
D_s	homgeneous diffusion coefficient	cm^2/s
H	plate height (HETP)	cm
h	reduced plate height, H/d_p	
K	equilibrium constant	
k'	retention factor	
K_d	steric exclusion factor	
k_f	external mass transfer coefficient	cm/s
K_m	over-all mass transfer coefficient	cm/s
k_p	pore-phase mass transfer coefficient	cm/s
k_q	solid-phase mass transfer coefficient	cm/s
k_s	mass transfer coefficient for homgeneous diffusion	cm/s
p	constant, $\epsilon/(1-\epsilon)K_d\epsilon_p$	
Pe	column Pecelét number Lv/D_a	
Q	volumetric flow rate	mL/min
q	solid phase concentration	g/L
q_0	solid phase concentration at the interface	g/L
q_F	equilibrium feed concentration in the solid phase	g/L
q_{max}	maximum equilibrium concentration	g/L
Re	Reynolds number, $vd_p\rho/\mu$	
Sc	Schmidt number, $\mu/\rho D$	
Sh	Sherwood number for the mobile phase, $k_f d_p/D$	
St_i	Stanton number, $6k_iL/vd_p$, with I=f, m, p, or q	
s	particle concentration, $K_d\epsilon_p(c_p+q)$	g/L
s_0	particle concentration at the interface	g/L

s_F	equilibrium feed concentration in the particle	g/L
s_{max}	maximum equilibrium concentration, $K_d \epsilon_p q_{max}$	g/L
v	interstitial velocity	cm/s
v_0	superficial velocity	cm/s
x	reduced mobile phase concentration, c/c_F	
x_0	reduced mobile phase concentration at the interface	
y	reduced solid phase concentration, q/q_F	
y_0	reduced solid phase concentration at the interface	

Greek letters

α	external mass transfer correlation parameter	cm/s
β	scaled concentration parameter bc_F and velocity exponent	
γ	ratio of the scaled solid and pore resistances, $k_p c_F / k_q q_F$	
δ	ratio of the scaled solid and film resistances, $k_f c_F / K_d \epsilon_p k_q q_F$	
ϵ	bed porosity	
ϵ_p	particle porosity	
Λ	resin capacity	M
λ	axial dispersion parameter	
μ	viscosity	g/cm s
ν	charge ratio	
ξ	dimensionless time, tv/L	
ρ	mobile phase density	g/cm^3
ψ	charge ratio correlation parameter	
ω	reduced solute velocityω	

Abreviations

ECEs	Extra column effects
LDF	Linear driving force
MTZ	The width of the mass transfer zone [t=time, ξ=dim. less, V=volume]

Introduction

This study concerns the mass transfer behaviour of ion-exchange resins as used primarily in the separation of macromolecules such as proteins. Combined with an equilibrium isotherm a model for mass transfer is essential to the design and optimisation of a preparative chromatographic separation step.

As an immediate impression the dependence of the mass transfer parameters on the solute, resin type, and particle diameter, which allows for a priori estimation, is the most relevant aspect of mass transfer. Coffman (1994) developed correlations of the intraparticle diffusivity for proteins in porous resins based on the pore size of the media and either the Stokes radius or the molecular weight of the protein. Lewus et al. (1998) discusses the application of an *effective-medium* model for predicting the diffusivity in gel-type resins from the molecular radius and the Darcy permeability. The relevance of a priori predictions is however somewhat restricted. Since a certain number of experiments must be performed in order to determine the right conditions for achieving separation, the mass transfer properties for the given solutes and resin can be estimated from relevant experimental data by use of an appropriate model. The main application of a model to process design therefore covers inter -and extrapolation of experimental data in order to redcuce the number of experiments.

In the progression of the present study it soon became evident that a fundamental aspect of mass transfer had to be addressed, namely which model to apply? The determination of mass transfer parameters is different from determining basic physical properties such as solubilities. The solubility of a component at specified conditions is an unambiguous property which can only be questioned through the applied experimental approach. A mass transfer coefficient or the corresponding diffusivity on the other hand is determined by comparing a model for the mass flux to experimental data and thus depends on the model applied.

The description of mass transfer in chromatographic resins consists primarily of two models known from general packed bed adsorption. In the *pore diffusion model* mass transfer occurs by hindered diffusion in the pores and the driving force is the gradient in the pore-phase concentration. In the *solid diffusion model* the driving force is the gradient in the concentration of the solute adsorbed in the resin. A general perception is that the pore diffusion model covers the mass transfer of truly porous resins, that is resins with liquid-filled pores, while the solid diffusion model describes the diffusional behaviour of gel-type resins. A third and less extensively used model is the *parallel diffusion model* in which intraparticle mass transfer occurs by both pore and solid diffusion. The pore and solid diffusion models are thus limiting cases of the parallel diffusion model.

The aim of this study is to determine which mechanisms should be included when describing the rate of mass transfer and to investigate whether a unified model description applies to ion-exchange resins ranging from macro porous to gel-type resins. The parallel diffusion model is chosen as the foundation since the relevance of pore, solid, and parallel diffusion can be investigated using this model. The model includes an expression for the external mass

transfer from the mobile phase to the particle surface. A fundamental understanding of mass transfer is sought through the interaction of experimental and theoretical studies, and for this purpose a simple model description including the linear driving force approximation is used. The linear driving force approximation is basically a mathematical approximation, a linearisation, of the Fickian diffusion term which provides simplified solutions while maintaining a physical foundation. The experimental conditions are chosen so that analytical model solutions apply and the mass transfer properties can thus be determined by a straight forward fitting procedure. The transparent nature of analytical solutions allows for a fundamental understanding of the model behaviour. The experimental work includes single solute adsorption and elution using common test solutes such as BSA and Lysozyme. The values of the mass transfer coefficients determined are therefore of minor interest except when comparing different resins, while the focus is on the qualitative behaviour of the mass transfer models in relation to the experimental data.

An excellent overview of preparative chromatography including short-cut engineering methods is given in Perrys Handbook (1997). For a thorough introduction to the parallel diffusion model, including reaction kinetics, the paper by Rice and Do (1987) is recommended. For applications of models for mass transfer the extensive work led by Giorgio Carta at the University of Virginia and the papers by Yoshida et al. (1984 and 1994) are recommended. The topic of mass transfer is in general not well covered and sometimes even mistreated in textbooks concerning preparative liquid chromatography, presumedly because the issue of mass transfer is usually considered secondary. For an introduction to mass transfer, textbooks describing general packed bed adsorption should be preferred.

The theoretical and experimental contents of this work can be divided into two parts comprising the study of mass transfer under linear and under strongly non-linear adsorbing conditions. The distinction arises from the availability of analytical solutions for the two cases. Chapters 2 and 3 concern non-linear mass transfer through the study of breakthrough curves. Chapters 4 and 5 describe the behaviour of the plate height (HETP) obtained from pulse injections under linear adsorbing conditions. Paper 1 is closely related to Chapter 3 while Paper 2 is closely related to Chapter 5. Although in both cases the related parts can be read independently the recommended order is to read the papers first, since these contain the primary results and the experimental procedures.

Experimental overview

Solute	Resin	Method	Reference
BSA	Resource 15Q	Frontal analysis	Paper 1
	Source 30Q	Frontal analysis	Paper 1
	Source 30Q [1]	Isocratic elution	Chapter 5, Table 2
	Q HyperD 20	Frontal analysis	Paper 1
	Q HyperD 35	Frontal analysis	Paper 1
	Poros HQ/M	Frontal analysis	Paper 1
Aprotinin	Resource 15S	Frontal analysis	Chapter 3, Table 1
	Resource 15S	Isocratic elution	Paper 2
	S HyperD 20	Isocratic elution	Paper 2
	Poros 50 HS	Isocratic elution	Chapter 5, Table 2
Tyrosine	Resource 15Q	Isocratic elution	Paper 2
	Q HyperD 20	Isocratic elution	Paper 2
	Poros 50 HQ	Isocratic elution	Chapter 5, Table 2
Lysozyme	Resource 15S	Frontal analysis	Chapter 3, Table 1

[1] Experimental data by Jensen (1999).

Chapter 1. General model

Chromatography can be described by general models for packed bed adsorption. A model comprises the column mass balance, an equation for the mass flux, an equilibrium isotherm, and reaction kinetics. While the mass balance is given, the flux equation, reaction kinetics, and isotherm must be chosen by considering the physical aspects of the process. The model applied in this work is general in the sense that it does not take into account explicit ion exchange mechanisms such as electric potentials. Mass transfer in the mobile and in the stationary phase is described by a linear driving force. Reaction kinetics is neglected since the rate of ion exchange is assumed to be much faster than the mass transport. For the equilibrium isotherm adequate models with a reasonable physical foundation are chosen, since the isotherm model is not essential in a study of mass transfer.

The chromatographic column

The column is packed with an adsorbing material, usually as spherical particles. The liquid (water) surrounding the particles is denoted the *mobile phase* since forced convection takes place due to the applied pressure. The mobile phase volume is given by the bed porosity as $V_M=V_{col}\,\epsilon$. The particles are divided into a *pore phase* comprising the liquid filled pores and a *solid phase* comprising the adsorbed state of the solute. The pore volume is given by the particle porosity as $V_P= V_{col}(1-\epsilon)\epsilon_p$. Depending on the size of the solute not all pores are accessible. The fraction of the pores accessible for the solute is expressed in the steric exclusion factor K_d so that the effective pore volume for a solute is $V_{P,i}=V_{col}(1-\epsilon)K_{d,i}\epsilon_p$ for species *i*. The functional groups which facilitates adsorption in the particles are placed on the inner surface of porous particles or in the three dimensional matrix found in gel-type adsorbents and rigid particles containing gel-filled pores. In both cases the solute can only reach the binding sites through the pores and both the pore and solid phase concentrations are therefore defined with respect to the accessible or effective pore volume. This provides some consistency since equilibrium is independent of the effective geometry of the adsorbing system, that is column packing, particle porosity and pore size. With the definitions above the total amount of solute in a column segment ΔV_{col} is

$$m = \Delta V_M c + \Delta V_p K_d (c_p + q) = \Delta V_{col}[\epsilon c + (1-\epsilon)K_d\epsilon_p(c_p + q)] \qquad (1)$$

where c is the mobile phase concentration while c_p and q are the average pore and solid phase concentrations respectively.

Mass balance

The differential mass balance for a column segment is

$$\epsilon v \frac{\partial c}{\partial z} + \epsilon \frac{\partial c}{\partial t} + (1-\epsilon)\frac{\partial s}{\partial t} - \epsilon(E_D + D_f)\frac{\partial^2 c}{\partial z^2} = 0 \qquad (2)$$

where s is the average concentration in the particles, $s=K_d\epsilon_p(c_p+q)$, and

$$\frac{\partial s}{\partial t} = K_d\epsilon_p\left(\frac{\partial c_p}{\partial t} + \frac{\partial q}{\partial t}\right) \qquad (3)$$

The mass balance states that the net transport into the segment by convection and axial diffusion equals the accumulation in the mobile phase and in the particles. Axial diffusion comprises the sum of ordinary diffusion and Eddy diffusion caused by the stochastic flow in the packed bed.

Mass transfer

Mass transfer can be divided into an external transport from the mobile phase to the particle surface and an intra particle transport from the interface to the solid phase. The external mass transfer is well described by the film expression:

$$\frac{\partial s}{\partial t} = \frac{6}{d_p}k_f(c-c_0) \qquad (4)$$

where c_0 is the interfacial concentration at the particle surface and k_f is the external -or film mass transfer coefficient. The intra particle mass transfer is not straight forward to describe because of the complex nature of most adsorbents. In this work the intra particle transport is assumed to occur by two distinct mechanisms, pore diffusion and solid diffusion, working in parallel inside the particles. Both mechanisms can be described by Fickian type diffusion with a gradient in the pore or solid phase concentration. The term *solid diffusion* covers both surface diffusion in porous particles and diffusion in gel-type resins since no distinction between the two phenomena is made. Assuming ideal behaviour the flux equation for parallel diffusion is

$$\frac{\partial s}{\partial t} = \frac{6}{d_p}K_d\epsilon_p\left[D_p\left(\frac{\partial c_p(r)}{\partial r}\right)_R + D_q\left(\frac{\partial q(r)}{\partial r}\right)_R\right] \qquad (5)$$

where D_p and D_q are the pore and solid diffusion coefficients respectively. Equation (5) states that the accumulation in the particles is given by the sum of the two fluxes at the interface (r=R). For ion-exchange the adsorption kinetics are assumed to be fast compared to mass

transfer and local equilibrium is therefore assumed between the pore and the solid phase, $q=q(c_p)$.

The linear driving force approximation

In order to simplify the flux equations the linear driving force (LDF) approximation is often used to describe mass transfer. In the LDF approximation mass transfer takes place over a small distance in a boundary layer -or film placed adjacent to the interface. Since the film thickness is small the concentration gradient can be linearised and the resulting expression is the product of the linear driving force, which is the difference between the average concentration and the concentration at the interface, and the mass transfer coefficient. For volumetric fluxes this expression is multiplied by the surface to volume ratio $6/d_p$ as found in equation (4) for the external transport. Although the LDF approximation is most accurate for describing the external film transport it can be applied to intra particle mass transfer in many cases (Yoshida, 1984). The intra particular mass transfer coefficients can be related to the relevant diffusivity by the expression $k_i=10D_i/d_p$, where subscript *i* denotes either pore (*p*) or solid (*q*), as shown by Glueckauff (1955).

When the intra particle mass transfer is controlled by either pore or solid diffusion it is straight forward to apply the LDF approximation. Combined with the external film expression this leads to two distinct models often applied in packed bed mass transfer:

The pore diffusion model

$$\frac{\partial s}{\partial t} = \frac{6}{d_p}k_f(c-c_0) = \frac{6}{d_p}k_p K_d \epsilon_p (c_0-c_p) \qquad (6)$$

The solid diffusion model

$$\frac{\partial s}{\partial t} = \frac{6}{d_p}k_f(c-c_0) = \frac{6}{d_p}k_q K_d \epsilon_p (q_0-q) \qquad (7)$$

where subscript *0* indicates a concentration at the interface at which the two phases pr. definition are in equilibrium while c_p and q are the average concentrations. The flux equation for a linear equilibrium isotherm is presented in Chapter 4. When both intra particle mass transfer mechanisms have to be taken into account and the equilibrium isotherm is non-linear application of the LDF approximation is not straight forward. Since the two phases are in local equilibrium an LDF expression can be obtained by linearisation of either or both gradients and it is not evident which formulation, if any, should be used. This general linearisation problem is discussed later in this work, since its relevance with respect to the experimental work is limited.

Mass transfer resistance

Depending on the conditions mass transfer can be dominated by one or several of the three mechanisms film diffusion, pore diffusion, and solid diffusion. In order to gain insight regarding mass transfer control it is convenient to interpret the finite mass transfer rate as originating from an over-all mass transfer *resistance*. The resulting over-all resistance consists of an external film resistance in series with a particle resistance comprising a pore resistance and a solid phase resistance placed in parallel. Two characteristic parameters can be defined for the system considered:

The ratio of the scaled solid and film resistances

$$\delta = \frac{k_f c_F}{k_q K_d \epsilon_p q_F} \tag{8}$$

and the ratio of the scaled solid and pore resistances

$$\gamma = \frac{k_p c_F}{k_q q_F} \tag{9}$$

where c_F is the feed concentration and q_F is the corresponding equilibrium concentration. For a linear isotherm the equilibrium ratio $q_F/c_F=A$ is constant.

Since pore and solid diffusion work in parallel the intra particular mass transfer is dominated by the fastest mechanism i.e. the smallest resistance. Therefore, when γ is large the solid phase resistance is larger than the pore phase resistance and pore diffusion predominates, and vice versa when γ is small. The pore and solid diffusion models represent two special cases $\gamma=0$ and $\gamma\to\infty$ of the parallel diffusion model. From an order of magnitude analysis pore diffusion control can be assumed for $\gamma>10$ and solid diffusion control for $\gamma<0.1$ while both resistances are significant when $0.1<\gamma<10$.

Since the mobile phase resistance and the particle resistance are placed in series, mass transfer is controlled by the largest resistance. The ratio of the scaled particle and mobile phase resistances is

$$\frac{\delta}{1+\gamma} = \frac{k_f c_F}{K_d \epsilon_p (k_p c_F + k_q q_F)} \tag{10}$$

which is small (<0.1) when the external film resistance is controlling and large (>10) when the particle resistance controls.

It is important to note that the relative significance of the three resistances is not determined by simply comparing the mass transfer coefficients but by comparing the coefficients scaled with the respective driving forces. Thus mass transfer control is closely related to the

equilibrium isotherm and is subject to change when the adsorbing conditions change. A schematic representation of mass transfer control is shown in Figure 1. The horizontal lines divide the particle resistance into three regions, solid control ($\gamma<0.1$), pore control ($\gamma>10$) and a mixed mode ($0.1\leq\gamma\leq10$). The curved lines represent values for the particle to film resistance ratio $r=\delta/(1+\gamma)$ of 0.1 and 10 from left to right. To the left of the line r=0.1 mass transfer is controlled by the film resistance while the particle resistance controls in the region to the right of r=10. For $\delta<0.1$ mass transfer is controlled by film diffusion regardless of the transport properties of the particle. On the other hand $\delta=10$ is not a sufficient condition for particle control since the (relatively) small flux from solid diffusion can be compensated by pore diffusion. By inserting appropriate values for the mass transfer coefficients and the equilibrium ratio it can be determined which transport mechanisms are relevant. Although this approach could have some merit in simplifying calculations when performing a simulation it is of little use in the general case where the mass transfer coefficients are not known. However, the changes regarding mass transfer control occurring when experimental conditions are varied can be studied qualitatively by use of Figure 1. For illustration the ratio $R_f= k_f/K_d\epsilon_p k_q$ is set to 50 and the ratio $R_p=k_p/k_q$ to 10 while the equilibrium ratio $A_F=q_F/c_F$ is varied from 0.1 to 1000 thereby obtaining the dashed line in Figure 1 given by $\gamma=\delta R_p/R_f$.

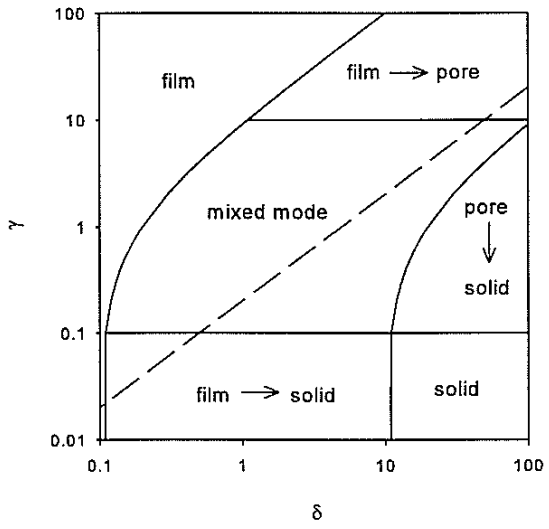

Figure 1: The significance of the mass transfer resistances. Curved lines are $\delta/(1+\gamma)=0.1$ and 10 from left to right. Dashed line is the development with the equilibrium ratio for $k_f/k_q=50$ and $k_p/k_q=10$.

When the equilibrium ratio is small, at approximately non-retained conditions, the intra particle mass transfer is slow compared to the external transport and controlled by pore

diffusion. For A_F small the dashed line therefore starts in the upper right corner of Figure 1 where mass transfer is dominated by pore diffusion. As the equilibrium ratio is increased solid diffusion becomes significant and finally controls the intra particle flux and in turn film diffusion control is facilitated as seen from the end point of the dashed line at high A_F. Changing R_f will shift the line in the horizontal direction while a change in R_p will shift the line vertically but neither will affect the slope.

In a general experimental study of mass transfer it is essential to vary the equilibrium ratio significantly in order to distinguish between the different mechanisms of mass transfer. Experimentally the equilibrium ratio can be varied by changing the feed concentration, the salt concentration, or pH.

Chapter 2. Non-linear mass transfer

In this work non-linear mass transfer is studied under frontal loading conditions where strong adsorption takes place and a constant concentration profile, referred to as *constant pattern*, develops in the column. For these conditions an approximate analytical solution to the model presented in Chapter 1 can be derived. Due to the strong adsorption it is assumed that the concentration in the particles can be approximated by the solid phase concentration and that the contribution from pore diffusion can be neglected, that is $q>>c_p$ and $\gamma<0.1$. Further, the contribution to band broadening from axial dispersion is neglected. Considering the resistance scheme in Figure 1 the flux model is thus confined to the region where the relative significance of the intra particle and external resistances $\delta/(1+\gamma)\approx\delta$ and mass transfer occurs by external film diffusion and solid phase diffusion. The validity of the assumptions are discussed in connection with the experimental work.

Constant pattern solution

Applying the above assumptions the flux equation becomes

$$\frac{\partial s}{\partial t} \approx K_d \epsilon_p \frac{\partial q}{\partial t} = \frac{6}{d_p} k_f (c - c_0) = \frac{6}{d_p} k_q K_d \epsilon_p (q_0 - q) \qquad \textbf{(11)}$$

corresponding to the solid diffusion model presented in chapter 1. Introducing the reduced concentrations $x=c/c_F$ and $y=q/q_F$ into the final equality gives

$$\delta (x - x_0) = (y_0 - y) \qquad \textbf{(12)}$$

which must be solved for the interfacial composition x_0.

The non-linear equilibrium is represented by the Langmuir isotherm

$$q = \frac{q_{max} bc}{1 + bc} \qquad \textbf{(13)}$$

where q_{max} is the capacity of the adsorbent for the species considered at the applied conditions i.e. pH and salt concentration. The Langmuir isotherm is chosen because it is simple and describes single component adsorption at fixed conditions well. In dimensionless form the Langmuir isotherm becomes

$$y = \frac{(1+\beta)x}{1 + \beta x} \qquad \textbf{(14)}$$

where $\beta=bc_F$.

Inserting this expression for the interface equilibrium equation (12) can be solved for x_0:

$$x_0 = D(x) + \sqrt{[D(x)]^2 + \frac{\delta x + y}{\delta\beta}} \qquad \textbf{(15)}$$

with

$$D(x) = \frac{1}{2}\left(x + \frac{y}{\delta} - \frac{1}{\beta} - \frac{1}{\delta} - \frac{1}{\delta\beta} \right) \qquad \textbf{(16)}$$

The frontal loading covers a step-up increase from 0 to c_F in the inlet concentration to an initially clean column at time zero. For constant pattern the column mass balance for these boundary conditions leads to the simple relation y=x. Inserting the constant pattern relation in the equations above x_0 is a function of x and the flux can be calculated from

$$\frac{ds}{dt} = K_d \epsilon_p q_F \frac{dx}{dt} = \frac{6}{d_p} k_f c_F (x - x_0) \qquad \textbf{(17)}$$

The resulting flux equation is an ordinary differential equation due to the constant pattern assumption. The model can be compared with experimental breakthrough curves x(t) by numerical integration or directly to the slope of the breakthrough curves, dx/dt.
For an irreversible isotherm $q(c)=q_{max}$ Yoshida et al. (1984) derived a general analytical solution of the solid diffusion model. The model is applicable for Langmuir adsorption when $bc_F > 20$.

Mass transfer behaviour

In this section the behaviour of the solid diffusion model for constant pattern is investigated. The flux expression on a scaled time basis is used:

$$\frac{ds}{d\xi} = St_f c_F (x - x_0) \qquad \textbf{(18)}$$

where $\xi = tv/L$ and St_f is the Stanton number for the mobile phase. The following parameters are used for the model system: $K_d\epsilon_p = 0.5$, $q_{max} = 200$ g/L, and b=20 L/g representing strong non-linear adsorption. $St_q = 3$ and $St_f = 286$ which corresponds to $\delta = 1$ when the feed concentration is 1 g/L.

Flux curves

The mass flux can be depicted as function of the reduced concentration x by use of the equations (15)-(18). Figure 2 shows the characteristic shape of the flux curve at c_F=1 g/L for the full model (δ=1), film diffusion control (δ→0) and solid diffusion control (δ→∞). The flux equations for the two limiting cases are

Film diffusion control

$$\frac{ds}{d\xi} = St_f c_F \frac{\beta x(1-x)}{1+\beta(1-x)} \tag{19}$$

Solid diffusion control

$$\frac{ds}{d\xi} = St_q K_d \epsilon_p q_F \frac{\beta x(1-x)}{1+\beta x} \tag{20}$$

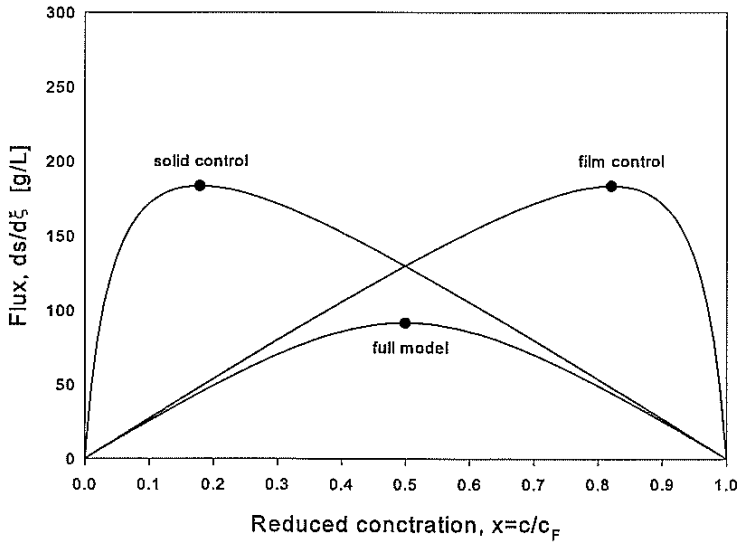

Figure 2: The flux in dependence of the reduced concentration. Symbols indicate the maximum flux and the corresponding inflection point.

For film diffusion control the flux is proportional to x for the main part of the curve since β(1-x)>>1 in equation (19). For solid diffusion control the flux is proportional to (1-x) for the main part of the curve since βx>>1 in equation (20). When δ=1 film and solid diffusion

contributes equally and the curve for the full model is therefore symmetric. The flux curve for the full model approaches the limiting solution of film and solid control when δ is decreased or increased respectively. The maximum flux for the full model is smaller than for the limiting cases since the model includes both resistances.

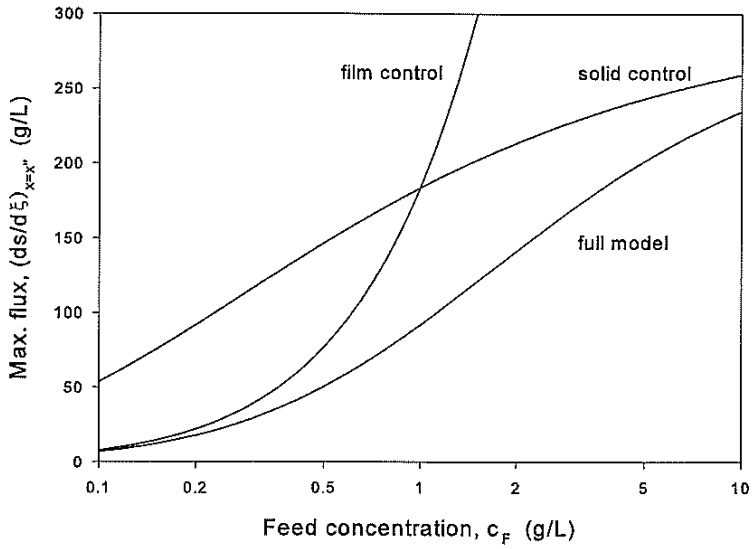

Figure 3: The maximum flux, corresponding to the flux at the inflection point, in dependence of the feed concentration.

A flux curve can be characterised by the maximum flux and the value of x at this maximum. The latter corresponds to the inflection point of the breakthrough curve. The inflection point is

$$x'' = \frac{1}{1+\delta}\left(1+\frac{(\delta-1)(\sqrt{1+\beta}-1)}{\beta}\right) \qquad (21)$$

and the maximum flux is found by inserting x″ into equations (15)-(18). For film and solid diffusion control the inflection points are

Film diffusion control

$$x'' = \frac{1+\beta-\sqrt{1+\beta}}{\beta} \qquad (22)$$

Solid diffusion control

$$x'' = \frac{\sqrt{1+\beta}-1}{\beta} \tag{23}$$

corresponding to $\delta \to 0$ and $\delta \to \infty$ in equation (21). It is noted that x'' for solid diffusion control equals $1-x''$ for film diffusion control. Figure 3 shows the maximum flux as a function of the feed concentration for the full model and the two limiting cases. The intersection of the lines for the limiting cases corresponds to $\delta=1$. The full model coincides with the model for film diffusion control at low feed concentrations and approaches the line for solid diffusion control when the feed concentration increases. The flux for the full model is always smaller than for the limiting cases. The inflection point as function of the feed concentration is depicted in Figure 4. The inflection point for the full model lies in between x'' for film and solid diffusion control.

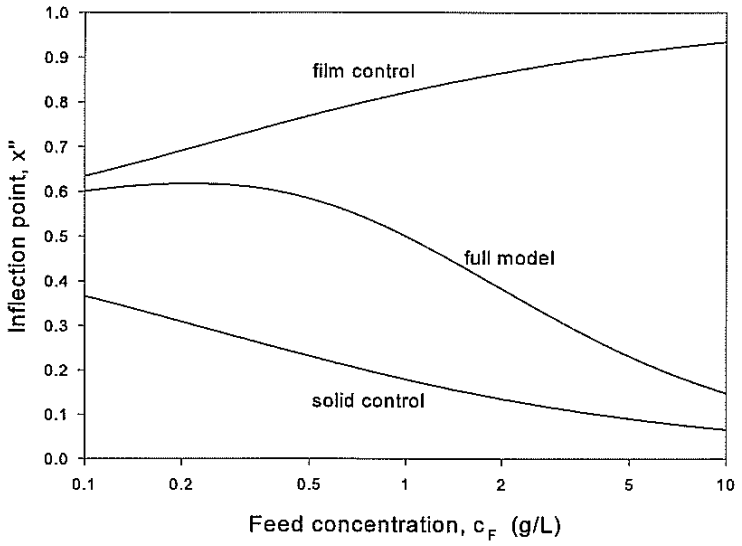

Figure 4: The inflection point as function of the feed concentration.

Figures 2, 3, and 4 describe the flux behaviour of the solid diffusion model. Starting at conditions where $\delta<0.1$ the flux curve coincides with the flux curve for film diffusion control. As the feed concentration is increased the flux curve moves to the left, i.e. the inflection point decreases, and the flux increases until the flux curve coincides with the curve for solid diffusion control.

The mass transfer zone

A breakthrough curve is the response x(t) to a step-up in the inlet concentration starting at x=0 and reaching one when the column is saturated. The retention time t_R is determined by the isotherm (and velocity) while the slope of the curve is determined by the isotherm and the mass transfer properties. Figure 5 shows the breakthrough curves $x(\xi-\xi_R)$, where $\xi_R=t_Rv/L$, corresponding to the flux curves in Figure 2. As for the flux curves the two limiting cases are mirror images.

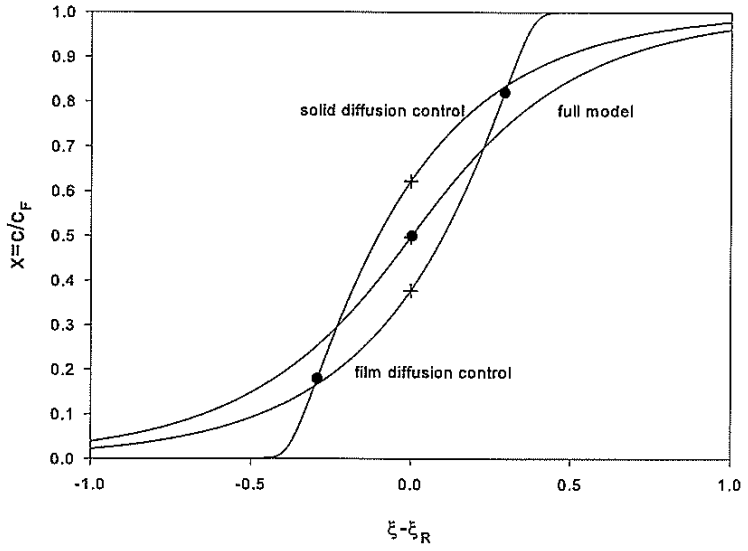

Figure 5: Breakthrough curves corresponding to the flux curves of Figure 2 including the inflection point (●) and the centre of mass (+).

The shape of the breakthrough curves are calculated by integrating the flux equations. The absolute location of the curves on the scaled time axis is found by calculating the centre of mass x_R and use (ξ_R,x_R) as a fixpoint. x_R is determined by solving

$$\int_0^1 [t(x)-t_R]\,dx = \int_0^1 \int_{x_R}^{w} \frac{dx}{x-x_0}\,dw = 0 \qquad (24)$$

For the full model the equation must be solved numerically. The breakthrough curves for the two limiting cases are calculated from

Film diffusion control

$$\frac{St_f c_F}{s_F}(\xi-\xi_R)=(1+\frac{1}{\beta})\ln x-\frac{1}{\beta}\ln(1-x)+1 \qquad (25)$$

Solid diffusion control

$$St_q(\xi-\xi_R)=\frac{1}{\beta}\ln x-(1+\frac{1}{\beta})\ln(1-x)-1 \qquad (26)$$

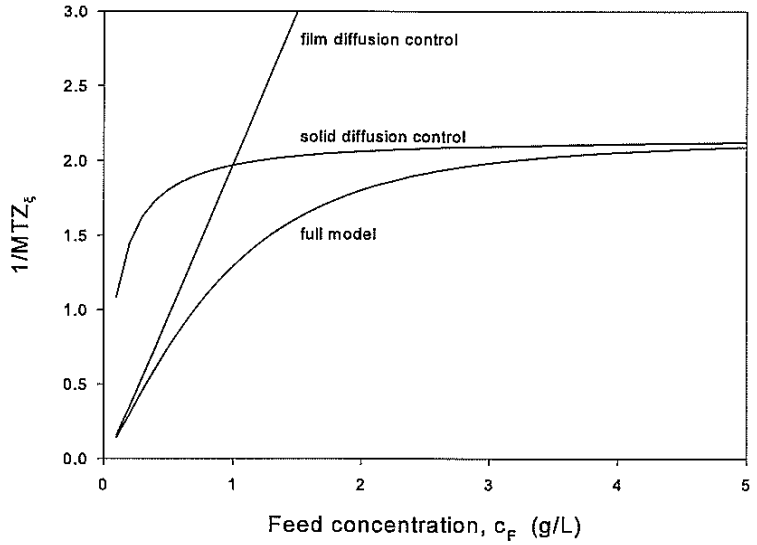

Figure 6: Development of the mass transfer zone with the feed concentration.

For completion, the centre of mass for the limiting cases can be determined from the equations

Film diffusion control

$$(\beta+1)\ln x_R - \ln(1-x_R) + \beta = 0 \qquad (27)$$

Solid diffusion control

$$(\beta+1)\ln(1-x_R) - \ln x_R + \beta = 0 \qquad (28)$$

The mass transfer zone is the region of the breakthrough curve where significant mass transfer takes place defined by a cut-off value x_{cut} so that the width of the zone in time units is $MTZ_t = t(1-x_{cut})-t(x_{cut})$. x_{cut} is usually in the range 0.1-0.3.The width of the mass transfer zone can be used to estimate the efficiency of the column and is also a convenient parameter to use when comparing several breakthrough experiments. Figure 6 shows the development of the mass transfer zone, given as $1/MTZ_\xi$, with the feed concentration. As for the maximum flux 1/MTZ is identical between the two limiting cases when $\delta=1$ ($c_F=1$) and always smaller for the full model.

Interpretation of experiments

The mass transfer behaviour of breakthrough experiments can be examined without prior knowledge of the isotherm and mass transfer parameters by creating plots similar to Figures 2-6. With a sufficient amount of data a straight forward approach is to plot $1/MTZ_t$ vs. the feed concentration. When b is large a practically straight line is obtained for film diffusion control since 1/MTZ is proportional to $c_F(1+bc_F)/(2+b_F)$. For solid control a close to horizontal line is obtained except at low feed concentrations since $1/MTZ \propto bc_F/(2+b_F)$. When both resistances are significant the line is convex approaching the two limiting cases at low and high feed concentrations. The flow rate dependence of the mass transfer zone is also of interest. For solid diffusion control $1/MTZ_t$ is independent of the flow rate since k_q is constant. For film control $1/MTZ_t$ is an increasing function of the flow rate since k_f increases with the velocity. However, the scaled resistance ratio δ increases with the velocity due to the velocity dependence of k_f. Thus, when both resistances are significant the flow rate dependence of $1/MTZ_t$ will be less pronounced as the flow rate increases since the influence of the external film resistance decreases. It can therefore be difficult to distinguish an apparent flow rate dependence of k_f, or rather MTZ_t, from an increased significance of the solid phase resistance.

The mass transfer parameters can be determined by fitting the model to experimental data for the width of the mass transfer zone or the flux. Even from a single experiment information regarding mass transfer can be extracted. If the inflection point of x(t) is greater than 0.5 film diffusion predominates while solid diffusion predominates when $x''<0.5$. In principle the ratio of the mass transfer coefficients can be found from the inflection point and the value of either coefficient from the flux maximum although this approach is not recommended. The issue of parameter fitting is discussed in Chapter 3.

Chapter 3. Frontal analysis

This chapter concerns application of the solid diffusion model to describe the experimental breakthrough behaviour. The study of a step response of a given system is known as *frontal analysis*. In the following, mass transfer coefficients determined from the flux and from the mass transfer zone are compared. Results for Aprotinin and Lysozyme are presented and compared with the results for BSA from Paper 1, and the results of the frontal analysis study are discussed in general. The experimental setup is described in Paper 1.

Data reduction and fitting procedures

In order to obtain the mass transfer parameters the flux model must be fitted to the experimental breakthrough curves. The fitting procedure is often a compromise between simplicity and robustness. In the most thorough but also tedious approach the full model is solved numerically and compared to the experimental curves. In order to simplify the fitting procedure two approaches can be taken. In the first the amount of experimental data is reduced either by extracting characteristic values for each curve, such as the width of the mass transfer zone, or by selecting breakthrough curves at specific representative conditions (film or solid phase diffusion control). In the second approach the model is simplified so that it only covers a specific set of conditions such as constant pattern or film diffusion control, which in return constrain the experimental conditions. In this work a combination of both approaches is used. The applied model is the constant pattern solution of the solid diffusion model derived in chapter 2. In the following the data reduction procedure and different fitting procedures will be examined and discussed in relation to a selected set of experimental results.

Reduction and smoothing

An experimental breakthrough curve easily consists of several thousands of data points given as UV signal vs. time. However, only the small fraction of the data representing the mass transfer zone are of interest when fitting the model. In this region the experimental curve can be fitted by fairly simple transient functions. As a result the experimental breakthrough curve x(t) is well described by a function with analytical derivatives containing perhaps five parameters. The original set of experimental curves are thus represented by empirical functions with a set of parameters for each curve. This approach, which can be compared to the use of spline functions, has two advantages apart from the reduced amount of data: By fitting with a continuous function the experimental curves are smoothed without using a *running average* type smoothing algorithm. Further, data manipulation is easier to perform since the determination of specific functional values and derivatives can be automated. As an example the width of the mass transfer zone, $MTZ(x_1,x_2)$, can be determined by solving $f(t)-x_i=0$ for t, where f(t) is the empirical transient function, and the procedure is easily repeated if alternative values for x_1 and x_2 are desired. This approach should be compared to

the straight forward alternative which includes scrolling through the data files to get the x-values and performing numerical differentiation to get the derivatives.

Flux curve procedure

By fitting the model to the derivative of the breakthrough curves numerical integration of the flux equation is avoided. This makes the parameter fitting straight forward and the procedure can be performed in a spreadsheet. The procedure was applied in Paper 1, where the experimental data for each breakthrough curve consisted of derivatives at ten selected values of the reduced concentration x. As discussed in Paper 1 fitting the model to the flux curves seems more sensitive than fitting to the width of the mass transfer zone. But more important, the enhanced sensitivity is pronounced when comparing the model to the experiments. In the extreme case, where only one experiment is performed the width of the mass transfer zone can be matched by any model, while the shape of the flux curve cannot. As the number of experiments and the variation among them is increased, the flux and the MTZ procedures should yield the same results, since the MTZ plots will also exhibit a characteristic shape as discussed in chapter 2.

MTZ procedure

The data for the width of the mass transfer zone consist of a value for MTZ for each experiment determined at a given cut-off. When fitting, the model must be integrated for each set of conditions (c_F, v), which puts certain demands on the software since a numerical integration must be incorporated into the fitting algorithm. The solid diffusion model was fitted to the mass transfer zone of the BSA data for Q HyperD 35 from Paper 1 and below the results are compared with the results obtained by the flux curve procedure.

Selective fit

In this approach the model is fitted to a single experiment performed at conditions where the mass transfer is controlled by one mechanism. In the present case this means either film or solid diffusion control, and the conditions must therefore correspond to a low and a high δ value respectively. The procedure is simple and elegant since it requires an understanding of the model behaviour to be applied in the planning of the experiments. However, some caution must be taken when using this approach since only the approximate relative increase in δ and not the absolute values can be controlled experimentally. If a rectangular isotherm is assumed, δ can be increased by a factor of 30 by changing the feed concentration from 0.1 to 3 g/L. In the best case this could correspond to δ=0.2 and δ=6, which is substantial for assuming film and solid diffusion control, but values of say 0.02 and 0.6 might also be encountered which would cause an underestimation of the solid phase mass transfer coefficient at "high" δ. Using this procedure individual values of k_f was determined from the BSA data for Q HyperD 35 for the lowest feed concentration c_F=0.5 g/L (δ low) at three

velocities and a value for k_q was determined from the highest velocity and feed concentration (δ high). The results for the film coefficients are shown in Figure 7. The concept of reducing the experimental work by considering the variation in δ is useful. A sufficient set of experiments could consist of a flow rate study at low c_F where the film resistance is most pronounced and a concentration study at an intermediate or high flow rate. Most importantly the combinations (low c_F, low v) and (high c_F, high v) should be included in this type of study.

Application to data for BSA on Q HyperD 35

The three procedures described above have been applied to the experimental data for Q HyperD 35 from Paper 1. For the flux and MTZ fit two approaches have been used. In the first the film coefficient was determined at each flow rate, in the second the film coefficient was represented by the expression $k_f=\alpha v^{\beta}$ with α and β as the fitting parameters. The latter approach should be preferred when results with a small contribution from the film resistance are included in the experimental data since the magnitude of the film coefficient at these conditions will be controlled by the conditions where this parameter is significant.

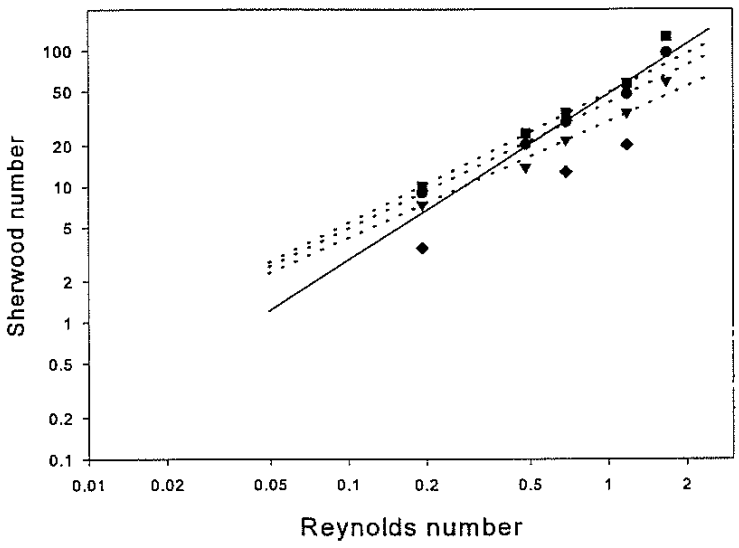

Figure 7: The Sherwood numbers for the film coefficients of BSA on Q HyperD 35 determined from MTZ_t at cut-off values of x_1,x_2 =(0.1,0.7) (●), (0.3,0.7) (▼), and (0.1,0.5)(■) by an individual fit of k_f and the correlation $k_f=\alpha v^{\beta}$ (dotted lines). The Sherwood numbers determined from c_F=0.5 g/L (◆) assuming film diffusion control. The solid line is the correlation from Paper 1.

Figure 7 shows the results for the film coefficients from the three procedures given as the

Sherwood number as function of the Reynolds number with physical parameters for the mobile phase identical to those of Paper 1. For the MTZ fit cut-off values of (x_1,x_2)=(0.1,0.7), (0.3,0.7) and (0.1,0.5) have been applied. Minor differences in the Sherwood numbers for the MTZ fit at different cut-off values are found, showing a trend where the highest Sherwood numbers are found when the cut-off is placed in the lower region of the breakthrough curves, (x_1,x_2)=(0.1,0.5). The dotted lines represent the fit obtained using the correlation for $k_f(v)$ and these results agree with the individual fit except at the highest Reynolds number. This indicates that the individual k_f for this velocity might not be well determined because of the minor influence of the film resistance. The correlation from Paper 1, which was obtained from a fit of the flux for several resins, is in agreement with the MTZ results for (x_1,x_2)=(0.1,0.7) although a slightly larger slope is found. The individual and the correlated fit of these flux data are almost identical as can be seen from Figure 7 in Paper 1. The most pronounced difference is found when comparing the results of the MTZ and flux procedures to the results of the selective fit performed at the lowest feed concentration. The smaller values found from the latter can be explained by the existence of a significant solid phase resistance at these conditions, see discussion above. For the MTZ procedure values of k_q in the range $3\text{-}4\times10^{-5}$ cm/s was found while $k_q=2.7\times10^{-5}$ cm/s for the fit to the highest velocity and feed concentration. These values should be compared to $k_q=k_s=2.9\times10^{-5}$ cm/s determined by the flux curve procedure in Paper 1.

From the comparison of the different fitting procedures it is concluded that a satisfactory agreement is found between the flux curve and the MTZ procedures. The approach of determining the parameters from selected experimental conditions by assuming mass transfer to be controlled by a single mechanism must be taken with caution.

Results

Mass transfer coefficients for BSA on five different resins was determined by frontal analysis and the results are presented in Paper 1. The experimental data showed a significant film resistance for all resins and a correlation of the film coefficients was possible revealing an unexpected strong Reynolds number dependence of the Sherwood number. Solid diffusion control was obtained only for Q HyperD 35, primarily because high flow rates could be applied to this resin. The results for Q HyperD 35 are therefore relevant in relation to the discussion of non-linear mass transfer behaviour in Chapter 2. Figure 8 shows the development of the mass transfer zone with the feed concentration at different flow rates for (x_1,x_2)=(0.1,0.7). For the lowest flow rate mass transfer is dominated by the film resistance and a close to straight line is observed. As the flow rate increases solid diffusion becomes significant (δ increases) and the lines become curved approaching the horizontal limit of solid diffusion control at high feed concentrations. The observed mass transfer behaviour is in agreement with the theoretical study from chapter 2.

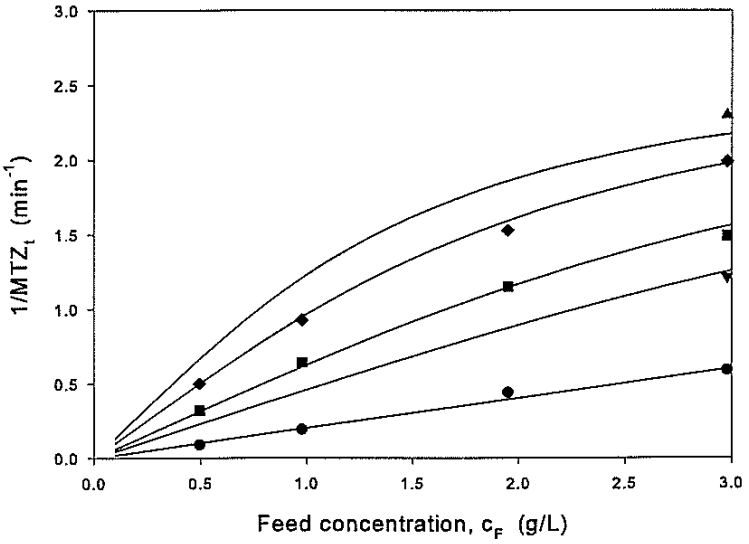

Figure 8: Data for the mass transfer zone of BSA on Q HyperD 35 at superficial velocities of 0.2 (●), 0.5 (▼), 0.7 (■), 1.2 (◆), and 1.7 cm/s (▲), and the solid diffusion model.

In the following additional frontal analysis results are presented. The velocity dependence of the film coefficient was the main objective in the experiments.

Aprotinin on Resource 15S

Breakthrough curves for Aprotinin in 50mM NaAc at pH 5 were determined on a Resource 15S column identical to that of Paper 2 where the mass transfer of Aprotinin is studied under linear adsorbing conditions. No salt was added to the mobile phase and the counter ion concentration was therefore $[Na^+]$=50 mM originating from the buffer. The experimental conditions and the results are presented in Table 1. The frontal analysis experiments where performed using the procedure described in Paper 1.

The Langmuir isotherm parameters where determined from the retention volumes approximated by $V(c/c_F=0.5)$ neglecting the amount of protein in the pores and using the bed porosity ϵ=0.48 determined in Paper 2. The constant pattern assumption was tested at c_F=0.5 g/L and v_0=0.25 cm/s using the gradient procedure described in Paper 1. Identical breakthrough curves with a mass transfer zone of 5 mL where observed for a step and a 20 mL gradient input thus supporting the constant pattern assumption. A general discussion of the procedure is found in Paper 1.

The flow rate dependence of the film coefficient was determined by two methods. In the first the film coefficients where determined from the width of the mass transfer zone as function of the flow rate at c_F=0.1 g/l assuming film controlled mass transfer. In the second both the

film and solid mass transfer coefficients where determined from a total fit of the MTZ data.

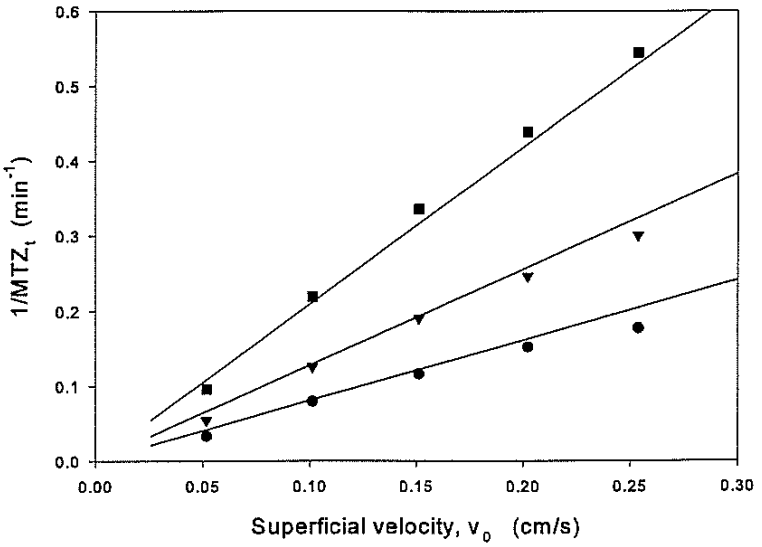

Figure 9: Data for the mass transfer zone for Aprotinin on Resource 15S at c_F=0.1 g/L and cut-off values of 0.1 (●), 0.2 (▼), and 0.3 (■), and the film diffusion control model, equation (25).

Figure 9 shows the data and model results for the fit at c_F=0.1 g/L depicted as $1/MTZ_t$ vs. the velocity. The parameters where determined by fitting the film control model equation (25) to the data at cut-off values of (x_1, x_2)=(0.1,0.9), (0.2,0.8), and (0.3,0.7) using the correlation $k_f=\alpha v^{\beta}$ where v is the interstitial velocity. The model fit is satisfactory and the data do not exhibit any significant influence of the solid resistance. If the solid resistance was significant the flow rate dependence given by the velocity exponent β would decrease with increasing flow rate as discussed in Chapter 2. Values of $\alpha=4.9\times10^{-3}$ cm/s and β=1.0 were obtained for this method.

The results of the total fit is depicted in Figure 10. The three data points c_F=1.9 g/L and v_0=0.1, 0.15 and 0.20 cm/s. where neglected in the fitting procedure. For these three experiments the width of the mass transfer zone in mL was considerably larger than for both the highest and lowest velocity at c_F=1.9 g/L. Within the present interpretation of the solid diffusion model the width of the mass transfer zone in volume units MTZ_V is a monotonic, usually increasing, function of the velocity and it is therefore likely that an experimental error might have occurred in the experiments for c_F=1.9 g/L. The experiments for the highest and lowest flow rate at c_F=1.9 g/L where performed in a multi-run (automated sequential runs) together with the experiments for c_F=0.2, 0.5, and 1 g/L and seem to correspond with the behaviour of these data. The experiments at the intermediate velocities where performed later

as the final runs of a sequence including the experiments for c_F=0.1 g/L. Since the system at the time had been running for more than twenty hours, due to the large retention time for c_F=0.1 g/L, the column and/or apparatus might have been affected and it was therefore decided to neglect these three experiments. For the total fit $\alpha=4.7\times10^{-3}$ cm/s, β=1.1, and $k_q=3.3\times10^{-5}$ cm/s. For these parameters a maximum value of δ=1.6 is found for v_0=0.25 cm/s and c_F=1.9 g/L. The results obtained by the two methods are in reasonable agreement and show a significant flow rate dependence of the external film mass transfer coefficient.

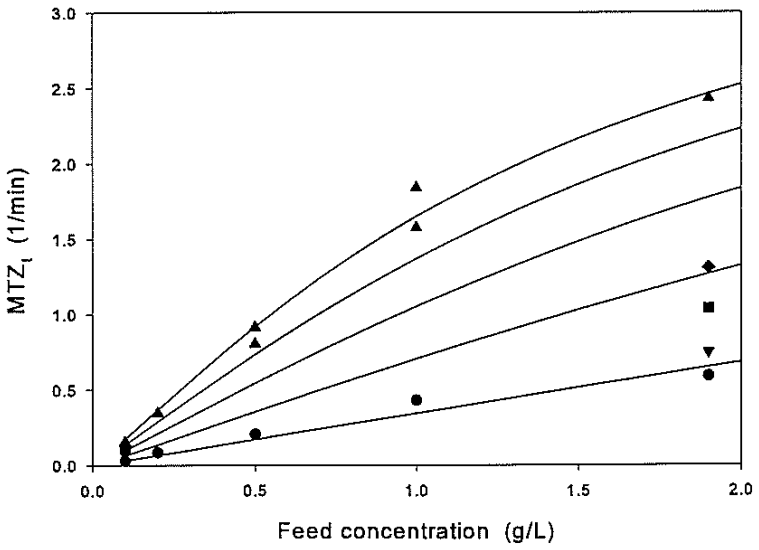

Figure 10: Data of the mass transfer zone for Aprotinin on Resource 15S (x_{cut}=0.1) at superficial velocities of 0.05 (●), 0.10 (▼), 0.15 (■), 0.20 (◆), and 0.25 cm/s (▲), and the solid diffusion model.

Lysozyme on Resource 15S

Breakthrough curves for Lysozyme (Lot 65H7025, Sigma) in 20 mM HPO_4Na_2 buffer at pH 6.5 (HCl) with 20mM NaCl added were determined on a Resource 15S 1 mL column identical to that of the Aprotinin experiments above and Paper 2. The counter ion concentration was [Na^+]=60mM. The experiments consist of a flow rate study at c_F=0.1 g/L and additional experiments in the range 0.2-1 g/L sufficient for estimating the isotherm parameters. The objective was to study the flow rate dependence of the film coefficient. As for Aprotinin the Langmuir parameters were determined from the volume at c/c_F=0.5. The experimental conditions and the results are presented in Table 1. Constant pattern was verified for c_F=0.5 g/L and v_0=0.15 cm/s by the procedure of Paper 1 using a 20 mL gradient. The correlation parameters α and β were determined by the first method described in the

section concerning Aprotinin.

Figure 11 shows the data and model results for Lysozyme at c_F=0.1 g/L. A satisfactory fit is obtained with $\alpha=4.2\times10^{-3}$ cm/s and β=1.2 although a minor deviance is found for (x_1, x_2)=(0.1,0.9). As for the Aprotinin data presented above the data for Lysozyme do not exhibit any significant influence of the solid phase resistance.

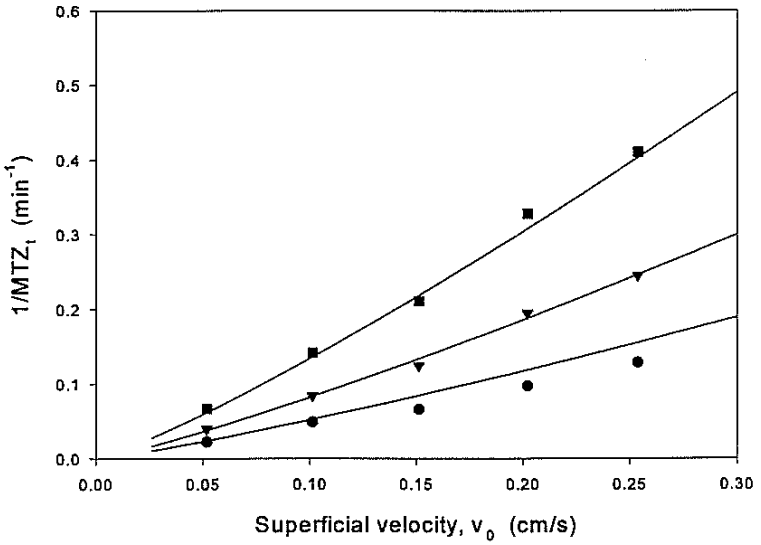

Figure 11: Data of the mass transfer zone for Lysozyme on Resource 15S at c_F=0.1 g/L and cut-off values of 0.1 (●), 0.2 (▼), and 0.3 (■), and the film control model, equation (25).

Discussion

Film coefficients

In modelling of chromatography the external film coefficients are most often estimated from existing packed bed correlations, and recent experimental data for the film coefficient are therefore sparse. For many applications the film coefficients are of minor importance since the film resistance is insignificant. Only when the rate of mass transfer in the particles is sufficient, as is the case for strong adsorption, the film resistance will be significant.

Figure 12 compares the film mass transfer coefficients for BSA, Aprotinin, and Lysozyme presented above and in Paper 1 to film coefficients calculated by two correlations often used for estimation when describing packed bed mass transfer. The correlations are

(Carberry, 1960)

$$Sh = 1.15 Re^{1/2} Sc^{1/3} \qquad (29)$$

(Wilson and Geankoplis, 1966)

$$Sh = \frac{1.09}{\epsilon}(Re\,\epsilon)^{1/3} Sc^{1/3} \qquad (30)$$

The Reynolds number is based on the interstitial velocity v.

For each of the three components the Sherwood numbers from this work are given by $Sh=\alpha Re^{\beta}$. For Aprotinin and Lysozyme the Sherwood numbers are calculated from the velocity correlations determined above while the correlation for BSA is given by equation (16) in Paper 1. The extend of the three lines represent the Reynolds number interval from which they were determined. The correlation by Carberry is valid for Re>1 while the correlation by Wilson and Geankoplis is valid for Re>0.0015 (Perrys Handbook, 1997). Fernandez et al. (1996) determined mass transfer coefficients for BSA from breakthrough experiments at Re close to one. Their results agree with the correlation by Carberry as shown in Paper 1. Koh et al. (1998) used the correlation by Wilson and Geankoplis in describing the breakthrough behaviour of L-phenylalanine but the validity of the film correlation was not examined.

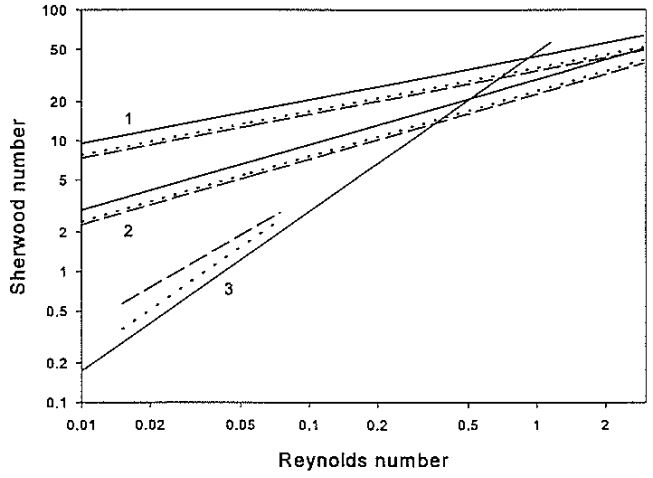

Figure 12: Sherwood numbers for BSA (solid), Lysozyme (dotted), and Aprotinin (dashed) determined by the correlations of Wilson & Geankoplis (1), Carberry (2), and this work (3).

The three correlations from this work exhibit the same Reynolds number dependence. Compared to the literature correlations the Sherwood numbers are significantly smaller and the Reynolds number exponent β greater by approximately a factor 2 and 3.

The difference between the Sherwood numbers of the three components as determined from the correlations (28) and (29) is small since the Schmidt number dependence is not pronounced. For Aprotinin, Lysozyme, and BSA the diffusion coefficients are 1.3, 1.1, and 0.6 $\times 10^{-6}$ cm^2/s respectively corresponding to Schmidt numbers of 1563, 9090, and 16667. The correlations from this work are also close but compared to the two literature correlations the order of the three components is reversed, most likely due to experimental uncertainties. It is noted that the film coefficients increase with the diffusion coefficient as would be expected.

It can be argued that the present Sherwood numbers seem unrealistic when compared to the literature correlations which are based on hydrodynamic considerations and a substantial amount of experimental data. However, it is beyond question that when describing the observed mass transfer using the mobile phase linear driving force approximation these correlations do not apply. At present the strong Reynolds number dependence of the Sherwood number determined from the breakthrough experiments have been neither verified nor contradicted by other experimental studies. The Reynolds number dependence is discussed further in Chapter 7.

		Resource 15S	
V_{col}	(mL)	1	
d_p	(µm)	15	
ϵ		0.48	
Solute		**Aprotinin**	**Lysozyme**
Buffer		50 mM NaAc	20 mM HPO_4Na_2
pH		5 (HCl)	6.5 (HCl)
c_{NaCl}	(M)	none added	0.02
c_{feed}	(g/L)	0.1-1.9	**0.1-1**
v_0	(cm/s)	0.05-0.25	0.05-0.25
s_{max}	(g/L particle)	120	127
b	(L/g)	53	80
$\alpha \times 10^3$	(cm/s)	4.9 (4.7)	4.2
β		1.0 (1.1)	1.2
$k_q \times 10^3$	(cm/s)	0.033	-
$D_q \times 10^6$	(cm^2/s)	0.50	-

Table 1: Parameters and conditions for frontal analysis on Resource 15S.

Apparent mass transfer coefficients

An apparent mass transfer coefficient can be determined by comparing a given model to a single experiment. Sajonz et al. (1996) determined the apparent solid phase mass transfer coefficient for BSA on Resource 15Q from the width of the mass transfer zone at experimental conditions identical to those of Paper 1. An apparent solid phase mass transfer coefficient was determined from each data point for MTZ using a model assuming solid phase diffusion control corresponding to equation (26). The apparent solid phase mass transfer coefficients could be correlated with the feed concentration by a linear expression at each flow rate, $k_{q,app.}=k_{q,0}+k_{q,1}c_F$. The parameters were $k_{q,0}=0.4\times10^{-6}$ cm/s and $k_{q,1}= 4.1\times10^{-6}$ cm·L/s·g for Q=1 mL/min, and $k_{q,0}=1.4\times10^{-6}$ cm/s and $k_{q,1}= 8.7\times10^{-6}$ cm·L/s·g for Q=2 mL/min. In Paper 1 it was found that the mass transfer for BSA on the Resource 15Q column was controlled by the external film resistance, contrary to the assumption made by Sajonz. Figure 5 of Paper 1 compares the flux curves for film diffusion control and apparent solid phase mass transfer. The width of the mass transfer zone for film and solid diffusion control are identical when $k_q=k_fc_F/q_F$. Thus when mass transfer is controlled by film diffusion the apparent solid phase mass transfer coefficient is an increasing function of the feed concentration and for a Langmuir isotherm the linear dependence $k_q=k_{q0}(1+bc_F)/s_{max}b$ is obtained. The correlation obtained by Sajonz is therefore merely a result of describing external film mass transfer by apparent solid phase diffusion.

Applying the relation between k_q and k_f to the results by Sajonz et al. k_f can be estimated for each flow rate resulting in Sherwood numbers of 0.8 and 1.6. These values are identical to the values determined in Paper 1 for the same flow rates, see Figure 7 of Paper 1. Thus, the Sherwood numbers determined from the results by Sajonz support the strong Reynolds number dependence found in this work.

Lewus et al. (1998) studied the batch and shallow bed uptake of Lysozyme on S HyperD-M and found mass transfer to be dominated by solid phase diffusion with some contribution from film diffusion. They showed that when using an apparent pore diffusion model to describe the data the pore diffusion coefficient had to increase when the salt concentration was lowered resulting in stronger adsorption. The reason is that the apparent flux for pore diffusion must match the flux for solid diffusion which in a simplified form corresponds to the relation $D_pc_F=D_qq_F$. An increase in q_F at fixed c_F caused by lowering the salt concentration therefore yields an increased apparent pore diffusion coefficient.

The approach of using apparent mass transfer coefficients is not very useful since intra -and extrapolation of the results to different equilibrium conditions and velocities is difficult. A model should contain mass transfer parameters that do not depend on the equilibrium conditions unless the dependence is substantiated by physical considerations. The topic of apparent diffusivities is treated further in relation to parallel mass transfer in Chapters 4-6.

Chapter 4. Linear mass transfer

When the equilibrium ratio q/c between the solid and liquid phase solute concentrations does not depend on the concentration in the liquid phase the adsorbing conditions are referred to as *linear* since q is a linear function of c at equilibrium. Mass transfer in linear systems is of interest primarily because analytical solutions of the various models are available providing a straight forward approach for estimation of the mass transfer properties.

In this work linear mass transfer is studied experimentally by pulse injections at conditions ranging from weak to strong retention. From the pulse response the number of theoretical plates and thus the plate height can be determined. The plate height is a measure of the column efficiency similar to the width of the mass transfer zone treated in chapters 2 and 3. From the experimental plate height data the mass transfer properties can be determined.

Parallel diffusion

For a linear isotherm the parallel diffusion equation presented in Chapter 1 can be expressed by

$$\frac{\partial s}{\partial t} = \frac{6}{d_p} K_d \epsilon_p (D_p + D_q A) \left(\frac{\partial c_p}{\partial r} \right)_R \qquad (31)$$

using the local equilibrium relation $q=Ac_p$. For the linear driving force approximation the flux equation is

$$\frac{\partial s}{\partial t} = \frac{6}{d_p} K_d \epsilon_p (k_p + k_q A)(c - c_p) \qquad (32)$$

Due to the linear relation between q and c_p this expression is independent of the choice of intra particle gradient to be linearised. This is not the case for non-linear conditions as discussed in Chapters 1 and 6.

The linear adsorbing conditions are useful for studying parallel diffusion since the flux equation is unambiguous and an analytical expression for the plate height exists. By changing the adsorbing conditions from weak to strong retention intra particle mass transfer ranging from pore to solid diffusion control can be studied.

The van Deemter equation

When the number of theoretical plates is sufficient the pulse response for linear adsorption results in a profile well approximated by the Gaussian distribution (Guiochon et al., 1994 and Wankatt, 1994). Comparing this approximation obtained from the plate theory to the expression obtained from the general rate model (mass balance and flux equation) van Deemter et al. (1956) derived an expression, later known as the *van Deemter equation*, which

relates the plate height for a given solute and column to relevant physical parameters. For conditions where the contribution from ordinary mobile phase diffusion to band broadening can be neglected and the axial dispersion coefficient is proportional to the velocity the reduced plate height $h=H/d_p$ from the van Deemter equation is given by

$$h = 2\lambda + 2\left[\frac{k'}{1+k'}\right]^2 \frac{\epsilon v}{6(1-\epsilon)K_m} \qquad (33)$$

where the two terms comprise the contributions from axial dispersion and mass transfer. The over-all mass transfer coefficient K_m corresponds to an over-all driving force in the liquid phase concentration, $c-c_p$. From the flux equation derived above and the external film expression the over-all mass transfer coefficient for parallel diffusion is

$$\frac{1}{K_m} = \frac{1}{k_f} + \frac{1}{K_d\epsilon_p(k_p + k_q A)} \qquad (34)$$

Inserting this expression and $k'=(1-\epsilon)K_d\epsilon_p(1+A)/\epsilon$ into the van Deemter equation the plate height for parallel diffusion becomes

$$h = 2\lambda + 2\left[\frac{1+A}{p+1+A}\right]^2 \frac{\epsilon v}{6(1-\epsilon)}\left(\frac{1}{k_f} + \frac{1}{K_d\epsilon_p(k_p + k_q A)}\right) \qquad (35)$$

where $p=\epsilon/(1-\epsilon)K_d\epsilon_p$.
Equation (35) reduces to the plate height for the solid and the pore diffusion model when $\gamma=k_p/k_qA$ goes to zero and infinity respectively.

Plate height behaviour

For a given solute and resin the plate height depends on the velocity and the equilibrium ratio. From experimental data for the plate height as function of the velocity performed at fixed adsorbing conditions only the over-all coefficient K_m can be determined as discussed in Paper 2. In order to determine the individual coefficients and distinguish between pore and solid diffusion significant variation in the equilibrium ratio is required. The development of the plate height with the equilibrium ratio is discussed in the following.
For the purpose of this study the van Deemter equation is written as

$$H^* = \frac{1}{N} = \frac{2}{Pe} + 2\left[\frac{1+A}{p+1+A}\right]^2 \frac{\epsilon}{(1-\epsilon)}\left(\frac{1}{St_f} + \frac{1}{K_d\epsilon_p(St_p + St_q A)}\right) \qquad (36)$$

where Pe is the axial dispersion Peclét number and $H^*=H/L=1/N$ is introduced for convenient

notation. The plate height represented by H* as function of the equilibrium ratio A is calculated using the parameters ϵ=0.5, $K_d\epsilon_p$=0.5, Pe=1000, St_f=600, and St_p=30, and St_q=6. Figure 13 shows the development of the resulting plate height and the individual contributions from axial dispersion, film, pore, and solid mass transfer. The contribution from axial dispersion is H_a^*=2/Pe. The contribution from film diffusion H_f is obtained from the last term in equation (36) including only $1/St_f$. The contributions from pore and solid diffusion H_p^* and H_q^* are obtained from the last term in equation (36) neglecting $1/St_f$ and setting St_q and St_p to zero respectively.

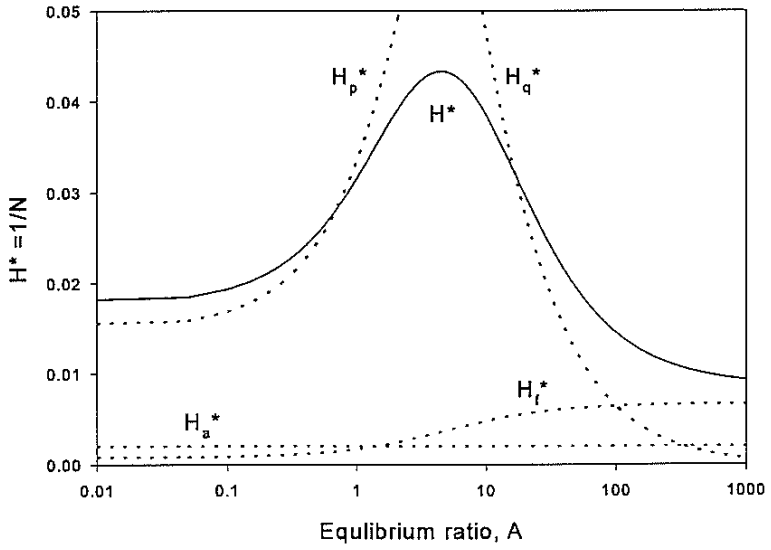

Figure 13: The resulting reciprocal plate number for parallel diffusion (solid) and the individual contributions (dotted) for axial dispersion (a), film diffusion (f), pore diffusion (p), and solid diffusion (q).

The plate height for intra particle mass transfer H_{pq}^* is dominated by the smallest of the contributions from pore and solid diffusion

$$\frac{1}{H_{pq}^*} = \frac{1}{H_p^*} + \frac{1}{H_q^*} = \frac{1+\gamma}{H_q^*} \qquad (37)$$

The resulting plate height is $H^*=H_a^*+H_f^*+H_{pq}^*$.

The plate height for pore diffusion H_p^* increases with A towards a constant value due to the term in the square brackets of equation (35) while the plate height for solid diffusion is a decreasing function of A approaching zero at strong retention. Therefore, the intra particle plate height given by equation (37) as function of A is a bell shaped curve coinciding with

H_p* at low retention (γ<0.1) and H_q* at strong retention (γ>10). This behaviour is also found in the curve for the resulting plate height H* in Figure 13 since the plate height in general is dominated by the contribution from intra particle mass transfer. The plate height for axial dispersion is independent of A while the plate height for film diffusion H_f* develops in the same manner as H_p* but is significantly smaller due to the higher Stanton number. When the equilibrium ratio becomes large intra particle mass transfer is relatively fast and the corresponding plate height contribution small. At high retention the resulting plate height therefore mainly comprises the contributions from axial dispersion and film diffusion as shown in Figure 13.

The plate height behaviour is consistent with the resistance scheme shown in Chapter 1. The plate height at low retention is dominated by pore diffusion corresponding to the starting point for the dashed line in the upper right corner of Figure 1 where γ>10. As the equilibrium ratio is increased solid diffusion becomes significant until the intra particle mass transfer rate becomes so high that the plate height is dominated by film diffusion (and axial dispersion) corresponding to the endpoint of the dashed line in the lower left corner of Figure 1 where $\delta/(1+\gamma)$<0.1. For Figure 13 the ratio of the scaled solid and pore mass transfer resistances γ is 0.1 and 10 for A=0.5 and 50 respectively, while the ratio of intra particle to film resistance $\delta/(1+\gamma)$ is 10 and 0.1 for A=5 and 1000.

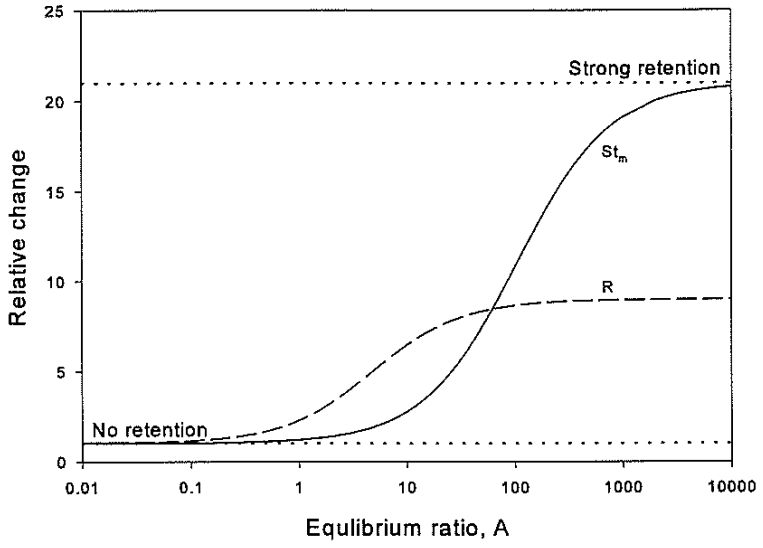

Figure 14: The relative change in the over-all Stanton number, $St_m(A)/St_m(A=0)$, (solid) with limits indicated (dotted) and the relative change in the retention term, $R(A)/R(A=0)$, (dashed).

The plate height for parallel diffusion does not vary to a great extend when the equilibrium

ratio is increased. The reason is that an increase in h from the term in the square brackets of equation (35) is somewhat compensated by an increase in the over-all mass transfer coefficient or Stanton number. Figure 14 shows the relative increase in the over-all Stanton number St_m and the retention term $R=(1+A)^2/(p+1+A)^2$ with the equilibrium ratio. The lines are scaled with the corresponding values at A=0. The over-all Stanton at number St_m is approximately $K_d\epsilon_p St_p$ at A=0 and St_f at very strong retention. In Figure 14 the ratio $St_m/St_m(A=0)$ therefore increases by approximately a factor of 20 corresponding to $St_f/K_d\epsilon_p St_p$. The retention term R increases by close to a factor 10 in Figure 14, more exact $(1+p)^2=9$. If an apparent over-all mass transfer coefficient is determined at non-retained conditions, equation (33) thus predicts that the plate height increases nine fold at strong retention when in fact the plate height for the present example decreases as shown in Figure 13. The figure illustrates that apparent over-all mass transfer coefficients are of little use in prediction of the mass transfer rate and thus the plate height. From an apparent over-all mass transfer coefficient determined at given retention the plate height at other retaining conditions cannot be predicted by use of equation (33). From Figure 13 it seems that it is a better approximation to assume the plate height independent of the equilibrium ratio than to assume a constant apparent over-all mass transfer coefficient, an issue discussed in chapter 5 and Paper 2 in relation to the experimental results.

Chapter 5. Isocratic elution

The linear isotherm can be considered a limiting case of the Langmuir isotherm valid when the product bc goes to zero. Linear conditions are realised experimentally by adding salt to the mobile phase in order to have a considerable counter ion concentration thereby reducing b and by applying a small feed sample which is diluted in the column. In this work linear mass transfer is studied experimentally by determining the plate height from pulse injections and isocratic elution at different counter ion concentrations. The retention volumes could be correlated using the mass action law for the equilibrium between the given species and counter ion, while the mass transfer properties were obtained from the plate height data. The experimental setup and fitting procedures are described in Paper 2.

Extra column effects

When working in small scale the experimental data must be corrected for the retention and band broadening caused by the experimental system, referred to as extra column effects (ECEs). The retention is caused by the dead volume in the tubing and valves while the band broadening originates from dispersion in the dead volume. For a linear system the first and second moments are additive and the true retention volume and variance of an experimental peak can therefore be calculated by subtracting the parameters determined from an identical experiment performed without the column. Determination of ECEs involves a significant uncertainty due to the small time scale of the experiment and the uncertainty is reflected in the corrected data. In general the best results are therefore obtained when the contribution from ECEs is less than perhaps 10% which can be achieved by using columns of a certain size. The significance of ECEs is less for large molecules such as proteins compared to small molecules such as inorganic ions or amino acids because the band broadening in the column is greater. The most uncertain data are those performed with small molecules on a small column at low retention and velocity.

Correction of experimental data

In order to avoid duplicating all experiments the ECEs for each solute where correlated with the flow rate. A constant dead volume of 0.4 mL was determined and an empiric correlation was used for the flow rate dependence of the variance. The correlation parameters were determined from data for each component obtained at different flow rates, injection volumes, and counter ion concentrations. It was found that the concentration of the counter ions had no effect on the variance of the peaks while a minor effect was observed when changing the injection volume. Figure 15 shows the variance determined without the column for Tyrosine, Aprotinin and BSA. Each set of data was correlated by the expression $\sigma_d^2=A+B/Q$ where σ_d^2 is the variance and Q the volumetric flow rate. For Tyrosine, Aprotinin and BSA the parameters were (A,B)=(0.007, 0), (0.005, 0.005), and (0.004, 0.005) respectively with A in mL^2 and B in mL^3/min. In the experimental work the problem of correcting for ECEs was

reduced by, when possible, using larger columns for the experiments performed at low retention where the variance is small.

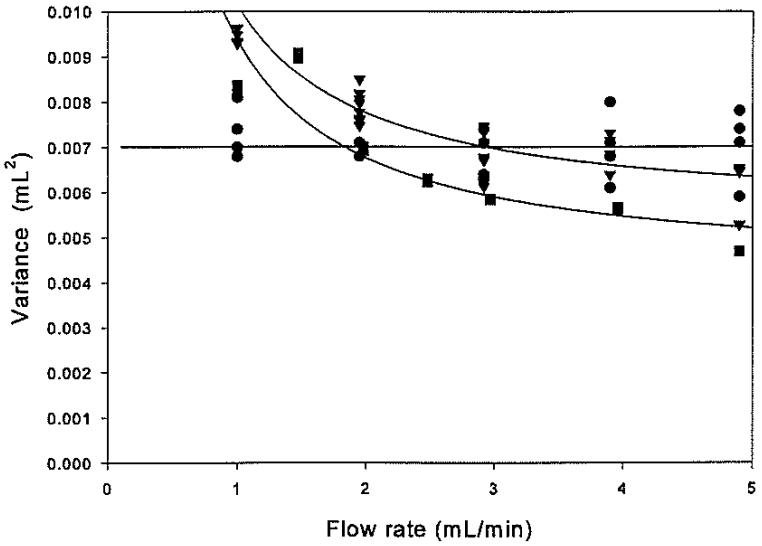

Figure 15: The BioCAD system peak variance for Tyrosine (●), Aprotinin (▼), and BSA (■), and correlation (solid lines) used for ECE correction.

Results

Experimental data for the plate height determined at different counter ion concentrations and velocities were correlated using the equilibrium ratio A obtained from the mass action law and the van Deemter equation for parallel diffusion presented in Chapter 4. Results for Tyrosine and Aprotinin on Resource 15 and HyperD 20 are presented in Paper 2. The observed plate height behaviour was consistent with the parallel diffusion model and it was concluded that the data could not be described by models including only pore or solid diffusion as the rate mechanism in the particles. In the following additional results obtained by the experimental and fitting procedures of Paper 2 are presented.

Aprotinin on Resource 15S

Figure 16 shows the results from Paper 2 for Aprotinin on Resource 15S including two additional velocities not shown in Figure 5 of Paper 2. The conditions and parameters are given in Table 1 of Paper 2. The data exhibit the characteristic bell like shape of parallel diffusion. For the lowest velocity the plate height is close to a constant since the contribution

from mass transfer is small compared to axial dispersion. As the velocity increases the variation of the plate height with the equilibrium ratio is more pronounced since the mass transfer term in the van Deemter equation is almost proportional to the velocity. The lines for h as function of the velocity are straight for low retention where mass transfer is controlled by pore diffusion. At strong retention the lines are slightly curved since the velocity dependence of the plate height is smaller due to the significant contribution from film mass transfer. The discrepancies between the model and the data found at high retention are most likely caused by the change in column size (see Paper 2 for discussion).

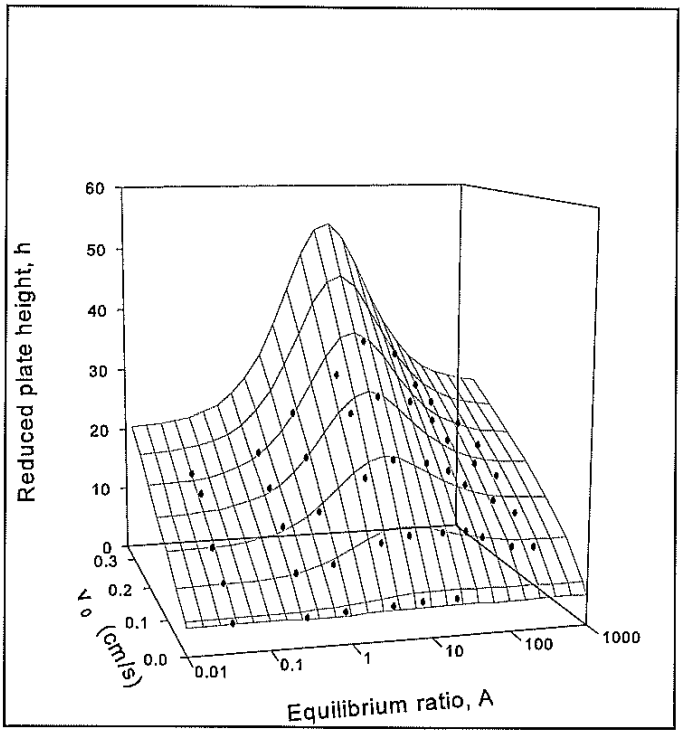

Figure 16: The experimental and the calculated reduced plate height for Aprotinin on Resource 15S. Starting at low v_0, lines 2-6 correspond to the experimental velocities.

Figure 17 shows the velocity dependence of the plate height for weak, intermediate, and strong retention. For v_0=0.2 cm/s the ratio of the scaled solid to pore resistances γ is 18, 0.6, and 0.01 for A=0.3, 8.5, and 392, while the ratio of the scaled particle to external resistances $\delta/(1+\gamma)$ is 4, 2, and 0.1. Thus, at strong retention mass transfer is dominated by the external film resistance. The figure shows that the plate height is almost proportional to the velocity and the rate of mass transfer is therefore not very dependent on the velocity even when film mass transfer dominates.

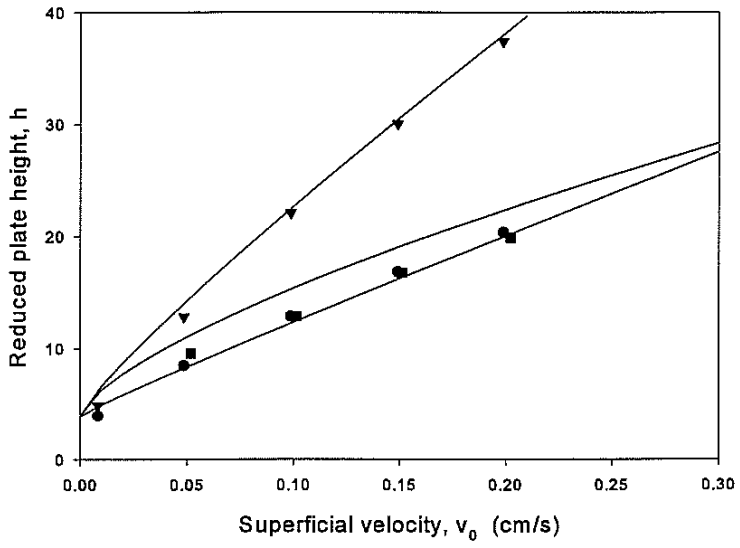

Figure 17: Experimental and calculated plate height for Aprotinin on Resource 15S at equilibrium ratios of A=0.3 (●), 8.5 (▼), and 392 (■).

Tyrosine on Poros 50 HQ

The Poros 50 HQ particles (Perseptive Biosystems) were packed in a 4.6 (ID) × 100 mm column at Novo Nordisk A/S, Denmark. The experimental conditions and procedures were identical to those for Tyrosine in Paper 2.

Figure 18 shows the plate height data and model as function of the equilibrium ratio at three velocities. The model parameters are reported in Table 2. The observed retention was not sufficient to obtain a decrease in the plate height as found for the Resource and HyperD resins. In order to investigate the existence of parallel diffusion the model is therefore compared to the pore diffusion model. For pore diffusion the over-all mass transfer coefficient is independent of the equilibrium ratio. For the fit of the pore diffusion model a constant over-all mass transfer coefficient K_m was therefore determined at each of the three velocities in Figure 18. The axial dispersion coefficient was set equal to the value obtained from the parallel diffusion model. The pore diffusion model cannot describe the observed plate height for A>1 since the variation of the plate height with A for this model is more pronounced than for the parallel diffusion model as discussed in Chapter 4.

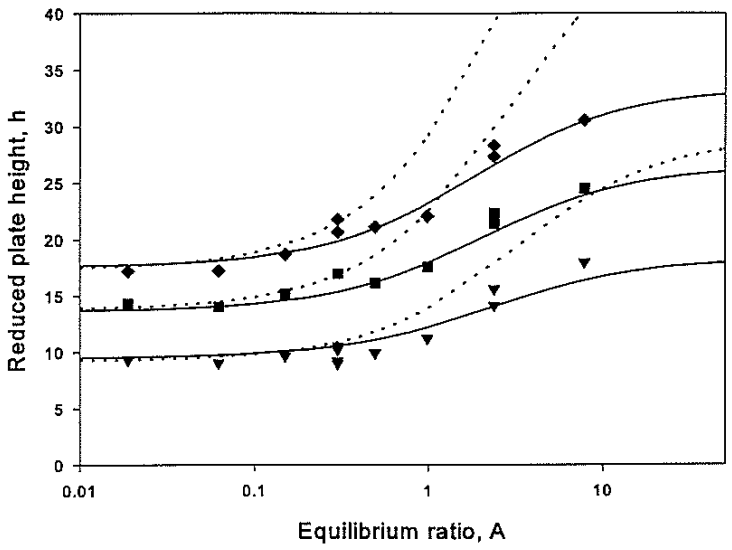

Figure 18: Comparison of the plate height data for Tyrosine on Poros 50 HQ at superficial velocities of 0.1 (▼), 0.2 (■) and 0.3 (◆) cm/s with the parallel diffusion model (solid) and the pore diffusion model (dotted).

Aprotinin on Poros 50 HS

The Poros 50 HS column (4.6×100 mm) was obtained from Perseptive Biosystems. The experimental conditions and procedures were identical to those for Aprotinin in Paper 2. Figure 19 shows the data and model fit at three velocities with parameters from Table 2. The observed plate height is almost independent of the equilibrium ratio and a pronounced axial dispersion contribution of 30 particle diameters is determined for this resin. The data for Tyrosine and Aprotinin could not be described satisfactory when setting λ equal for the two Poros resins. The difference in axial dispersion was investigated by determining the plate height for Tyrosine on the HS column and Aprotinin on the HQ column, both at high salt concentrations in order to avoid Donnan exclusion. Figure 20 compares the plate height for the two solutes on the two columns and it is evident that a significant difference in the apparent axial dispersion exists. The difference could be caused by different packing densities or perhaps wearing of the HS column. From Figures 18-20 it seems that the HQ column is applicable while the results for Aprotinin on the HS column must be interpreted with caution since the apparent irregularities in the column packing described by axial dispersion might influence other parameters.

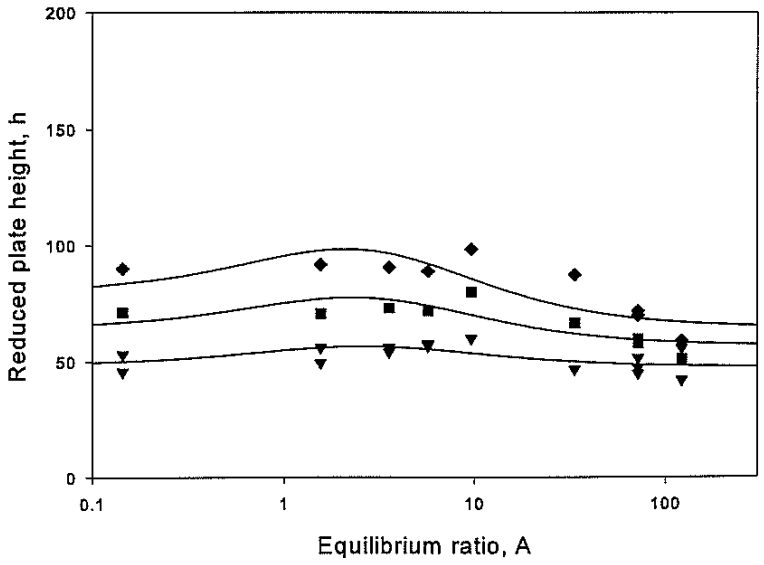

Figure 19: Experimental and calculated plate height for Aprotinin on Poros 50 HS at superficial velocities of 0.1 (▼), 0.2 (■) and 0.3 (◆) cm/s.

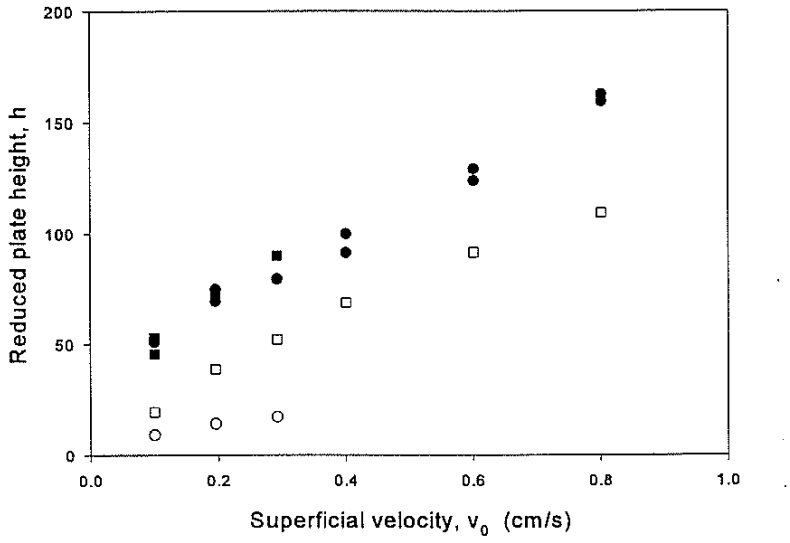

Figure 20: The plate height for Tyrosine (circles) and Aprotinin (squares) on Poros 50 HS (solid) and Poros 50 HQ (open) determined at non-retained conditions.

BSA on Source 30Q

The mass transfer and retention properties for BSA on Source 30Q (Pharmacia) packed in a 10 (ID)×104 mm column have been determined from the data provided by Jensen (1999). The experimental conditions and model parameters are found in Table 2. A bed porosity of 0.5 was assumed.

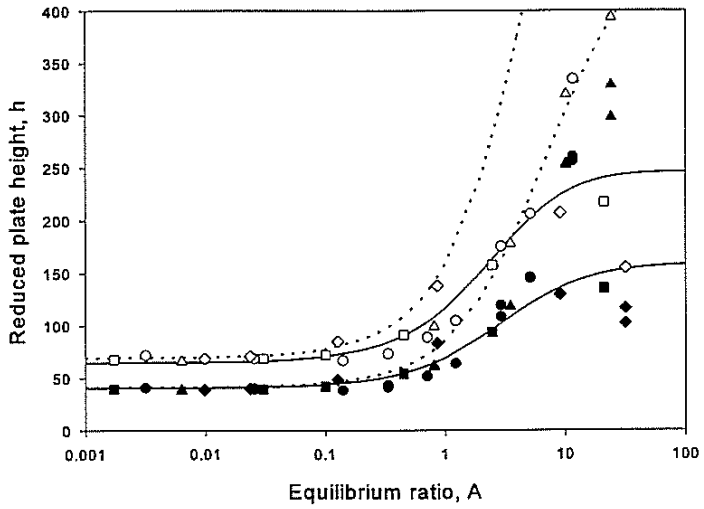

Figure 21: The plate height for BSA on Source 30Q at pH 6 (●), 7 (▲),8 (■), and 9 (◆) and superficial velocities of 0.06 (solid) and 0.12 cm/s (open). The parallel diffusion model (solid) and the pore diffusion model (dotted) were fitted to data for A<10 only. Data by Jensen (1999).

Plate height data for BSA are in general not well suited for investigating parallel diffusion since the peaks at moderate to high retention tend to be disturbed by impurities resulting in an ambiguous variance. However, the data by Jensen 1999 are interesting since a significant variation in pH was applied. The driving forces and mass transfer parameters in the present model are independent of the counter ion concentration and the charge of the solute which depends on pH. The mass transfer properties and thus the plate height for a given equilibrium ratio should therefore be independent of how the pH and the salt concentration were combined in order to obtain the given retention.

The retention volumes could be correlated satisfactory by the method of Paper 2 using a linear dependence of the adsorbing charge ratio ν on pH:

$$A = K\left(\frac{\Lambda}{c_s}\right)^{\psi(pH-pI)} \qquad (38)$$

Λ is the concentration of equivalents or binding sites in the resin, K is the equilibrium constant, pI is the isoelectric point, and ψ is an empirical constant.

Figure 21 shows the plate height data and model for BSA. The data for A>10 were not included in the fitting procedure due to the problem of impurities mentioned above. For A<10 the experimental data are very similar at different pH. As for Tyrosine on Poros 50 HQ the parallel diffusion model is compared to the pore diffusion model with an over-all mass transfer coefficient determined at each velocity. The pore diffusion model fails to describe the data when A>1.

Discussion

At present not many data for the intra particle diffusivities of Aprotinin and Tyrosine are available. The results for Tyrosine on Resource 15Q and Q HyperD 20 are compared to data from a few references in Paper 2.

The intra particle diffusion coefficients for Aprotinin can be evaluated to some extend by comparing with data for Lysozyme since the two proteins are of similar size. Nash et al. (1998) determined effective pore diffusion coefficients $D_{pe}=K_d\epsilon_p D_p=0.7\times10^{-6}$ cm^2/s for Lysozyme on Source 15 (same as Resource) which is higher than the value for the smaller molecule Aprotinin, $D_{pe}=0.24\times10^{-6}$ cm^2/s from Paper 2. Weaver and Carta (1996) determined $D_{pe}=0.1\times10^{-6}$ cm^2/s for Lysozyme on Poros 50 HS using a moderated shrinking core model. The value for Aprotinin calculated from Table 2 is 0.3×10^{-6} cm^2/s. No data were found for the pore diffusion coefficients of HyperD since mass transfer in this resin is usually described by solid or homogeneous diffusion. In general the pore diffusion coefficients of this work seem realistic as the ratios of the effective pore diffusivity to the free diffusivity are less than unity.

Weaver and Carta (1996) determined an effective solid diffusion coefficient $D_{qe}=K_d\epsilon_p D_q=0.008\times10^{-6}$ cm^2/s for Lysozyme on S HyperD M (dp=78 μm). From Table 1 of Paper 2 the value for Aprotinin on S HyperD 20 is 0.012×10^{-6} cm^2/s. No data were found for the solid diffusion coefficients of Poros since mass transfer in this resin is usually described by pore diffusion. The solid diffusion coefficient for Aprotinin is significantly larger than the one determined by frontal analysis in chapter 3. However, for the breakthrough experiments the solid resistance was relatively small wherefore a determination of the solid phase mass transfer coefficient is uncertain. The apparent difference in the solid diffusion coefficient of Aprotinin is discussed further in Chapter 6.

An apparent flow rate dependence of the pore diffusion coefficients for *Poros* resins, which results in a flow rate independent plate height, have been reported by several authors

(Rodrigues et al. 1996, Horvarth et al. 1994, and Nash et al. 1998) and is generally referred to as *perfusion*. No apparent flow rate dependence was observed for either Tyrosine or Aprotinin on the present Poros resins in the experimental range v_0=0.1-0.8 cm/s as seen from Figure 20.

Film coefficients

The film mass transfer coefficient was described by the correlation $k_f=\alpha v^{\beta}$. A global value of β=1/3 was chosen by observing the fitting residuals for different values while α was fitted for each set of experimental data. As discussed in Paper 2 the film correlations could not all be determined with confidence since in some cases the film resistance for the main part of a given set of data was not significant. Further the two parameters are coupled i.e. the value of α is influenced by the choice of β. However, when depicting the plate height as function of the velocity at strong retention, where the film resistance dominates, only a minor flow rate dependence indicated by a slightly curved line, see Figure 17, was observed and the velocity exponent β must therefore be small.

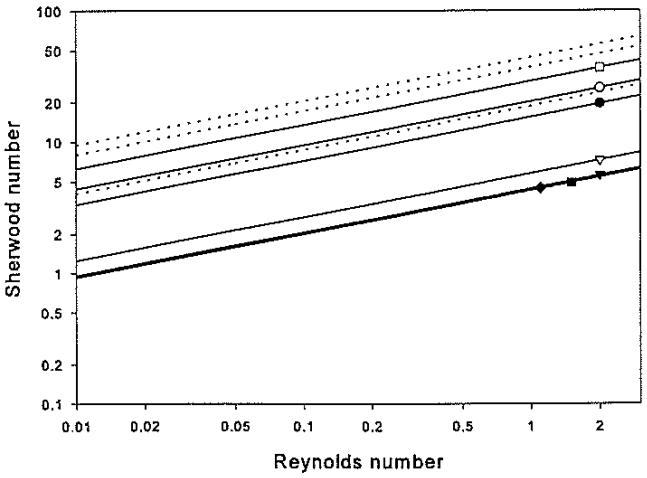

Figure 22: Sherwood numbers for Tyrosine, Aprotinin, and BSA (solid lines). The symbols indicate: Tyrosine (solid) and Aprotinin (open) on Resource 15 (●), HyperD 20 (▼), and Poros 50 (■) and BSA on Source 30Q (◆). The dotted lines are the correlation by Wilson and Geankoplis with Tyrosine, Aprotinin, and BSA in ascending order.

Figure 22 shows the film correlations determined from the data reported in this chapter and in Paper 2. The results are compared to the correlation by Wilson and Geankoplis (1966).

Since the Sherwood number is in principle independent of the resin, except for a possible dependence on the bed porosity, the lines for Tyrosine indicated by the solid symbols (excluding BSA) should be close to identical as should the lines for Aprotinin indicated by the open symbols. For Tyrosine the Sherwood numbers for HyperD and Poros are identical while Sh for Resource is significantly higher. For Aprotinin the Sherwood numbers for Resource and Poros are similar while Sh for HyperD is significantly lower. The ratios between the Sherwood numbers for Aprotinin and Tyrosine are almost identical for Resource and HyperD, whereas the same ratio for the Poros resin is much higher. The Sherwood numbers for Aprotinin on Poros 50 HS are somewhat doubtful due to the high apparent axial dispersion found for this resin.

In general the film correlations are not in agreement with the correlation by Wilson and Geankoplis except for the fixed velocity or Reynolds number exponent. Compared to the correlations presented in Chapter 3 the Reynolds number dependence of the Sherwood number (β) in Figure 22 differs by a factor of three. Further, the Sherwood numbers for Aprotinin on Resource 15S are significantly higher than determined by frontal analysis. In both the frontal analysis and the pulse experiments for Aprotinin on Resource 15S film diffusion control could be achieved, in the latter case at strong retention. The plate height and MTZ data are poorly described when interchanging the two correlations. The discrepancies between the film coefficients determined at linear and non-linear conditions are discussed further in chapter 6.

Composition dependent diffusivities

Since the equilibrium ratio is varied experimentally by changing the counter ion concentration it is relevant to examine whether the observed change in the rate of intra particle mass transfer could be caused by a counter ion concentration dependent pore diffusion coefficient. Thus, the increased diffusivity observed when A increases might originate from a pore diffusion coefficient which increases as the counter ion concentration decreases. In Paper 2 the relative change of the free solution diffusion coefficients for Tyrosine and Aprotinin were estimated by applying the Nernst-Planck equation, equation (7) of Paper 2. Assuming that the relative change in the free diffusivity applies to the pore diffusivity it was found that the change obtained from the Nernst-Planck equation was far less than the observed change in the effective intra particle mass transfer rate.

For the BSA results on Source 30Q reported above the relative change in the free solution diffusion coefficient was determined from the Nernst-Planck equation using the approach described in Paper 2. For each pH the Na^+ concentration for A=10 and the charge determined from the empirical correlation of equation (38) was used together with the feed concentration of BSA. These conditions provide the maximum effect of the Nernst-Planck equation. The relative change in the diffusivity was between 1.05 (pH 9) and 1.8 (pH 7). Assuming a similar behaviour the effective diffusion coefficient for intra particle mass transfer should

thus increase by no more than a factor of two when going from A=0 to A=10. The values are most likely overestimated since the feed concentration is much higher than the average concentration of BSA in the column. From the parameters of Table 2 the effective diffusion coefficient for intra particle mass transfer, D_p+AD_q, increases by approximately a factor of five from A=0 to A=10. The Nernst-Planck equation thus underestimates the change in the effective diffusivity and predicts different values for each pH. The observed plate height for A<10 in Figure 21 suggests that the rate of mass transfer does not depend directly on the counter ion concentration or pH but only on the retention obtained, and this is in correspondence with the present parallel diffusion model.

Apparent over-all mass transfer coefficients

For linear adsorbing conditions an apparent over-all mass transfer coefficient can be determined since the equilibrium ratio at the particle surface is linear. For parallel diffusion the apparent over-all mass transfer coefficient is given by equation (34). Over-all coefficients as a measure of the rate of mass transfer are useful for comparing the efficiency of different resins at fixed conditions and can be used in scale-up. However, an apparent over-all coefficient determined at given adsorbing conditions cannot in general be used for prediction of the mass transfer rate at other conditions as discussed briefly in Chapter 4.

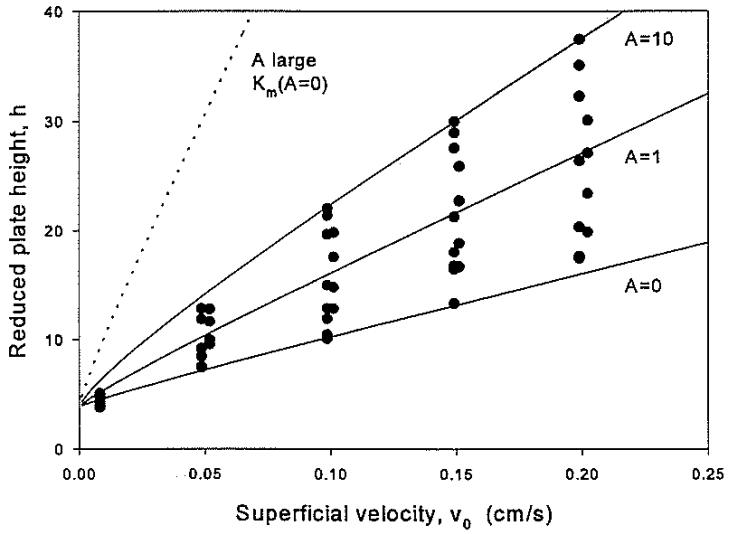

Figure 23: The plate height for Aprotinin on Resource 15S (entire set) and model for A=0, 1, and 10. Dotted line is $h(v_0)$ at strong retention calculated using the apparent over-all mass transfer coefficient for A=0.

In liquid chromatography the van Deemter equation is often presented by the simple

expression h=A+Cv where A and C are constants or the more detailed expression given by equation (33). In Paper 2 it was argued that the simple expression is a better approximation than equation (33) when a constant apparent over-all mass transfer coefficient K_m is assumed. This is supported by the discussion regarding Figures 13 and 14 in Chapter 4. Figure 23 shows the observed plate height for Aprotinin on Resource 15S (same as Figure 16) as function of the velocity including the lines for A=0, 1, and 10 obtained from the parallel diffusion model. The dotted line is the plate height at strong retention obtained from equation (33) with K_m calculated from equation (34) at A=0. The dotted line thus represents the plate height at strong retention as predicted using a constant apparent over-all mass transfer coefficient determined at non-retained conditions. The figure shows that the variation of the plate height when assuming K_m constant is much greater than the observed variation. A better representation of the data is achieved by using the line for A=1 corresponding to approximately k′=1. All data of the present study exhibit a behaviour similar to Figure 23. If an approximate model for the plate height is needed for prediction it is better to use the expression h=A+Cv with C determined at moderate retention, k′=1-2, than to use equation (33) with a constant K_m determined at any conditions.

		Tyrosine	**Aprotinin**	**BSA** [1]
Buffer		none	50 mM NaAc	20 mM BisTris propane
pH		11 (NaOH)	5 (HCl)	6,7,8,9 (HCl)
c_{feed}	(g/L)	0.3	1	5
$D \times 10^6$	(cm^2/s)	10	1.3	0.6
Resin		**Poros 50 HQ**	**Poros 50 HS**	**Source 30Q**
V_{col}	(mL)	1.7	1.7	8.0
d_p	(μm)	50	50	30
ϵ		0.44 [2]	0.44 [2]	0.5
ϵ_p		0.68	0.68	$K_d\epsilon_p$=0.32
v_0	(cm/s)	0.1-0.8	0.1-0.8	0.065, 0.13
c_{NaCl}	(M)	0.03-1	0.27-1.05	0.08-1.0
K_d		1	0.71	$K_d\epsilon_p$=0.32
B	(M^{ν})	0.019	0.18	K=0.15, Λ=0.3 M
ν		1.72	4.96	ψ=2.64, pI=4.8
λ		1.9	15.6	6.3
$\alpha \times 10^3$	(cm/s)	6.8	6.0	0.58
β		1/3	1/3	1/3
$k_p \times 10^3$	(cm/s)	7.4	1.2	0.42
$k_q \times 10^3$	(cm/s)	6.3	0.83	0.19
$D_p \times 10^6$	(cm^2/s)	3.7	0.6	0.13
$D_q \times 10^6$	(cm^2/s)	3.1	0.42	0.06

Table 2: Parameters and conditions for the plate height studies.

[1] Experimental data by Jensen (1999). [2] Bisgaard-Frantzen (1998).

Chapter 6. Non-linear parallel diffusion

When both pore and solid diffusion must be taken into account and the adsorbing conditions are non-linear application of the linear driving force approximation is not straight forward since the model is ambiguous in regards to linearisation of the concentration gradients at the particle surface. An experimental and in depth study of non-linear parallel diffusion is not included in this work and this chapter should therefore be considered a preliminary study investigating parallel diffusion at non-linear adsorbing conditions and the application of the LDF approximation.

Linear driving force models

Using the local equilibrium assumption equation (5) can be written as

$$\frac{\partial s}{\partial t} = \frac{6}{d_p} K_d \epsilon_p \left[D_p + D_q \left(\frac{\partial q(r)}{\partial c_p(r)} \right)_R \right] \left(\frac{\partial c_p(r)}{\partial r} \right)_R \tag{39}$$

and

$$\frac{\partial s}{\partial t} = \frac{6}{d_p} K_d \epsilon_p \left[D_p \left(\frac{\partial c_p(r)}{\partial q(r)} \right)_R + D_q \right] \left(\frac{\partial q(r)}{\partial r} \right)_R \tag{40}$$

Application of the LDF approximation to the two interfacial gradients results in

Model 1: LDF for pore gradient

$$\frac{\partial s}{\partial t} = \frac{6}{d_p} K_d \epsilon_p \left[k_p + k_q \left(\frac{\partial q}{\partial c_p} \right)_R \right] (c_0 - c_p) \tag{41}$$

Model 2: LDF for solid gradient

$$\frac{\partial s}{\partial t} = \frac{6}{d_p} K_d \epsilon_p \left[k_p \left(\frac{\partial c_p}{\partial q} \right)_R + k_q \right] (q_0 - q) \tag{42}$$

Alternatively, The LDF approximation can be applied to both the pore and the solid phase

concentration gradient in equation (5) giving

Model 3: LDF for pore and solid gradient

$$\frac{\partial s}{\partial t} = \frac{6}{d_p} K_d \epsilon_p \left[k_p (c_0 - c_p) + k_q (q_0 - q) \right] \qquad \textbf{(43)}$$

Combined with the flux expression for the external film and neglecting axial dispersion equations (41)-(43) constitutes three possible models, denoted model 1, 2, and 3, for non-linear parallel diffusion using the linear driving force approximation. Constant pattern solutions can be obtained for each model by determining the pore-phase concentration c_p from the mass balance and solving for the interfacial concentration c_0, the latter resulting in a cubic equation for models 1 and 2 when using the Langmuir isotherm.

From the present experimental work it is not possible to evaluate the models directly since the breakthrough data did not exhibit a parallel diffusion behaviour and the three models are identical when the isotherm is linear. However, the validity of the models can be investigated to some extend by considering the observed and the theoretical mass transfer behaviour.

In Chapter 3 and Paper 1 the observed non-linear flux behaviour was described by the solid diffusion model presented in Chapter 2. The model has the ability to change the shape, or the inflection point, of the flux curves as shown in Figure 2 and this reflects the observed flux behaviour especially for the BSA data on Q HyperD 35, see Figure 4 of Paper 1. A model for parallel diffusion must therefore contain this ability, in other words the parallel diffusion model must reduce to the solid diffusion model when pore diffusion is negligible. A theoretical study of model 1 showed that the inflection point x″ as function of the feed concentration in general develops similar to the inflection point for the pore diffusion model given by equation (6). This seems reasonable considering that both models describe intra particle mass transfer by a linear driving force in the pore-phase concentration. The inflection point of the pore diffusion model is identical to that of film diffusion control, equation (22) shown in Figure 4, where the inflection point is always greater than 0.5. Model 1 is thus unable to describe the flux behaviour at conditions where $x'' < 0.5$, that is when solid diffusion predominates.

In model 2 the equilibrium relation at the interface is given by the isotherm as $q_0(c_0)$ and transport from the mobile phase to the particles takes places via this interfacial equilibrium relation. At conditions where no adsorption takes place (high counter ion concentration), $\partial q/\partial r = 0$ and $q = q_0 = 0$, the model predicts that nothing is transported across the interface thus neglecting the mass transfer between the mobile phase and the pores.

From the form of equation (43) it is obvious that model 3 include the pore and the solid diffusion models as limiting cases when $\gamma = k_p c_F / k_q q_F$ goes to infinity and zero respectively. It is therefore concluded that if the linear driving force approximation can be applied to non-

linear parallel diffusion, model 3 given by equation (43), which comprises linearisation of both intra particle gradients, should be used. It is noted that the validity of applying the LDF approximation to both gradients is not obvious.

Reported experimental studies

In general it can be difficult to discriminate between pore and solid diffusion since the two diffusive contributions are additive resulting in an effective intra particle mass transfer rate and neither mass transfer coefficient depends on the velocity. Experimental verification of parallel diffusion therefore requires a significant variation in the applied equilibrium ratio as found in the plate height studies in Chapter 5 and Paper 2.

Koh et al. (1998) studied the breakthrough behaviour of L-phenylalanine on a Duolite C-20 cation-exchange resin. The experimental data where described by pore, solid, and parallel diffusion models using a Fickian diffusion term in the particles and including both external film diffusion and axial dispersion. All three models could describe the observed breakthrough behaviour. However, for an increasing equilibrium ratio in the range 50-450 applied by changing the feed concentration the apparent pore diffusion coefficient increased while the apparent solid diffusion coefficient decreased. The data could be described satisfactory by the parallel diffusion model with constant diffusivities assuming local equilibrium and using $(\partial c_p/\partial r)_R$ as the interfacial gradient corresponding to equation (39). The results can be explained qualitatively by comparing the scaled diffusivities for the three models, $D_{pa}c_F=D_{qa}q_F=D_pc_F+D_qq_F$, where a indicates the apparent diffusivities for the pore and solid diffusion models. If c_F is doubled the scaled diffusivity for parallel diffusion increases by a factor 1-2 depending on the relative values of the two coefficients. In order to match this diffusivity the apparent pore diffusion coefficient must decrease while the apparent solid diffusion coefficient must increase. It was concluded that mass transfer was dominated by solid phase diffusion with a significant contribution from pore diffusion.

Yoshida et al. (1994) studied the batch and shallow bed uptake of BSA on the highly porous anion exchangers chitopearl 2503 and 2507. The experimental data could be correlated by the homogeneous diffusion model where the concentration gradient in the particles is expressed in the total particle concentration s, i.e. $\partial s/\partial t \propto (\partial s/\partial r)_R$. For strong adsorption the homogeneous and the solid diffusion models are almost identical since $s \approx K_d\epsilon_p q$. The contribution from the external film diffusion could be neglected. The intra particle gradient was described by Fickian diffusion using a mean effective diffusivity $D_e=D_q+D_pc_F/q_F$, where c_F/q_F is the mean value of $\partial c_p/\partial q$. The model is thus similar to equation (40). Both pore and solid diffusion were significant in the two resins.

Lewus et al. (1998) studied the batch and shallow bed uptake and desorption of Lysozyme on S HyperD-M at various salt concentrations (NaCl). The data were correlated using the homogeneous diffusion model with Fickian diffusion described above and a constant homgeneous diffusivity D_s. External film diffusion was included . The equilibrium data for

each salt concentration where correlated using the Langmuir isotherm q=ac/(1+bc). No adsorption was detected for $c_s \geq 300$ mM. The main results are summarised in Table 3. For the experimental data measured under strong adsorbing conditions mass transfer was dominated by homogeneous diffusion ($D_s=0.0075\times10^{-6}$ cm^2/s) with some contribution from film diffusion. For the desorption studies performed at high salt concentrations the homogeneous diffusion coefficient D_s was increased ($D_s=0.020\times10^{-6}$ cm^2/s) in order to match the observed desorption curves. It was concluded that "The electrostatic interaction responsible for solute binding apparently increases diffusional hindrance within the gel". From the present discussion concerning apparent solid and pore diffusivities in relation to parallel diffusion, the increase in the homogeneous diffusivity reported by Lewus et al. might be caused by a significant contribution from pore diffusion at weak adsorbing conditions. For this reason the model results by Lewus are investigated in the following.

	Lysozyme on S Hyper M		
Buffer	20 mM HPO_4Na_2, pH=6.5 (HCl)		
d_p (μm)	78		
ϵ_p	0.65		
$k_f\times10^3$ (cm/s)	2.9 for v_0=0.94 cm/s		
c_{NaCl} (mM)	100	150	300, 500 ,1000
$a=s_{max}b$ (g/L)	823	199	0
b (L/g)	3.77	0.7	0
$D_s\times10^6$ (cm^2/s)	0.0075	0.0075	0.020
	LDF approximation		
$k_s\times10^3$ (cm/s) [1]	0.0096	0.0096	0.026
$k_p\times10^3$ (cm/s)	0.026	0.026	0.026
$k_q\times10^3$ (cm/s)	0.0096	0.0096	0.0096

Table 3: Parameters and conditions from Lewus et al. (1998) and the parameters used in the present study. [1] $k_s=10D_s/d_p$.

Application of the LDF model to the results by Lewus et al. (1998)

For a shallow bed the axial position is not included in the model and the concentrations are therefore constant throughout the column. Lewus et al. used a Fickian diffusion term in the particles and integrated the concentration gradient $\partial s/\partial r$ in order to get the flux at the particle surface $(\partial s/\partial r)_R$. Applying the LDF approximation, $k_s(s_0-s)$, for homogeneous diffusion the calculated uptake and desorption curves are in agreement with the results of Lewus et al. and can be used to represent their model curves. For parallel diffusion, model 3 given by equation (43) was applied. The homogeneous and parallel diffusion models are related by

$$\frac{\partial s}{\partial t} = \frac{6}{d_p} k_s (s_0 - s) = \frac{6}{d_p} K_d \epsilon_p \left[k_p (c_0 - c_p) + k_q (q_0 - q) \right] \qquad \textbf{(44)}$$

For strong adsorption $k_q q_F >> k_p c_F$ ($\gamma \approx 0$) and the two models are identical setting $k_s = k_q$. For weak or no adsorption $\gamma \approx \infty$ and the models are identical when $k_s = k_p$. The two diffusivities determined by Lewus at strong and weak adsorbing conditions can therefore be used as approximate solid and pore diffusivities. The corresponding mass transfer coefficients are given in Table 3. Using the LDF approximation the model has time as the only independent variable.

Figure 24 shows the model desorption curves reported by Lewus et al. calculated from the homogeneous model (LDF approximation) and the curves calculated from the parallel diffusion model, both including external film diffusion. For each model the lines for $c_s \geq 300$ mM are identical since a=b=0. The calculations were performed using the following approach:

1) Determine c_p and q for the parallel diffusion model (local equilibrium from desorption isotherm) from the particle mass balance $s = \epsilon_p (c_p + q)$.
2) Determine c_0 for the two models, calculate the fluxes from $ds/dt = (6/d_p) k_f (c - c_0)$ with c=0 initially.
3) Calculate $s_{i+1} = s_i + (ds/dt)\Delta t$ (Δt=1 sec.), repeat from 1.

Comparing with the paper by Lewus et al. their experimental data are well represented by the homogeneous diffusion model (LDF approximation) when $k_s = 0.0096 \times 10^{-3}$ cm/s for $c_s = 100$ and 150 mM and $k_s = 0.026 \times 10^{-3}$ cm/s for $c_s \geq 300$ mM corresponding to the diffusivities reported by Lewus, see Table 3. These "pseudo experimental" curves given by the homogeneous diffusion model are matched satisfactory by the parallel diffusion model using the fixed mass transfer coefficients $k_q = 0.0096 \times 10^{-3}$ cm/s and $k_p = 0.026 \times 10^{-3}$ cm/s. The increase of the apparent homogeneous diffusion coefficient might thus be explained by the existence of parallel diffusion. Unfortunately the applied salt concentrations divide the data into a solid diffusion controlled region ($c_s \leq 150$ mM) and a pore diffusion controlled region ($c_s \geq 300$ mM) while no data were measured at conditions where both pore and solid diffusion are significant. Both models can therefore describe the data using two parameters for the intra particle mass transfer although the change in the homogeneous diffusivity is somewhat empirical. If parallel diffusion exists, the parallel diffusion model parameters would not have to be modified when applying salt concentrations in the region 150-300 mM while the apparent homogeneous diffusivity necessary to describe the data would vary in the region D_s= 0.0075 to 0.020×10^{-6} cm^2/s.

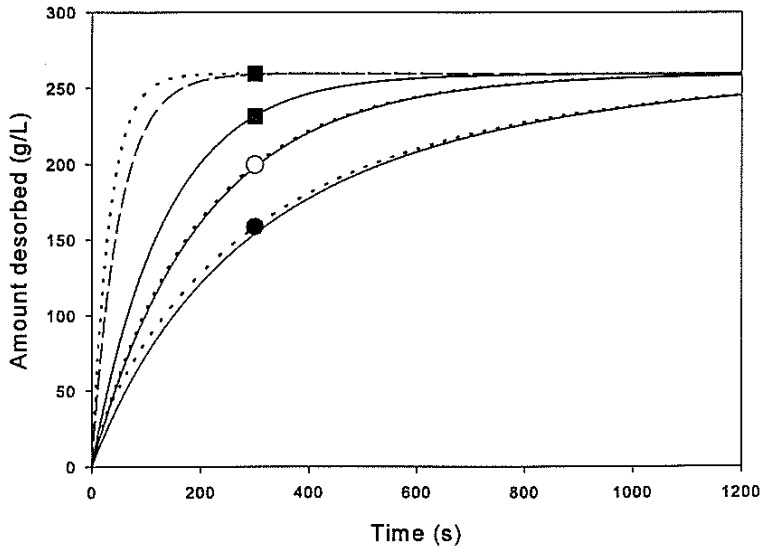

Figure 24: Desorption curves for Lysozyme on S HypeD-M obtained from the results reported by Lewus et al. (1998). Symbols indicate NaCl concentrations of 100 (●), 150 (○), and 300, 500, 1000 mM (■). The shallow bed was equilibrated at c_F=1 g/L with no salt added, prior to wash and desorption and the superficial velocity was 0.94 cm/s. The solid lines are calculated using the homogeneous diffusion model with $k_s=0.0096\times10^{-6}$ cm/s. The dashed line is calculated using the homogeneous diffusion model with $k_s=0.026\times10^{-6}$ cm/s ($c_s\geq300$mM only). The dotted lines are calculated using the parallel diffusion model with $k_q=0.0096\times10^{-6}$ cm/s and $k_p=0.026\times10^{-6}$ cm/s.

Chapter 7. General discussion

The linear driving force (LDF) approximation is perhaps the most simple concept for describing mass transfer while maintaining a reasonable physical foundation. More complex models can include Fickian diffusion, a radial velocity distribution in the column, and a detailed description of the particles comprising pore connectivity and pore size distributions. On the thermodynamic level nonidealities can be introduced in the form of activity coefficients and electrostatic interactions. It is outside the present framework to discuss the validity of the LDF approximation in regards to models with a higher level of detail.
In this concluding chapter a coherent description of the development of the present study is presented and the assumptions made in frontal analysis are investigated within the model frame of the LDF approximation.

Evolvement of the Rationale

The theory and experimental results of this work have been presented in a straight forward manner based on the parallel diffusion model while a comparison with related models is given primarily in Papers 1 and 2. This approach was chosen in order to focus on the results obtained rather than the models disregarded. Understanding the mass transfer behaviour has of course been an evolving process. To provide a deeper perspective the evolvement of the rationale is outlined in the following.
The starting point consisted primarily of the pore diffusion model and the solid diffusion model, two popular models widely used in the literature. Initially it seemed that both models are valid merely by choice although the general understanding is that the pore diffusion model is valid for porous resins while the solid diffusion model is valid for gel type resins. In some papers the external film resistance is included and found significant while in most cases it is neglected often based on a priori estimations from existing correlations. The initial literature study raised the questions: How can experimental studies comprising single solute mass transfer behaviour result in such different conclusions? Does any model apply as a result of some fitting exercise? Investigating the fundamental assumptions and the models it became clear that the most important aspect is the relation between the rate of mass transfer and the equilibrium conditions and that the discrepancies between the results reported to some extend could be explained by the different experimental conditions applied, i.e. strong or weak adsorption. If the equilibrium ratio is constant basically any model applies especially in the linear range of the isotherm as found in the numerous plate height studies performed at non-retained conditions. In order to differentiate between the various models the focus has therefore been on the relation between the equilibrium conditions and the rate of mass transfer.
From the frontal analysis study of BSA in Paper 1 it was found that the mass transfer in both porous and gel type resins was well described using the solid diffusion model including an external film resistance while the pore diffusion model was not able to describe the data.

Since the breakthrough experiments were performed under strong adsorbing conditions the rate of mass transfer in the particles was relatively high due to the large driving force and the mass transfer resistance was therefore in general dominated by the velocity dependent external film resistance.

Plate height data for BSA determined at non-retained conditions exhibited a linear dependence on the velocity corresponding to a rate of mass transfer independent of the velocity, apparently in contrast to the strongly velocity dependent rate found in the breakthrough study. But since the driving force in the particles was strongly reduced the resistance in the particles had become the rate limiting step and the external resistance was therefore negligible. The plate height was however greatly over estimated when replacing the over-all mass transfer coefficient K_m in the van Deemter equation, equation (33), with the solid phase mass transfer coefficient determined by frontal analysis. Apparently, the mass transfer coefficient determined at strong adsorbing conditions did not apply to the non-retained conditions. A fundamental question was what happens to the rate of intra particle diffusion when nothing is adsorbed? It seems reasonable that at non-adsorbing conditions the particle can be considered an inert porous shell and that mass transfer therefore occurs by pore diffusion.

Inspired by the papers of Yoshida (1994) and Rice and Do (1987) a parallel diffusion mechanism was incorporated into the van Deemter equation resulting in the expression for the over-all mass transfer coefficient given by equation (34). Three different forms of the van Deemter equation or rather the over-all mass transfer coefficient now existed comprising pore, solid, and parallel diffusion, each with a distinguished shape for the plate height as function of the equilibrium ratio as seen from Figure 1 of Paper 2. The theoretical discovery of a maximum in the plate height as function of the equilibrium ratio for parallel diffusion was supported by sparse data for BSA but not substantiated by any reported plate height studies. The study of linear mass transfer, which had initially been somewhat neglected since apparently any model applied, was suddenly the key to distinguishing between the three models since the difference between them is found in the shape of the curves for the plate height as function of the equilibrium ratio and is not an issue of merely improving the residuals between the model and the data. The results of Paper 2 show that the pore and solid diffusion models cannot describe the plate height data while a satisfactory description is obtained when applying the parallel diffusion model. The topic of the van Deemter equation has gone full circle in a somewhat ironic manner since due to the moderate variation of the plate height with the equilibrium ratio the simple and often used expression H=A+Cv, where A and C are constants, is in general an acceptable approximation.

Assumptions in frontal analysis

The breakthrough and the plate height data of this work were described satisfactory by the parallel diffusion model neglecting axial dispersion and pore diffusion in the former case.

The model is able to interpolate between the experimental data and for the isolated cases of non-linear and linear mass transfer the parameters determined for different solutes and resins seem consistent i.e. the intra particle diffusion coefficients decrease for larger solutes and the flow rate dependence is independent of the solute. However, the mass transfer parameters for Aprotinin measured under linear and non-linear conditions are not in agreement and the exponent in the flow rate dependence of the film coefficients is approximately 1 for the breakthrough data compared to 1/3 for the plate height data. In order to investigate possible explanations for these discrepancies the assumptions made in frontal analysis are examined in the following.

Experimental

The procedure for measuring the breakthrough curves is presented in Paper 1. The experimental curves were corrected for the dead volume but not the band broadening originating outside the column in the tubing and valves. However, since the breakthrough profiles used for the constant pattern validation obtained from a step and a linear gradient input are identical the band broadening originating before the column has no influence on the results. Further, the mass transfer zone of profiles determined at non-adsorbing conditions are small compared to the profiles determined at strong adsorption and the extra column band broadening must therefore be relatively small . Finally, the experimental data for BSA on Resource 15Q are in agreement with the results by Sajonz et al. (1996), which makes it most unlikely that major systematic experimental errors have been made.

Pore concentration and pore diffusion

For the strong adsorbing conditions it was assumed that $q>>c_p$ and for the isotherms determined this assumption is valid. The smallest equilibrium ratio q_F/c_F was approximately 120 calculated for c_F=2 g/L from the isotherm of the Poros HQ/M column in Paper 1 assuming $K_d\epsilon_p$=0.5.

The influence of pore diffusion is somewhat difficult to evaluate for the present results since the breakthrough profiles were in general dominated by film diffusion. For the cases where the pore mass transfer coefficient has been determined the ratio of the scaled solid and pore resistances $\gamma=k_pc_F/k_qq_F$, calculated for a small and a large feed concentration, is presented in Table 4. The influence of pore diffusion is negligible when using the solid phase mass transfer coefficient obtained from plate height data, while a minor influence is found when using the coefficient determined by frontal analysis. The difference in the solid phase mass transfer coefficients determined by the two methods is discussed below. In conclusion the pore phase mass transfer coefficients are larger than the solid phase coefficients, but due to the strong adsorption the driving force in the solid phase is much larger than in the pores and the influence of pore diffusion is therefore small.

Resin	Resource 15S	Resource 15S	Resource 15Q	Source 30Q	Source 30Q
Solute	Aprotinin	Aprotinin	BSA	BSA	BSA
$k_p \times 10^3$ (cm/s)	3.2 (P2)	3.2 (P2)	1.7[3]	0.42 (T2)	0.42 (T2)
$k_q \times 10^3$ (cm/s)	0.033 (**T1**)	0.58 (**P2**)	0.036 (P1)	0.051 (**P1**)	0.19 (**T2**)
$q_{max}=s_{max}/K_d\epsilon_p$ (g/L)	235 (T1)[1]	235 (T1)[1]	228 (P1)[2]	206 (P1)[2]	206 (P1)[2]
b (L/g)	53 (T1)	53 (T1)	20 (P1)	20 (P1)	20 (P1)
γ (c_F=0.1)	0.05	0.003	0.03	0.006	0.002
γ (c_F=2)	0.8	0.05	0.4	0.08	0.02

Table 4: The significance of pore diffusion in frontal analysis. T and P signifies *Table* and *Paper*.
[1] $K_d\epsilon_p$ from Paper 2. [2] $K_d\epsilon_p$ from Table 2 (Source 30Q). [3] Approximate, determined at non-retained conditions.

Axial dispersion

To investigate the influence of axial dispersion the solution of the solid diffusion model for constant pattern presented in Chapter 2 obtained when neglecting axial dispersion is compared to solutions including axial dispersion. The derivation and comparison of the various solutions are outlined in the following.

When axial dispersion is neglected the mass balance for constant pattern relates the reduced mobile and solid phase concentrations by x=y . When including axial dispersion the mass balance in dimensionless form becomes

$$\frac{1}{Pe\omega(1-\omega)}\frac{dx}{d\xi} + x = y \tag{45}$$

where ω is the reduced solute velocity

$$\omega = \frac{u_s}{v} = \frac{\epsilon}{\epsilon + (1-\epsilon)\frac{s_F}{c_F}} \tag{46}$$

Differentiating equation (45)

$$\frac{1}{Pe\,\omega(1-\omega)}\frac{d^2x}{d\xi^2} + \frac{dx}{d\xi} = \frac{dy}{d\xi} \tag{47}$$

which combined with the LDF expression for the particle

$$\frac{dy}{d\xi} = St_q \epsilon_p K_d (y_0 - y) \tag{48}$$

and equation (45) results in

$$\frac{1}{St_q Pe}\frac{d^2x}{d\xi^2} + \left(\frac{1}{Pe} + \frac{\omega(1-\omega)}{St_q}\right)\frac{dx}{d\xi} = \omega(1-\omega)(y_0 - x) \tag{49}$$

An approximate model is obtained when the first term on the left hand side is negligible, an assumption introduced by Rhee and Amundson (1972) valid when St_q and Pe are large. The coupled effect of solid phase mass transfer and axial dispersion is thus neglected and the two contributions are additive. The assumption corresponds to neglecting the first term in equation (47) thereby obtaining the relation

$$\frac{dx}{d\xi} = \frac{dy}{d\xi} \tag{50}$$

for the mass balance at constant pattern conditions.
Neglecting the second order term in equation (49) and combining with the external film mass transfer gives

$$(\theta + \delta)(x - x_0) = (y_0 - x) \tag{51}$$

where θ indicates the significance of axial dispersion

$$\theta = \frac{c_F St_f}{s_F Pe\,\omega(1-\omega)} \approx \frac{(1-\epsilon)St_f}{\epsilon Pe} \tag{52}$$

Equation (51) resembles the relation obtained when neglecting axial dispersion given by equation (12) in Chapter 2 (inserting y=x) and the solutions of the present approximate model is found by replacing δ with $\delta+\theta$ and y with x in equations (15) and (16).
The approximate model and the model neglecting axial dispersion describe the same flux or breakthrough curve when St_f is identical and

$$\frac{1}{St_q} = \frac{1}{St_{qa}} + \frac{1}{Pe\,\omega(1-\omega)} \approx \frac{1}{St_{qa}} + \frac{(1-\epsilon)s_F}{\epsilon c_F Pe} \tag{53}$$

where *a* indicates the model including axial dispersion. If axial dispersion is significant the

solid phase mass transfer coefficient will therefore be underestimated when applying the model neglecting axial dispersion. The two approximative terms in equations (52) and (53) are valid when the reduced velocity ω is small corresponding to $(1-\epsilon)s_F/\epsilon c_F >> 1$ as is the case for strong adsorption.

The influence of axial dispersion on the parameters determined by frontal analysis was evaluated by calculating θ using the approximate expression in equation (52). For Aprotinin on Resource 15S the Stanton number for the external film is approximately 50 while the Peclet number

$$Pe = \frac{Lv}{D_a} = \frac{Lv}{\lambda v d_p} = \frac{L}{\lambda d_p} \qquad (54)$$

is 1053 using $\lambda=1.9$ determined from the plate height data in Paper 2. From these numbers $\theta \approx 0.05$ and the influence of axial dispersion is seemingly small.

The full model including the second order term in equation (49) can be evaluated by calculating y and $dy/d\xi$ from equations (45) and (47) inserting $dx/d\xi$ and $d^2x/d\xi^2$ obtained from the empirical transient functions used for smoothing the breakthrough curves as discussed in Chapter 3. Using $\lambda=1.9$ from Paper 2 no significant difference was found between dy/dt and dx/dt for Aprotinin on Resource 15S and the second order term is therefore negligible. The flux curves for Aprotinin on Resource 15S where fitted to the model including axial dispersion using both $\lambda=1.9$ and $\lambda=0$ in order to compare the flux fit with and without axial dispersion to the results obtained from the width of the mass transfer zone. The parameters were almost identical to the ones presented in Table 1 with the most significant difference found in $k_q=0.035\times10^{-3}$ cm/s for $\lambda=1.9$ compared to 0.033×10^{-3} cm/s from Table 1. The minor increase in k_q when including axial dispersion is consistent with equation (53). In conclusion axial dispersion was negligible for Aprotinin on Resource 15S and from estimated values of θ axial dispersion is also negligible for the remaining frontal analysis data. Thus, the large difference between the solid phase mass transfer coefficients determined from the frontal analysis and the plate height data cannot be explained by a significant contribution from axial dispersion.

Velocity dependence of the external film coefficient

The external film coefficient has been correlated successfully with the interstitial velocity by the expression $k_f=\alpha v^\beta$ in both the breakthrough and the plate height studies and no apparent lower limit of the film coefficient or Sherwood number was found for $v\rightarrow0$ ($Re\rightarrow0$) as briefly discussed in Paper 1. The velocity dependence of the film coefficient is an issue not easily addressed as confirmed by the numerous existing correlations including different values for β. The approach taken in this work has been to determine the velocity dependence from the experimental results in order to avoid biasing of the other parameters caused by the choice

between existing correlations. The results of the frontal analysis experiments contain the most explicit information on film diffusion since mass transfer was dominated by the external resistance. The data showed that the correlations most commonly used in chromatography did not apply and that if the mobile phase linear driving force approximation is valid a velocity exponent β of approximately 1 must be included. In the plate height study the influence of the film resistance was in general minor except at strong retention. The data showed that the velocity dependence of the film coefficient was not pronounced and in the model a value of $\beta=1/3$ was sufficient. However, the information regarding the film resistance obtained from the plate height study is somewhat implicit since the film coefficient appear in context with several other parameters. In fact the plate height data for Aprotinin on the Resource 15S resin are well described neglecting the film resistance and introducing a velocity dependence in the form $D_a \propto v^{4/3}$ for the axial dispersion coefficient as found in the Knox equation, $H=Av^{1/3}+Cv$, see Guiochon et al. (1994), while this is not the case for the breakthrough data.

The film coefficients determined in the frontal analysis study are thus the most rigorous which is further substantiated by the close to identical velocity exponents determined independently for the three solutes Aprotinin, Lysozyme, and BSA , see Figure 12. However, the film correlations determined at non-linear adsorbing conditions in the frontal analysis study do not apply to the plate height data determined at linear conditions. A discussion regarding the values and the velocity dependence of the film coefficient in respect to existing correlations and pakced bed fluid dynamics is of minor interest as long as the discrepancies between the breakthrough and plate height data are not resolved.

Conclusions

The results of the breakthrough and plate height studies are in agreement with the parallel diffusion model. The experimental observations correspond to the resistance scheme presented in Figure 1. A general model comprising parallel diffusion using the LDF approximation can be used for describing mass transfer in both porous and gel-type resins. The plate height data for Tyrosine and Aprotinin show that when the conditions are varied from weak to strong adsorption the pore and the solid diffusion model do not apply.

In the breakthrough experiments the mass transfer resistance consisted primarily of the external film resistance. The external film coefficient has an unexpected strong velocity dependence contrary to the dependence found in commonly used correlations.

The results for Aprotinin show a discrepancy between the parameters determined at linear and non-linear conditions and in general the strong velocity dependence found in the correlations of the external film coefficient determined by frontal analysis do not apply to the plate height data. At present this problem cannot be resolved and it seems reasonable that further experimental studies should be performed before considering a theoretical explanation.

The experimental studies included three types of resins comprising a porous media (Source and Resource), a gel-type media (HyperD) and a macro porous media (Poros). In general the intra particle diffusion coefficients for the three resins are found in the order Poros>Source>HyperD, while the order of the adsorption capacities is the reverse.
This study have showed that the influence of the equilibrium conditions on the rate of mass transfer is essential for understanding the mass transfer behaviour of a chromatographic resin. Depending on the adsorbing conditions the rate of mass transfer is governed by different mechanisms. In the optimisation of a preparative separation step different approaches should thus be taken depending on the applied loading and eluting conditions.

Future work

The aim of the present work has been to investigate mass transfer in a broad sense and the experimental work have therefore included several resins and solutes rather than focusing on the detailed description of a single system. A continuation of the present work should comprise closing the gap between the linear and non-linear mass transfer behaviour and challenge the validity of the parallel diffusion model in its present form.
Experimentally a shallow bed contactor seems an excellent choice for the study of mass transfer since the conditions can be varied from weak to strong adsorption using the same procedure and model solution. The primary question is why the apparent velocity dependence of the film coefficient changes when the experimental conditions are changed from weak to strong adsorption?
An important issue not treated in the present work is the fundamental understanding of solid phase diffusion. While pore diffusion is a straight forward phenomena it is not easy to comprehend the nature of solid phase diffusion, which in the present and many other cases is merely defined by choosing the solid phase concentration as the driving force. This issue is closely related to the validity of the LDF approximation or rather the use of concentrations as the driving forces. The present model does not distinguish between ion-exchange and hydrophobic interaction (HIC) or reversed phase chromatography (RPC). In order to investigate the nature and validity of solid phase diffusion, experiments on HIC or RPC resins would therefore be interesting for comparison since the hydrophobic forces are of a different nature and much weaker than the electrostatic interactions of ion exchange.

References

Bisgaard-Frantzen, H.; *Characterization of column packings for chromatography of proteins. Ph.D. thesise, Technical University of Denmark*, **1998**.

Carberry, J. J., *A boundary-Layer Model of Fluid-Particle Mass Transfer in Fixed Beds*. A.I.Ch.E. J., **1960**, 6, 460

Coffman, J.L. *Protein Diffusion in Chromatographic Media*, Ph.D. thesis, University of Winsconsin-Madison, **1994**

van **Deemter**, J.J.; Zuiderweg, F.J.; Klinkenberg, A. *Longitudinal diffusion and resistance to mass transfer as causes of nonideality in chromatography.* Chem. Eng. Sci. **1956**, 5, 271.

Do, D.D.; Rice, R.G. *On the relative importance of pore and surface diffusion in non-equilibrium adsorption rate processes*. Chem. Eng. Sci., **1987**, 42, 2269-2284

Fernandez, M. A.; Laughinghouse, W. S.; Carta, G. *Characterization of protein adsorption by composite silica-polyacrylamid gel anion exchangers II. Mass transfer in packed columns and predictability of breakthrough behaviour*. J.Chromatogr. A, **1996**, 746, 185

Glueckauff, E. Trans Faraday soc., **1955**, 51, 540

Guiochon, G.; Sadroddin, G.S.; Katti, A.M. *Fundamentals of Preparative and Nonlinear Chromatography*, Academinc Press, London, **1994**

Horvarth, J.; Boschetti,E.; Guerrier, L.; Cooke, N. *High-performance protein separations with novel strong ion exchangers*. J. Chromatogr. A, **1994**, 679, 11-22

Jensen, M.B. *Ionbytningskromatografi af valleproetiner* (in Danish), preliminary master thesis, Technical University of Denmark, **1999**

Koh, J.-H.; Wankatt, P.C.; Wang, N.-H. *Pore and Surface Diffusion and Bulk-phase Mass Transfer in Pakced and Fluidized Beds*. Ind. Eng. Chem. Res., **1998**, 37, 228-239

Lewus, R.K.; Altan, F.H.; Carta, G. *Protein Adsorption and Desorption on Gel-Filled Rigid Particles for Ion Exchange*. Ind. Eng. Chem. Res., **1998**, 37, 1079-1087

Nash, D.C. and Chase, H.A. *Comparison of diffusion and diffusion-convection matrices for use in ion-exchange separation processes.* J.Chromatogr.A, **1998**, 807, 185.

Perry, R.H. and Green, D.W. *Perrys Chemical Engineers' Handbook*, 7th ed., ch. 16, McGraw-Hill, New York, **1997**.

Rhee, H.-K. and Amundson, N.R. *A study of the shock layer in Nonequilibrium Exchange Systems*. Chem. Eng. Sci., **1972**, 27, 199

Rodrigues, A.E.; Chenou, C.; de la Vega, M.R. *Protein separation by liquid chromatography using permeable POROS Q/M particles*. Chem. Eng. Jou., **1996**, 61, 191-201

Sajonz, P.; Guan-Sajonz, H.; Zhong, G.; Guiochon, G. *Application of the Shock Layer Theory to the Determination of the Mass Transfer Rate Coefficient and Its Concentration*

Dependence for Proteins on Anion Exchange Columns. Biotechnol. Progr., **1997**, 13, 170

Wankat, P.C., *Rate Controlled Separations*, chapter 8, Chapman & Hall, Great Britain, **1994**

Weaver, Jr.,L.E. and Carta, G. *Protein adsorption on Cation Exchangers: Comparison of Macorporous and Gel-Composite Media.* Biotechnol. Prog., **1996**, 12, 342-355

Wilson, E.J. and Geankoplis, C.J. *titel* Ind. Eng. Chem. Fundamen. **1966**, 5, 9.

Yoshida, H.; Kataoka, T.; Ruthven, D. M. *Analytical Solution of the Breakthrough Curve for Rectangular Isotherm Systems*. Chem. Eng. Sci. **1984**, 39 (10), 1489

Yoshida, H.; Yoshikawa, M.; Kataoka, T. *Parallel Transport of BSA by surface and Pore Diffusion in Strongly Basic Chitosan*. A.I.Ch.E. J, **1994**, 40 (12), 2034

Paper 1

Application of the two-film theory

to the determination of mass transfer coefficients

for bovine serum albumin on anion-exchange columns.

Ernst Hansen and Jørgen Mollerup*

Engineering Research Centre IVC-SEP, Department of Chemical Engineering

The Technical University of Denmark, DTU

Building 229, 2800 Lyngby, Denmark

Fax: +45 4588 2258, phone: +45 4525 2866, e-mail: jm@kt.dtu.dk

NB: In Paper 1 the symbol q refers to the particle concentration corresponding to $s=K_d\epsilon_p q$ in Chapters 1-7, and the solid phase mass transfer coefficient is denoted k_s.

ELSEVIER

Journal of Chromatography A, 827 (1998) 259–267

JOURNAL OF CHROMATOGRAPHY A

Application of the two-film theory to the determination of mass transfer coefficients for bovine serum albumin on anion-exchange columns

Ernst Hansen, Jørgen Mollerup*

Engineering Research Centre IVC-SEP, Department of Chemical Engineering, Technical University of Denmark, DTU. Building 229, 2800 Lyngby, Denmark

Abstract

The paper describes a method of simultaneous determination of the external and the solid-phase mass-transfer coefficients from frontal analysis data. The protein flux to the solid particles is determined from the slope of the breakthrough curve and the mass-transfer coefficients are determined by fitting the two-film model to the experimentally determined flux. The two-film model is compared with two apparent overall driving force models: the apparent overall mobile phase driving force model and the apparent overall solid-phase driving force model. The experiments show that the apparent overall driving force models fail to describe the flux correctly and this is substantiated by the theory. Results obtained with bovine serum albumin on the anion-exchange media Q HyperD, Source, and Poros show that the external film resistance is significant for Reynolds numbers less than one. The experimental Sherwood numbers are lower than expected and their dependence on the Reynolds number are much higher than expected.

Keywords: Mass transfer; Adsorption isotherms; Albumin

1. Introduction

For large molecules such as proteins the dispersion in an ion-exchange chromatographic column is caused mainly by the mass-transfer resistance. The resistance can be divided into an external film resistance covering the transfer from the mobile phase to the particle surface and a particle resistance covering the transfer from the interphase to the adsorbing phase. The particle resistance includes either pore diffusion, solid (surface) diffusion or both (parallel diffusion). The mass transfer can in most cases be described by the linear driving force approximation. Although a more correct description for the solid-phase mass transfer is obtained using a diffusion term, the linear driving force approximation is adequate in most cases. For solid diffusion Yoshida et al. [1] showed that the approximation is satisfactory when the scaled mass-transfer resistance ratio (solid over external) is less than 5.

A simple approach is the use of an apparent overall driving force model in which the mass flux is calculable as an overall linear driving force multiplied by an overall mass-transfer coefficient. This approach is, however, only applicable when the isotherm is linear or when pore diffusion controls. The apparent overall driving force model is often thought of as a one parameter model. However, the overall mass-transfer coefficient is a lumped parameter comprising the velocity dependent external film resistance, the solid-phase resistance, and in the case

*Corresponding author. Tel.: +45 4525 2866; fax: +45 4588 2258; e-mail: jm@kt.dtu.dk

0021-9673/98/$ – see front matter
PII: S0021-9673(98)00791-2

of solid diffusion, the equilibrium ratio which depends on the salt concentration and the pH in the mobile phase. The resistances are only additive if the equilibrium ratio is independent of the solute concentration, as it is for linear isotherms.

When the isotherm is non-linear and solid diffusion dominates over pore diffusion an overall mass-transfer coefficient is of cause still calculable. Unfortunately, owing to the non-linear isotherm, it becomes a function of the interfacial and the bulk compositions of the solute, therefore it is no longer convenient to use the concept of overall mass-transfer coefficients [2]. In the case of non-linear mass-transfer, the flux equation must be solved simultaneously with the algebraic expression for the equilibrium relation to determine the interfacial composition [3]. The model parameters are, a velocity dependent external film resistance, a constant solid-phase resistance and the isotherm. This subject will be addressed in the paper.

To model parallel diffusion in the solid particle requires a knowledge of the diffusion coefficients in the pore phase and in the solid-phase as well. It has been investigated by Yoshida et al. [4] in cases where the external film resistance can be neglected. We have investigated this model but our data do not permit to discriminate between his approach and our approach where the particle resistance is modelled by a single resistance.

2. Theory

In this work we use the single porosity model where the particles are considered a single homogenous phase. The flux is described by film models using the linear driving force approximation.

2.1. Apparent overall driving force models

Two distinct apparent overall driving force models for the system are considered, the apparent overall mobile phase driving force model and the apparent overall solid-phase driving force model. The corresponding flux equations are:

Apparent overall mobile phase driving force model

$$\frac{\partial q}{\partial t} = \frac{6}{d_p} \cdot K_c(c - c^*) \tag{1}$$

Apparent overall solid-phase driving force model

$$\frac{\partial q}{\partial t} = \frac{6}{d_p} \cdot K_q(q^* - q) \tag{2}$$

where c^* is a hypothetical mobile phase concentration in equilibrium with q, and q^* is a hypothetical solid-phase concentration in equilibrium with c, K_c and K_q are the respective apparent overall mass-transfer coefficients, and $6/d_p$ is the surface to volume ratio for spherical particles. The apparent overall driving forces are $(c-c^*)$ and (q^*-q), respectively.

2.2. Two-film model

In the two-film theory the linear driving forces are $(c-c_0)$ and (q_0-q) where subscript 0 denotes a concentration at the interface of the two-films at which c_0 and q_0 per definition are in equilibrium, that is

$$\frac{\partial q}{\partial t} = \frac{6}{d_p} \cdot k_f(c - c_0) = \frac{6}{d_p} \cdot k_s(q_0 - q) \tag{3}$$

In this work k_f is a velocity dependent external mass-transfer coefficient and k_s is the solid-phase mass-transfer coefficient. $1/k_f$ and $1/k_s$ are denoted the external and solid-phase resistances.

2.3. Constant pattern solutions

2.3.1. The apparent overall driving force models

The Langmuir isotherm often describes the adsorption of a single protein on an ion-exchange medium quite well, therefore it is used in this work. The hypothetical equilibrium concentrations in the apparent overall driving force models, Eqs. (1) and (2), are calculable as

$$q^* = \frac{q_{max} bc}{1 + bc} \text{ and } c^* = \frac{q}{b(q_{max} - q)} \tag{4}$$

where q_{max} is the maximum capacity.

At constant pattern the mobile and solid-phase concentrations are related by [5]

$$\frac{q}{q_F} = \frac{c}{c_F} \tag{5}$$

where c_F is the feed concentration and q_F the corresponding equilibrium concentration. For constant pattern the flux equations become ordinary differential equations. It is convenient to introduce the dimensionless concentrations $x = c/c_F$ and $y = q/q_F$, therefore the constant pattern relation, Eq. (5), becomes $y = x$. Inserting the Eqs. (4) and (5) in the Eqs. (1) and (2), the flux can be expressed as a function of x

$$\frac{dq}{dt} = q_F \cdot \frac{dx}{dt} = \frac{6}{d_p} \cdot K_c c_F \cdot \frac{\beta x(1-x)}{1+\beta(1-x)} \tag{6}$$

and

$$\frac{dq}{dt} = q_F \cdot \frac{dx}{dt} = \frac{6}{d_p} \cdot K_q q_F \cdot \frac{\beta x(1-x)}{1+\beta x} \tag{7}$$

where $\beta = bc_F$.

2.3.2. Two-film model

Inserting the Langmuir expression and the constant pattern relation in the two-film model, Eq. (3), yields

$$\delta(x - x_0) = \frac{(1+\beta)x_0}{1+\beta x_0} - x \tag{8}$$

where δ is the scaled mass-transfer resistance ratio

$$\delta = \frac{k_f c_F}{k_s q_F} \tag{9}$$

The dimensionless interfacial mobile phase concentration x_0 is obtained by solving Eq. (8), which in the present case can be solved analytically. The flux in the two-film model is expressed as a function of x by solving Eq. (8) for x_0 and inserting in Eq. (3). The solution is

$$\frac{dq}{dt} = q_F \cdot \frac{dx}{dt} = \frac{6}{d_p} \cdot k_f c_F (x - x_0) \tag{10}$$

where

$$x_0 = D(x) + \sqrt{[D(x)]^2 + \frac{x(1+\delta)}{\delta\beta}} \tag{11}$$

with

$$D(x) = \frac{1}{2} \cdot \left(x + \frac{x}{\delta} - \frac{1}{\beta} - \frac{1}{\delta} - \frac{1}{\delta\beta} \right) \tag{12}$$

2.4. The breakthrough curves

The breakthrough curves, $x(t)$, are obtained by integrating the flux expressions. The apparent overall driving force models, the Eqs. (6) and (7), have analytical solutions while the two-film model does not. The main difference between the apparent overall driving force model and the two-film model is that where as the driving force in the apparent overall driving force models depends on the isotherm parameters and feed concentration alone, the driving force in the two-film model depends also on the scaled mass-transfer resistance ratio δ because x_0 depends on δ.

The inflection point on the breakthrough curves corresponds to the maximum of the flux curves. The stationary points of the three models, Eqs. (6), (7), (10) are

The apparent overall mobile phase driving force model

$$x'' = \frac{1+\beta-\sqrt{1+\beta}}{\beta} \tag{13}$$

The apparent overall solid-phase driving force model

$$x'' = \frac{\sqrt{1+\beta}-1}{\beta} \tag{14}$$

The two-film model

$$x'' = \frac{1}{1+\delta} \cdot \left(1 + \frac{(\delta-1)(\sqrt{1+\beta}-1)}{\beta} \right) \tag{15}$$

where x'' is the value of x at the inflection point corresponding to a maximum of the flux. The inflection point in the two-film model depends on the scaled mass-transfer resistance ratio δ and $\beta = bc_F$, whereas it in the apparent overall driving force models depends on β only. When δ in Eq. (15) approaches 0, that is when $\delta < 0.1$, it indicates that the flux is controlled by the external film resistance therefore Eq. (15) reduces to Eq. (13). On the other hand, when δ becomes large, $\delta > 10$, the solid-phase resistance is controlling and Eq. (15) reduces to Eq. (14). The two-film model thus coincide with the

apparent overall driving force models when a single resistance controls.

3. Experimental

3.1. Chemicals

Bovine serum albumin, BSA (A6918) and Bis–Tris buffer (B-9754) were from Sigma (St. Louis, MO, USA) both with a purity of 98% according to the manufacturer. NaCl (1.06404.1) was from Merck (Darmstadt, Germany) and 5 *M* HCl (Lab00440) and 5 *M* NaOH (Lab00334) were from Bie & Berntsen, Denmark. Standard solutions for the pH meter calibration were from Radiometer (Copenhagen, Denmark).

3.2. Equipment

A BioCAD Chromatographic Workstation was from Perseptive Biosystems (Cambridge, MA, USA), Milton Roy Spectronic 3000 spectrophotometer and a pH meter (pHM 92) were from Radiometer and 0.45-μm HV filters were from Millipore. The following prepacked columns were used: Resource 15Q (No. 531030) from Pharmacia Biotech (30×6.4 mm), Poros HQ/M (No. 305) from Perseptive Biosystems (100×4.6 mm) and Q HyperD 20 (lot No. 5155) and Q HyperD 35 (lot No. 5266) from BioSepra (100×4.6 mm). A Source 30Q (lot No. 230 230) from Pharmacia Biotech (100×4.6 mm) was packed at Novo Nordisk.

3.3. Procedures

The buffer solutions were prepared by dissolving 25 m*M* Bis–Tris and titrating with HCl to pH 6. Parent solutions were prepared by adding 3 g BSA/l to the buffer and the desired sample solutions were prepared by mixing parent and buffer solutions. Solutions for the non-binding conditions were prepared by adding 0.5 *M* NaCl to the buffer solution. The pH meter was calibrated with standard solutions at pH 4.01 and 7.00. All solutions were filtered through 0.45-μm filters. The concentration in the feed solutions was determined on the Milton Roy spectrophotometer at 280 nm. The breakthrough curves were detected at 280 and 254 nm.

3.4. Experimental measurements

The column was equilibrated with 20 CVs (column volumes) buffer and 40 ml of sample solution was pumped through the system while bypassing the column. The 40 ml was enough to ensure a plateau in the UV signal and the UV detector was zeroed. The sample solution was then passed through the column and the data collection started. The solution was passed through the column well after the breakthrough until a close to constant signal was reached. The column was then bypassed with 5 ml sample solution. The resulting experimental curve is a UV window which starts at zero, passes through a negative plateau and ends with the breakthrough followed by a near constant plateau and finally a step-up to zero from the second bypass. The procedure of bypassing has two purposes: it ensures a step injection originating close to the column and it provides a signal at the feed concentration to be compared with the plateau reached after the breakthrough and finally with the signal from the second bypass whereby one can estimate a possible shift in the detector response. The column was regenerated with 20 CVs of 1 *M* NaCl solution followed by 20 CVs buffer solution. The volume of buffer used in the equilibration and regeneration was later reduced to 10 CVs with no change in the column performance. After approximately 5–10 runs the column was cleaned using the procedure of Sajonz et al. [6]: 5 CVs of 1 *M* NaCl, 5 CVs of 1 *M* NaOH, 5 CVs of 1 *M* HCl, and finally 5 CVs of 1 *M* NaCl. All regeneration and cleaning procedures were carried out at a flow-rate of 0.5 CVs/min. The experimental conditions for the various media are shown in Table 1.

3.5. Data reduction procedure

The model parameters can be obtained by fitting the integral of the flux equations Eqs. (6), (7), (10) to the experimental breakthrough curves or by fitting the flux equations to the experimental flux determined from the slopes of the breakthrough curves. We have chosen the latter method in order to avoid

Table 1
Parameters and experimental conditions

	Q HyperD 35	Q HyperD 20	Source 30Q	Source 15Q	Poros HQ/M
d_p (μm)	49 [7]	20	30	15	20
c_F (g/l)	0.5–3	2	0.2–3	0.1–3 2	
u_0 (cm/h)	400–6000	400–1100	400–1100	200–550	400–1100
ϵ	0.5	0.5	0.5	0.5	0.5
q_{max} (g/l particle)	203	119	66	73	60
b (l/g)	50	50	20	20	20
$k_s \cdot 10^5$ (cm/s)	2.9	4.5	5.1	3.6	13
δ	0.07–7.5	0.06–0.2	0.03–1.0	0.04–0.7	0.08–0.3

numerical integration in the fitting procedure. Further, it is our experience that comparing the experimental flux to the model is a more sensitive way of evaluating the model than comparing the breakthrough curves. The experimental flux was determined by fitting the breakthrough curves to flexible functions with analytical derivatives. The results of this method agreed with results obtained by smoothing and numerical differentiation. The models were fitted to the experimental flux data in the range $0.1<x<0.7$ which covers the mass-transfer zone. The maximum capacity, q_{max}, was determined by matching the model retention time at the centre of mass to the experimental retention time. Due to the extreme non-linearity of the isotherms a confident determination of the b parameter is difficult, therefore it was estimated with appropriate values for each medium.

3.6. Constant pattern evaluation

To verify whether a constant pattern profile was reached in the experiments the following procedure was used: for a given flow-rate and feed concentration the width of the breakthrough curve in milliliters was estimated from the output signal. The experiment was then repeated with a gradient input profile over a significantly larger volume than the estimated width of the breakthrough curve. By comparing the profiles obtained from the step input and various gradient inputs a qualitative measure of the deviation from constant pattern can be obtained. If a constant pattern is reached the profiles will be identical; if not, the profile resulting from the step input must be steeper than the profiles resulting from the gradient inputs. The outlined procedure was applied to the Source 30Q column at a feed concentration of 1 g/l and a superficial velocity of 1060 cm/h. The breakthrough curves for the frontal input (bypass procedure) and the most shallow gradient are compared in Fig. 1. The result is quite convincing; constant pattern is definitely achieved. Since the mass-transfer properties of the media investigated do not differ to a great extent, we assume that a constant pattern has been reached in all the experiments.

4. Results and discussion

Fig. 2 shows a sample breakthrough curve for Q HyperD 35, Source 30Q and Poros HQ/M. It is a characteristic for all our experiments that the feed concentration can only be reached after a very long time. The pseudo plateau is reached at approximately

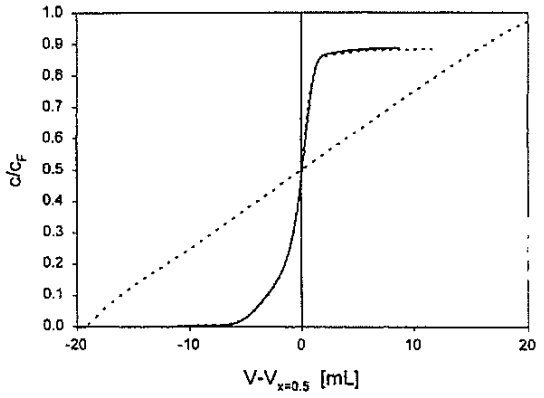

Fig. 1. Breakthrough profiles for Source 30Q at a feed concentration of 1 g/l and a superficial velocity of 1060 cm/h with a step-up input and a 40-ml gradient input.

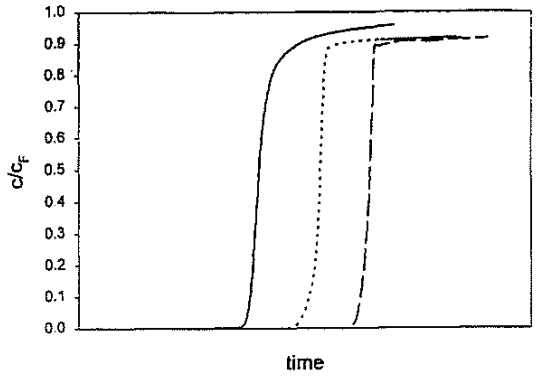

Fig. 2. Breakthrough profiles for Q HyperD 35 (solid line, $c_F=3$ g/l, $u_0=2527$ cm/h), Source 30Q (dotted line, $c_F=2$ g/l, $u_0=1060$ cm/h) and Poros HQ/M (dashed line, $c_F=2$ g/l, $u_0=707$ cm/h).

0.9 c_F for the Source and Poros columns, and at 0.95 c_F for the Q HyperD column.

4.1. Model comparison

The calculated breakthrough curves of the three models for Q HyperD 35 at $c_F=3$ g/l and $u_0=2527$ cm/h are compared with the experimental breakthrough curve in Fig. 3. The results were obtained by integrating the Eqs. (6), (7), (10) using the estimated model parameters. The mass-transfer coefficients in the two-film model, k_f and k_s, were determined by fitting the model to all the experimental flux curves for Q HyperD 35 using a velocity dependent k_f and a constant k_s. The mass-transfer coefficients of the overall driving force models were determined by a fit to the flux data at the conditions shown in Fig. 3. None of the models can of course account for the flattening of the experimental profile observed at high x-values since this phenomenon is not included in any of the models. A plot like Fig. 3 is not a very sensitive way to evaluate the models, since they all seem to give a reasonable description of the steeper part of the breakthrough curve. A more sensitive comparison is to compare the flux profiles. Fig. 4 compares the flux from the experimental breakthrough curve with the three models shown in Fig. 3. The flux is proportional to the slope of the breakthrough curve and its maximum value is at the inflection point of the breakthrough curve, $x=x''$. The location of the inflection point in the apparent overall driving force models is determined by the parameter $\beta=bc_F$ only, see Eqs. (13) and (14), whereas in the two-film model it is greatly influenced by the scaled mass-transfer resistance ratio δ, see Eq. (15). For the data shown in Fig. 4 $\delta=1.9$, indicating that both resistances are important. The two-film model provides a satisfactory fit of the experimental data. The overall models cannot fit the flux data,

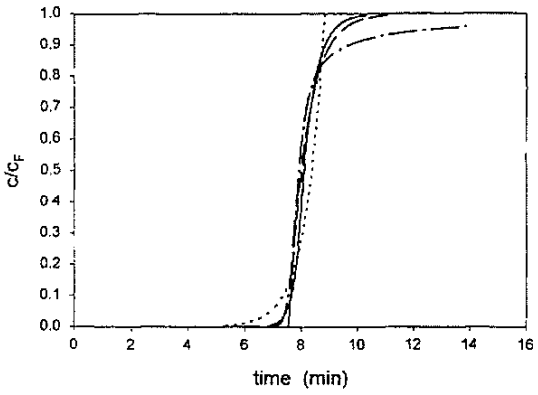

Fig. 3. Comparison of the experimental breakthrough profile for Q HyperD 35 (dash–dotted line, $c_F=3$ g/l, $u_0=2527$ cm/h) and the model profiles for the two-film model (solid line), the apparent overall mobile phase driving force model (dotted line) and the apparent overall solid phase driving force model (dashed line).

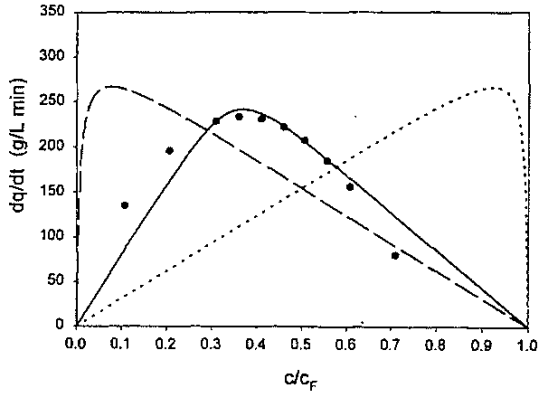

Fig. 4. Comparison of the experimental flux profile for Q HyperD 35 (solid circles, $c_F=3$ g/l, $u_0=2527$ cm/h) and the calculated flux profiles for the two-film model (solid line), the apparent overall mobile phase driving force model (dotted line) and the apparent overall solid phase driving force model (dashed line).

even though the over all mass-transfer coefficients where determined by fitting exclusively to the experimental data as shown in Fig. 4.

When the experimental conditions are varied, either by changing the feed concentration or the velocity, δ changes. Thus the relative importance of the resistances can shift depending on the experimental conditions. The apparent overall driving force models cannot account for this. In general, neither of the overall driving force models can describe the data well when the scaled mass-transfer resistance ratio is in the region $0.1<\delta<10$.

4.2. Comparison with other data

We have measured breakthrough curves for BSA on Resource 15Q under the same experimental conditions as Sajonz et al. [6] and our experimental results are in agreement with theirs. They estimated the apparent overall solid-phase mass-transfer coefficients from the shock layer thickness (SLT). The SLT is the width of the breakthrough curve, usually in time units, between two defined values of x, most often $x=1-\theta$ and $x=\theta$, i.e. $\mathrm{SLT}=t_{(1-\theta)}-t_{\theta}$ where θ is in the range 0.1–0.3. In this way, the model is fitted to match the distance between two points on the breakthrough curve without taking the shape of the breakthrough curve into account. Using this procedure they found an overall mass transfer coefficient proportional to the velocity. We have used their procedure on our experimental results and determined the same values for the parameters.

Fig. 5 compares the experimental flux to the two overall driving force models and the two-film model for Resource 15Q. The overall mass-transfer coefficients were determined from the SLT. The profiles for the overall mobile phase driving force model and the two-film model are almost identical, which indicates that the flux is dominated by the external resistance as can be seen from the values of δ in Table 1 ($\delta\approx0.2$ for Fig. 5). The overall solid-phase driving force model does not describe the flux data well, even though the SLT is the same for the three models.

4.3. Mass-transfer coefficients

Fig. 6 depicts the flux at the inflection point as a function of the superficial velocity for Q HyperD 35, Source 30Q and Poros HQ/M at constant feed concentration. The fluxes show a strong velocity dependence which indicate that the resistance to mass transfer for the three media is strongly dependent on the velocity in the mobile phase. The values for the estimated solid-phase mass-transfer coefficients, the isotherm parameters, and the range of the scaled mass-transfer resistance ratio δ are shown in Table 1. Fernandez et al. [7] determined a k_s value of $1.9\cdot10^{-5}$ cm/s for Q HyperD F. Fig. 7 shows the

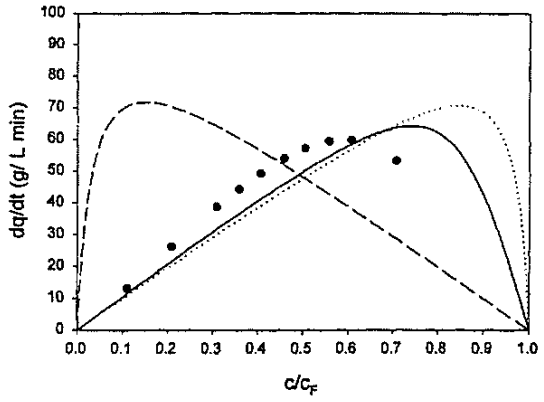

Fig. 5. Comparison of the experimental flux profile for Resource 15Q (solid circles, $c_F=1.5$ g/l, $u_0=187$ cm/h) and the calculated flux profiles for the two-film model (solid line), the apparent overall mobile phase driving force model (dotted line) and the apparent overall solid phase driving force model (dashed line).

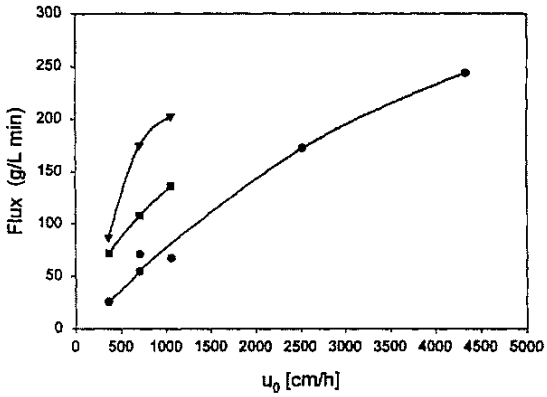

Fig. 6. Experimentally determined velocity dependence of the flux at the inflection point of the breakthrough profile ($c_F\approx2$ g/l) for Q HyperD 35 (●), Source 30Q (▲) and Poros HQ/M (■).

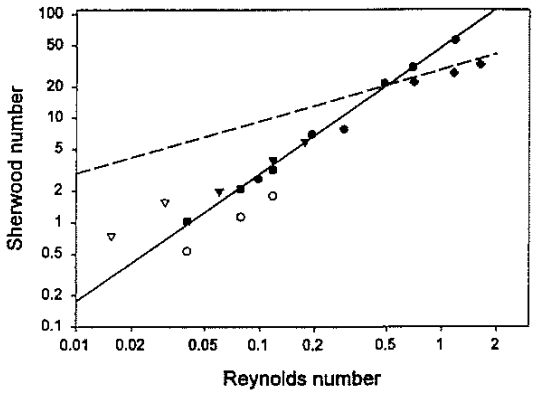

Fig. 7. Sherwood numbers for Q HyperD 35 (●), Q HyperD 20 (○), Source 30Q (▲), Source 15Q (△), Poros HQ/M (■), and data by Fernandez et al. [7] (◇). The solid line represents a correlation of the experimentally determined data by Eq. (16) and the dashed line is the correlation of Carberry [8].

Sherwood number for the external mass-transfer coefficient as function of the Reynolds number. All the data exhibit the same velocity dependence, while the data for the Source 15Q and Q HyperD 20 media fall on each side of the full line representing the best fit to the data given by

$$Sh = 47.5Re^{1.22} \quad (16)$$

This correlation is compared with the correlation by Carberry [8]

$$Sh = 1.15Re^{1/2}Sc^{1/3} \quad (17)$$

The Reynolds numbers where calculated assuming a bed porosity of $\epsilon = 0.5$ for all columns. The diffusion coefficient of BSA is $6 \cdot 10^{-7}$ cm^2/s [9] corresponding to a Schmidt number of 16 667. This correlation was used by Fernandez et al. [10]. At low Re, our estimated Sherwood numbers are considerably less than predicted by the correlation of Carberry and show a much stronger velocity dependence. Fernandez et al. [10] estimated Sherwood numbers from experimental data for Q HyperD F at three flow-rates and their results are included in Fig. 7. They concluded that the external resistance was significant. For Resource 15Q Sajonz et al. [6] determined an overall mass-transfer coefficient proportional to the velocity at the same Reynolds numbers as applied here.

The Sherwood numbers we have determined do not reach an asymptotic value of 2 when $Re \rightarrow 0$ corresponding to a film thickness of half the particle diameter [11]. Carberry [8] stated that it is not inconceivable that at very low flow-rates the boundary layer in a packed bed may develop over a distance greater than one particle diameter. He concluded that in this case the film thickness is proportional to the inverse Reynolds number and as a result the film coefficient will be proportional to the velocity.

Since the Sherwood numbers we have determined exhibit an unexpectedly strong dependence on the velocity, it is appropriate to investigate possible sources of errors. In Eqs. (9)–(12) the parameters q_F and k_f only enter as the ratio k_f/q_F, therefore the estimated values of k_f are proportional to the estimated maximum column capacity but the maximum capacity does not influence the estimated values of k_s. The uncertainty in the column capacities is 15–20%, including the uncertainty in the bed porosity, therefore the uncertainty in k_f is 15–20%. This uncertainty, however, is only reflected in the magnitude of the Sherwood numbers and not in the velocity dependence. The isotherms are strongly non-linear, therefore even a large uncertainty of the b-parameter in the Langmuir isotherm will not influence the estimated mass-transfer coefficients significantly. Thus, the uncertainties in the data reduction procedure cannot explain the strong velocity dependence of the Sherwood number.

The influence of the flat upper region of the experimental breakthrough profiles on the estimation of the mass-transfer coefficients is difficult to assess. We find it plausible that this phenomenon has some influence on the location of the inflection point, and to a lesser degree also on the steepness of the breakthrough curve. In our parameter estimation we have included data points up to $x = 0.7$. If only data up to 0.5 were included it would in general increase the Sherwood numbers by no more than 10–20%, but still the estimated Sherwood numbers at low Reynolds numbers would be less than a limiting number of 2.

Symbols

b	Langmuir parameter, (l/g)
c	Mobile phase concentration, (g/l)
c_0	Mobile phase concentration at the interphase, (g/l)
c_F	Feed concentration, (g/l)
CV	Column volume,
d_p	Particle diameter, (μm)
D	Diffusion coefficient, (cm^2/s)
k_f	External film mass-transfer coefficient, (cm/s)
k_s	Solid-phase film mass-transfer coefficient, (cm/s)
q	Solid-phase concentration, (g/l particle)
q_0	solid-phase concentration at the interface, (g/l particle)
q_F	Equilibrium feed concentration in particle, g/l particle
q_{max}	Maximum equilibrium capacity, g/l particle
Re	Reynolds number, $ud_p\rho/\mu$
Sc	*Schmidth number*, $\mu/\rho D$
Sh	*Sherwood number*, $k_f d_p/D$
u	Interstitial velocity, cm/s
u_0	Superficial velocity, cm/h
x	*Reduced mobile phase concentration*, c/c_F
x_0	Reduced *concentration at the interphase*, c_0/c_F
y	Reduced solid-phase concentration, q/q_F

Greek letters

β	parameter, bc_F
δ	Scaled mass-transfer resistance ratio, $k_f c_F/k_s q_F$
ϵ	Bed porosity,
μ	Viscosity, g/cm s
ρ	Mobile phase density, g/cm^3

Acknowledgements

The authors wish to thank Pharmacia Biotech for supplying the Resource 15Q column and Novo Nordisk for their support.

References

[1] H. Yoshida, T. Kataoka, D.M. Ruthven, Chem. Eng. Sci. 39(10) (1984) 1489.
[2] J. Mollerup, E. Hansen, J. Chromatogr. A 827 (1998) 235.
[3] R.E. Treyball, Mass-Transfer Operations, Ch. 5, McGraw-Hill, New York, 1955.
[4] H. Yoshida, M. Yoshikawa, T. Kataoka, AIChE J. 40(12) (1994) 2034.
[5] P.C. Wankat, Rate Controlled Separations, Ch. 8, Chapman & Hall, 1994, Ch. 8.
[6] P. Sajonz, H. Guan-Sajonz, G. Zhong, G. Guiochon, Biotechnol. Progr. 13 (1997) 170.
[7] M.A. Fernandez, G. Carta, J. Chromatogr. A 746 (1996) 169.
[8] J.J. Carberry, AIChE J. 6 (1960) 460.
[9] M.E. Young, P.A. Carroad, R.L. Bell, Biotechnol. Bioeng. 12 (1980) 947.
[10] M.A. Fernandez, W.S. Laughinghouse, G. Carta, J. Chromatogr. A 746 (1996) 185.
[11] W.L. McCabe, J.C. Smith, P. Harriot, Unit Operations of Chemical Engineering, McGraw-Hill, 5th edition, Singapore, 1993, Ch. 21.

Paper 2

The Influence of retention on the plate height in ion-exchange chromatography

Ernst Hansen and Jørgen Mollerup*

Engineering Research Centre IVC-SEP, Department of Chemical Engineering

The Technical University of Denmark, DTU

Building 229, 2800 Lyngby, Denmark

Fax: +45 4588 2258, phone: +45 4525 2866, e-mail: jm@kt.dtu.dk

Submitted to Journal of Chromatography, December 1999

Abstract

The plate heights for Tyrosine (anion exchange) and Aprotinin (cation exchange) have been determined on a porous media (Resource 15) and a gel-filled media (HyperD 20) at salt concentrations ranging from weak to strong retention. The measurements show that going from high towards low salt concentrations at constant velocity the plate height increases, goes through a maximum, and finally decreases as the salt concentration is lowered further. The band broadening in the columns is caused by axial dispersion and mass transfer.The rate of mass transfer in the particles is described by three models comprising pore diffusion, solid diffusion, and parallel diffusion as the rate mechanism. The van Deemter equation was used to model the data in order to determine the mass transfer properties.The development of the plate height with increasing retention reveals a characteristic behaviour for each model. For pore diffusion the plate height increases towards a constant value at strong retention while the plate height for solid diffusion decreases approaching a constant value at strong retention. In the parallel diffusuion model both pore and solid diffusion takes place. The model coincides with the pore diffusion model at weak retention and with the solid diffusuion model at strong retention while a maximum is reached at intermediate conditions resulting in a bell shaped curve.This model behaviour corresponds to the observed variation of the plate height at constant velocity. The pore and solid diffusion models cannot describe the experimental data while a satisfactory fit of the parallel diffusion model was obtained.

Introduction

At linear adsorbing conditions the plate height (HETP) can be determined from the variance of the response to a pulse injection. The plate height depends on the velocity, mass transfer coefficients, retention behaviour, as well as the particle diameter and the porosities. Experimental data for the plate height can be correlated by the van Deemter equation.The plate height has an explicit and an implicit dependence on retention; implicit because the rate of mass transfer depends on the equilibrium conditions. The scope of this study is to determine how the plate height depends on retention and use the van Deemter equation to investigate different models for mass transfer.The plate height for an amino acid (Tyrosine) and a protein (Aprotinin) have been measured over a wide range of salt concentrations, ranging from weak to strong retention, on two different resins, a porous media (Resource 15Q&S) and a gel-filled media (Q&S HyperD 20).

For a linear system the rate of mass transfer is given by an over-all mass transfer coefficient comprising the contributions from film and intra particle mass transfer. The model for intra particle mass transfer can include either *pore diffusion*, *solid diffusion*, or both usually referred to as *parallel diffusion*. Often the over-all mass transfer coefficient is determined by measuring the plate height as function of the velocity under non-retained

conditions ([1]-[3]). However, from experiments performed at constant retention the nature of the rate mechanism in the particles cannot be investigated since the plate height at constant retention can be matched by any of the three models. Therefore, in order to distinguish between the various models the plate height must be determined at conditions having a significant variation in retention.

Theory

The van Deemter equation is used to model the plate height data. The rate of mass transfer is described by the linear driving force approximation and local equillibrium assumed between the two phases in the particles.

For the applied conditions the contribution from ordinary diffusion to band broadening can be neglected. Assuming the Eddy diffusion coefficient proportional to the velocity, the reduced plate height $h=H/d_p$ given by the van Deemter equation is [4]

$$h = 2\lambda + 2\left(\frac{k'}{1+k'}\right)^2 \frac{\epsilon v}{6(1-\epsilon)K_m} = 2\lambda + 2\left(\frac{1+A}{p+1+A}\right)^2 \frac{\epsilon v}{6(1-\epsilon)K_m} \qquad (1)$$

where λ is a constant related to the axial dispersion coeffcient, $D_{ax}=\lambda v d_p$, usually in the range 1-3 and $p=\epsilon/(1-\epsilon)K_d\epsilon_p$ is in the range 1-2. K_m is the over-all mass transfer cofficient corresponding to an over-all driving force in the liquid phase concentration $c-c^*=c-c_{pore}$ and $A=q/c_{pore}$ is the equilibrium ratio between the solid and pore phase concentrations in the particles. The solid and pore concentrations are defined with respect to the accesible pore volume so that the retention factor is $k'=(1-\epsilon)K_d\epsilon_p(1+A)/\epsilon$.

The development of the plate height with increasing retention depends on the term in the brackets of Eq. (1) as well as the variation of the over-all mass transfer coeffcient and is discussed below in regards to possible mechanisms of intra particle mass transfer. A detailed discussion of intra particle mass transfer is found in Perrys Handbook [5].

Pore diffusion

When intra particle mass transfer is controlled by pore diffusion the over-all mass transfer coeffcient is

$$\frac{1}{K_m} = \frac{1}{k_f} + \frac{1}{K_d\epsilon_p k_p} \qquad (2)$$

where k_f is the velocity dependent film coefficient for the external mass transfer and k_p is the mass transfer coefficient for the pores. The product $K_d\epsilon_p$ is the effective particle porosity for a given solute. Since the over-all mass transfer coefficient is a constant at fixed

velocity the plate height for pore diffusion will increase with A and approach a constant value when the term in the brackets of Eq. (1) goes to unity.

Solid diffusion

In solid diffusion the driving force for mass transfer is expressed in the solid phase concentration q and the over-all mass transfer coefficient is

$$\frac{1}{K_m} = \frac{1}{k_f} + \frac{1}{K_d \epsilon_p A k_q} \qquad (3)$$

where k_q is the solid phase mass transfer coeffcient. Inserting this expression in the van Deemter equation the plate height for solid diffusion is a decreasing function of the equilibrium ratio approaching a constant for large values of A. A deficiancy in the solid diffusion model is that the plate height goes to infinity at non-retained conditions ($A \rightarrow 0$).

Parallel diffusion

In the parallel diffusion model intra particle mass transfer occurs by both pore and solid diffusion i.e. the two mechanisms work in parallel.

$$\frac{1}{K_m} = \frac{1}{k_f} + \frac{1}{K_d \epsilon_p (k_p + A k_q)} \qquad (4)$$

Due to the parallel nature of the transport the rate of mass transfer in the particles will be controlled by the fastest mechanism. At low retention where $k_p >> Ak_q$ mass transfer occurs by pore diffusion while solid diffusion dominates as the equilibrium ratio becomes large. Since the plate height increases with A for low to moderate retention and decreases with A for strong retention a maximum in the plate height as function of the equilibrium ratio must be reached at conditions in between. Finally, it is noted that the pore and solid diffusion models, Eqs. (2) and (3), are limiting cases of the general parallel diffusion model Eq. (4).

Figure 1 shows the reduced plate height as function of the equilibrium ratio for the three models. For simplicity the contribution from the external film resistance is neglected. At low retention pore diffusion dominates and the plate height for parallel diffusion $h_{par} \approx h_{pore}$ increases with A. At moderate to strong retention solid diffusion dominates and $h_{par} \approx h_{solid}$ decreases with A. At intemediate conditions a transition from the pore to the solid diffusion domain takes place and the plate height goes through a maximum. The resulting variation of h_{par} with A is smaller than for both pore and solid diffusion.

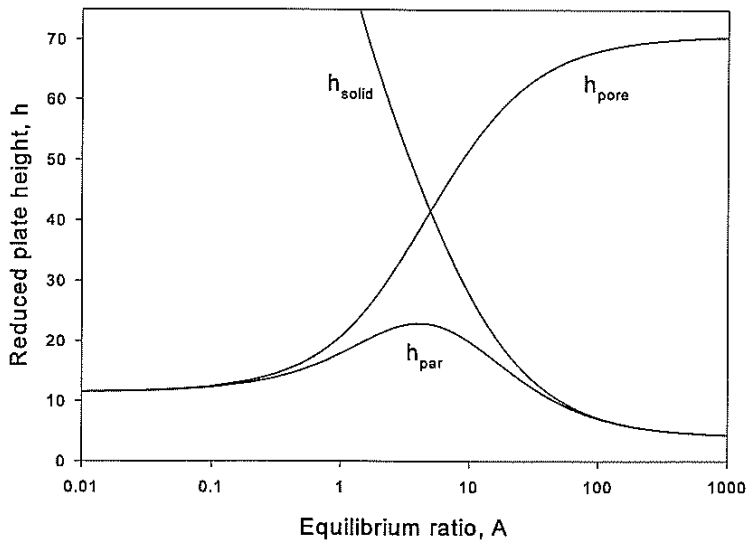

Figure 1: Plate height behaviour for pore, solid and parallel diffusion calculated from Eqs. (1) and (2)-(4) with $\epsilon=0.5$, $\epsilon_p=0.5$, $\lambda=2$, $k_p=2\times10^{-3}$ cm/s, $k_q=0.4\times10^{-3}$ cm/s at $v_0=0.1$ cm/s and negelcting the film resistance.

Experimental data for the plate height obtained at constant retention can be matched by any of the three models. Thus from a plot of the plate height versus the velocity (the so called van Deemter plot) we cannot in general distinguish between the models. However, with significant variation in the equilibrium ratio a plot of h versus A at constant velocity will have a distinguished shape for each of the three models as shown in Figure 1. Thus by determining the plate height as function of the equilibrium ratio we can investigate the significance of the three models for intraparticle mass transfer.

Linear equilibrium

The equilibrium ratio depends on the concentration of the counter ion and is described by the mass action law :

$$A = \frac{q}{c_p} = K\left(\frac{\Lambda}{c_s}\right)^{z_{solute}/z_{salt}} = B\,c_s^{-\nu} \qquad (5)$$

where K is the equilibrium constant, Λ is the concentation of equivlalents in the adsorbing matrix and c_s is the concentration of the counter ion. z_{solute} is the effective or binding charge of the solute as encountered by the adsorbing matrix. For large molecules such as proteins, where several configurations of attachment are possible, this value can vary between

adsorbents and moderate differences in the charge ratio ν should be expected.

Experimental

Chemicals

Aprotinin from Novo Nordisk, Tyrosine (T-3754) and NaAc (S5889) from Sigma, $NaNO_3$ (1.06537) and NaCl (1.06404) from Merck, 5 N HCl (Lab00440) and 5 N NaOH (Lab00334) from Bie & Berntsen. Standard solutions for calibration of the pH meter from Radiometer (pH=4.01, 7.00, and 10.01).

Equipment

BioCAD Chromatographic Workstation from Perseptive Biosystems, pH meter (pHM 92) from Radiometer, 0.45 μm HV filters from Millipore.
Columns: Resource 15S (no.510566), 30×6.4 mm (1mL), Resource 15S (no. 300734) and 15Q (no. 301572), 30×16 mm (6mL) from Pharmacia Biotech. Q HyperD 20 (lot 5155) and S HyperD 20 (lot 4206), 100×4.6 mm (1.7 mL) from BioSepra.

Procedures

The experimental conditions are summarised in Table 1. The mobile phase solutions for Aprotinin were prepared by dissolving buffer and NaCl before titrating with HCl to pH 5. The solutions for Tyrosine were prepared by dissolving NaCl before titrating with NaOH to pH 11. The high pH for the Tyrosine experiments was selected in order to have a negative charge close to 2. From the Bjerrum diagram it was found that the charge is not sensitive to the pH in this region. The pH meter was calibrated with standard solutions at pH 4.01 and 7.00 or 7.00 and 10.01. All solutions were filtered through 0.45 μm filters. The pulse response curves where measured at 254 and 280 nm. Feed solutions for the injections where prepared by dissolving the components in the relevant mobile phase. The injection volume was preferably 100 μL. In order to test whether the conditions could be considered linear, experimental runs with different injection volumes were performed at low to moderate salt concentrations.

Data reduction

The first and second moment of a peak was determined by fitting the response curve to the Exponentially Modified Gaussuian (EMG) function. The retention volume was calculated by subtracting the dead volume from the first moment and the variance was calculated by subtracting the variance measured without the column from the second moment. Finally, the plate number N was calculated from the retention volume and the variance. The bed porosities ϵ for the Resource 15S (1 mL) and S HyperD 20 columns were determined from injections of a dextrane conjugate (MW $8 \cdot 10^6$) dissolved in 1 M NaCl. The total porosities $\epsilon_t = \epsilon + (1-\epsilon)\epsilon_p$ were determined by injection of water after saturation with 1 M $NaNO_3$.

Identical porosities were assumed for the Q and S form of the resins and for the two Resource 15S columns.
The retention volume for the linear adsorbing conditions is

$$V_R = V_{col}\epsilon[1+k'] = V_{col}[\epsilon+(1-\epsilon)K_d\epsilon_p(1+A)] = V_{col}[\epsilon+(1-\epsilon)K_d\epsilon_p(1+B\,c_s^{-\nu})] \quad (6)$$

The three solute dependent retention parameters K_d, B and ν were determined by fitting Eq. (6) to the retention volumes at all velocities as function of the counter ion concentration (Na^+ or Cl^-). For the cation exchange of Aprotinin a value of 50 mM Na^+ originating from the buffer was added to the nominal salt concentration.
The mass transfer and axial dispersion coefficients where determined by fitting Eq. (1) with K_m from the parallel mass transfer model Eq. (4) to the data for $h=L/Nd_p$ as function of the counter ion concentration and velocity using the smoothed expression for A obtained from Eq. (6). The film mass transfer coefficient was correlated by the expression $k_f=\alpha v^\beta$, where α and β are constants. In the fitting procedure constraints were introduced so that the exponent β was a global parameter and the axial dispersion parameter λ independent of the applied solute.

Results

Tyrosine

Figure 2 shows the experimental retention volumes for Tyrosine and Aprotinin and the model fit obtained from Eq. (6) as function of the salt concentration. The retention volumes have been scaled with the volume at non-retained conditions. The porosities and retention parameters are reported in Table 1. The relative charge ν corresponds to the numerical value of the binding charge since the counter ions are monovalent. For Tyrosine the value of ν for both the Resource 15Q and the Q HyperD 20 resin is close to the theoretical value of 1.9 at pH 11. This indicates that the entire charge of the amino acid molecule is involved in the adsorption. As seen from Figure 2 the adsorbing behaviour for the two resins regarding Tyrosine is almost identical.
The experimental plate height data and model fit at three selected velocities are shown in Figures 3 and 4. The axial dispersion and mass transfer coefficients are given in Table 1. The results for the Resource 15Q resin exhibit the characteristic shape of parallel diffusion shown in Figure 1. For the Q HyperD resin the data are somewhat scattered which is partially due to the increased uncertainty introduced when performing experiments with small molecules on a small column, where the influence of extra column effects can be significant. Comparing Figure 4 with Figure 1 the data exhibit a much smaller variation with the equilibrium ratio than would be observed if intra particle mass transfer was controlled by pore or solid diffusion. For both resins a satisfactory fit of the parallel diffusion model to the data was obtained.

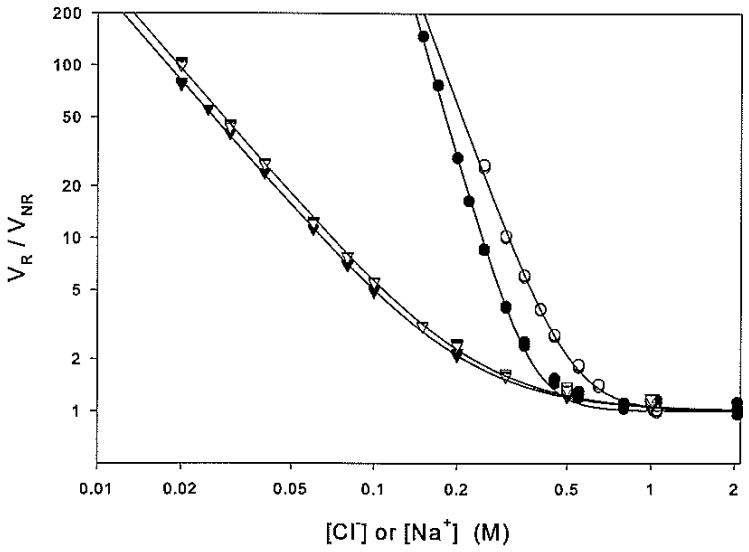

Figure 2: Retention behaviour of Tyrosine (▼) and Aprotinin (●) on Resource 15 (solid) and HyperD 20 (open) as function of the counter ion concentration, [Cl^-] for Tyrosine and [Na^+] for Aprotinin. The lines are the best fit of the retention volume model Eq. (6).

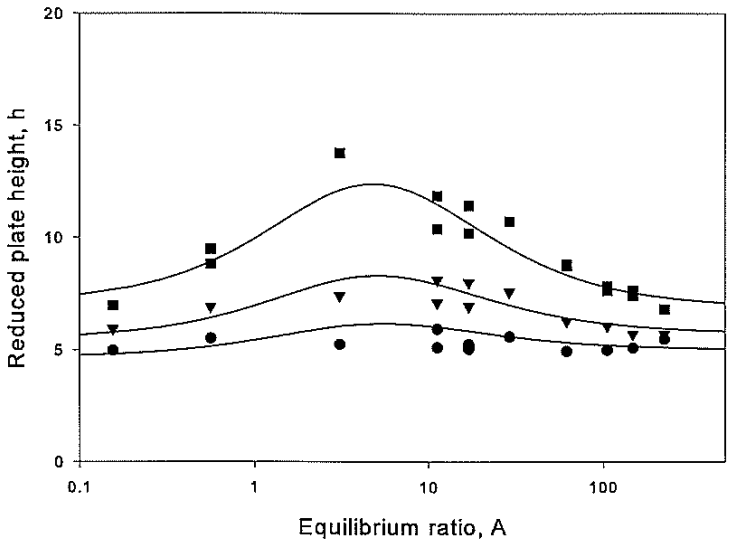

Figure 3: Reduced plate height and fit of the parallel diffusion model for Tyrosine on Resource 15Q at superficial velocities of v_0=0.05 (●), 0.1 (▼), and 0.2 cm/s (■).

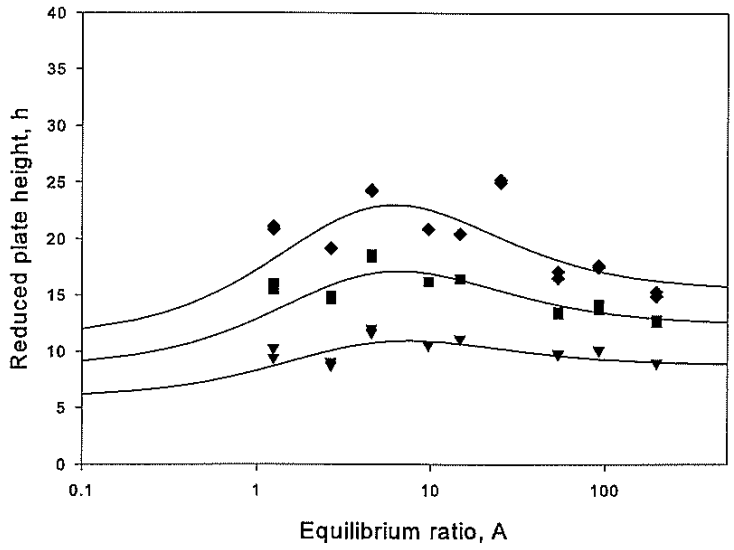

Figure 4: Reduced plate height and fit of the parallel diffusion model for Tyrosine on Q HyperD 20 at superficial velocities of v_0=0.1 (▼), 0.2 (■), and 0.3 cm/s (◆).

Aprotinin

The relative binding charge for Aprotinin is significantly larger than for Tyrosine wherefore 0the retention volumes for this component increase more rapidly with decreasing salt concentration as shown in Figure 2. The difference in retention between the two resins is more pronounced for Aprotinin than for Tyrosine, and from Table 1 a difference in the charge ratio ν for Aprotinin is found. Although this indicates that adsorption of Aprotinin on the two resins does not involve the same number of charges, it is noted that the retention parameters B and ν are correlated and the true binding charges might therefore be more alike.

The plate height as function of the equilibrium ratio for Aprotinin is shown in figures 5 and 6. Since Aprotinin is a large molecule compared to Tyrosine a lower rate of mass transfer, corresponding to a larger plate height, should be expected. Comparing Figures 5 and 6 with Figures 3 and 4 the plate height has increased approximately by a factor of three for the Resource resin and a factor of ten for the HyperD resin. For both resins a maximum in the plate height is reached and a satisfactory fit is obtained using the parallel diffusion model. There are some discrepancies between the model and the data for the Resource resin in the region to the right of the maximum ($A > 40$). For these conditions the column size was changed from 6 to 1 mL and we therefore explain the deviations thereby.

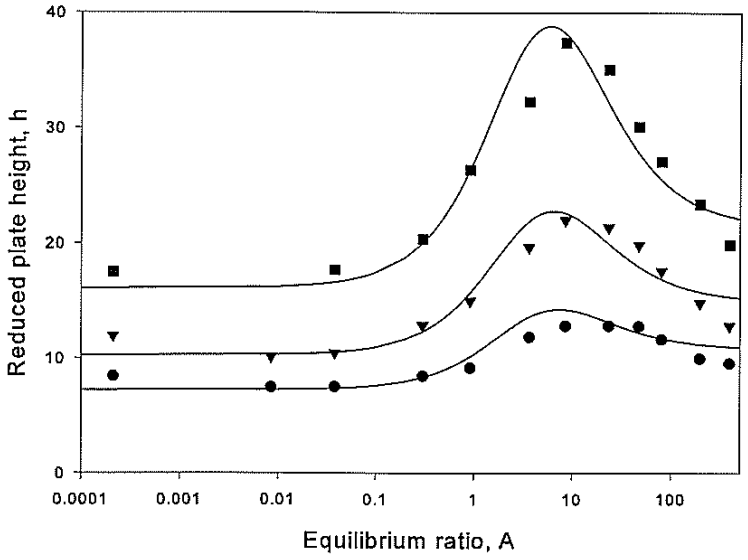

Figure 5: Reduced plate height and fit of the parallel diffusion model for Aprotinin on Resource 15S at superficial velocities of v_0=0.05 (●), 0.1 (▼), and 0.2 cm/s (■).

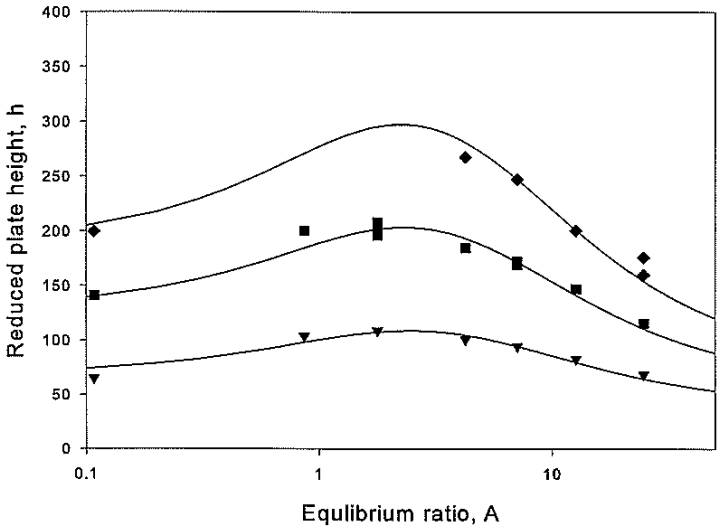

Figure 6: Reduced plate height and fit of the parallel diffusion model for Aprotinin on S HyperD 20 at superficial velocities of v_0=0.1 (▼), 0.2 (■), and 0.3 cm/s (◆).

Discussion

Model evaluation

When comparing the experimental results for Tyrosine and Aprotinin to the characteristic behaviour of the three mass transfer models it is evident that only the parallel diffusion model can describe the data satisfactory. The pore diffusion model predicts an asymptotic maximum plate height to be reached at strong retention, but the experiments show that this is not the case. The monotonic decrease of h predicted by the solid diffusion model cannot match the experimental data as well.

In the experimental work the equilibrium ratio has been varied by changing the salt concentration. If the diffusion coefficient depends on the salt concentration the effect described by parallel diffusion might instead originate from a concentration dependent diffusion coefficient. To investigate this we consider a model where mass transfer occurs by pore diffusion and the diffusion coefficient in free solution is given by the Nernst-Planck equation

$$D_{eff} = \frac{D_A D_B (z_A^2 c_A + z_B^2 c_B)}{D_A z_A^2 c_A + D_B z_B^2 c_B} \qquad (7)$$

where A and B represent the two diffusing ions which in the present case is either Tyrosine and Na^+ or Aprotinin and Cl^-. For these approximate calculations it is assumed that the relative change in the pore diffusion coefficient correspond to the change in D_{eff} from the Nernst-Planck equation. For Aprotinin the diffusion coefficient is determined from the correlation by Young et al. [6] as $D=1.3\times10^{-6}$ cm^2/s, for Cl^- it is 20.3×10^{-6} cm^2/s [7]. The charge z is set to 5 for Aprotinin and the feed concentration 1 g/L=0.15 mM is used together with the lowest chloride concentration applied which is 100 mM in order to get the maximum effect from the Nernst-Planck expression. For these numbers a value for the ratio D_{eff}/D of 1.04 is obtained. For Tyrosine the diffusion coefficient was determined from the Wilke-Chang correlation as $D=10\times10^{-6}$ cm^2/s and the value for Na^+ is 13.3×10^{-6} cm^2/s [7]. The lowest Na^+ concentration applied was 20 mM and the feed concentration for Tyrosine is 0.3 g/L=1.7 mM. Inserting these concentrations and z=-1.9 for Tyrosine the ratio D_{eff}/D is 1.2. In comparison the effective mass transfer coefficient k_p+Ak_q, which is proportional to the effective diffusion coefficient for the particle, changes by a factor of 20 for Tyrosine on the Resource resin when the equilibrium varies from 0 to 100. Thus a concentration dependent pore diffusion coefficient described by the Nernst-Planck equation cannot account for the observed variation of the plate height.

The linearity of the isotherm has been tested at low to moderate salt concentrations where a signifcant non-linear effect might exist. These experiments showed that a non-linear isotherm has a much larger impact on the the variance of the peak than on the retention volume. For experiments where the retention volume was reduced by 5-10% when

increasing the feed volume the variance was increased by up to 50%. Since the retention volume decreases and the variance increases when the adsorbing conditions become non-linear the combined effect is a significant increase in the plate height. This effect is in contrast to the decrease found at moderate to strong retention, wherefore experimental errors of this kind cannot explain the observed plate height behaviour.

Mass transfer behaviour

The values obtained for the axial dispersion parameter λ are between 1 and 2 corresponding to a plate height contribution of 2-4 particle diameters. From the present experimental data it is not possible to estimate robust parameters for α and β in the film coefficient expression $k_f=\alpha v^{\beta}$. This is partially due to the minor contribution of film diffusion to the plate height except at strong retention and partially because the variation of the velocity in some cases was not substantial to ensure a decoupling of α and β in the fitting procedure. For Tyrosine on the Resource resin a satisfactory fit could be obtained when setting the velocity exponent β between 0.1 and 0.6, but the contribution from film diffusion could not be disregarded. Thus the applied global value of $\beta=1/3$ is somewhat arbitrary, although consistent with commonly used correlations ([8] and [9]), and the magnitude of the α parameters are influenced by this choice. For a given solute the ratio of α between resins depends on the column characteristics only and should therefore be the same for Tyrosine and Aprotinin. From Table 1 the ratio is 5.9 for both solutes which indicates that α has some physical relevance and is not merely a fitting parameter.

In order to compare the two resins diffusion coefficients are calculated from the mass transfer coefficients for the pore and solid phase using the relation $k_i=10D_i/d_p$, where *i* is either p or q. The solid diffusion coefficients are lower than the pore diffusion coefficients which again are significantly lower than the diffusion coefficients in free solution. The intra particle diffusion coefficients for Tyrosine on the Resource and the HyperD resins are similar as indicated by the similar plate height behaviour in Figures 3 and 4. For Aprotinin the diffusion coefficients for HyperD are small compared to Resource, especially the pore diffusion coefficient. Although many factors influence the pore diffusivity it seems reasonable that the diffusion of large molecules is more hindered in a gel-filled pore. To ensure that the apparantly low intra particle diffusivities did not originate from the assumptions regarding the porosities, experiments with Tyrosine on S HyperD 20 at 1 M NaCl where performed. The retention and the plate height at 1 M NaCl were very similar between the S and Q form thus justifying the assumption of identical porosities. The significant difference in the Aprotinin diffusion coefficients between the Resource and the HyperD resin is supported by studies of BSA which showed that the maximum reduced plate height at $v_0=0.1$ cm/s is approximately 150 for Resource 15Q and 500 for Q HyperD 20.

Saunders et al. [10] studied pore and solid diffusion of Tyrosine by batch uptake on an

Amberlite 252 cation exchange resin with a particle diameter of 800 μm. They found values of $D_p' = 2.3\times10^{-6}$ cm^2/s and $D_q' = 0.018\times10^{-6}$ cm^2/s, where $D_i' = K_d\epsilon_p D_i$. Using the same experimental approach Jones and Carta [11] determined solid diffusion coefficients for various amino acids on seven different Dowex resins with particle diameters in the range 450-850 μm. The values of D_q' for phenyl alanine, which resembles Tyrosine, are in the range 0.02-0.1$\times10^{-6}$ cm^2/s with one exception of 3×10^{-6} cm^2/s. The values for Tyrosine determined in this work are $D_p' = 0.84$ and 1.2×10^{-6} cm^2/s and $D_q' = 0.17$ and 0.15×10^{-6} cm^2/s for Resource and HyperD respectively.

The primary application of the van Deemter equation is to characterize and thereby compare different resins, and often approximate shortcut methods with a minimum number of experiments are needed. In regards to this an interresting observation can be extracted from the present study: If an approximate expression for the plate height as function of the velocity and the retention factor is needed, it is better to us the van Deemter equation in the simple form $H=A+Cv$, where A and C are constants, than to use Eq. (1) with a constant over-all mass transfer coefficient K_m. The reason is that the term $[k'/(1+k')]^2$ varies to a much greater extend than the experimental plate height as seen from the pore diffusion model in Figure 1. The experimental data in Figures 3-6 indicate that a representative value of C can be determined from a flow rate study at low (but significant) retention, approximately $k' = 1$-2. For proteins this corresponds to a NaCl concentration of perhaps 0.3-0.4 M.

Conclusions

The mass transfer behaviour of a protein and an amino acid on a porous and a gel-type resin have been studied by determining the plate height as function of the equilibrium ratio and velocity. It was found that intra particle mass transfer is not well described by a model containing either pore or solid diffusion as the rate mechanism. By combining the two mechanisms in a parallel diffusion model a satisfactory fit of the model to the four sets of experimental data was obtained. Although caution must be taken when introducing an additional parameter, we find that the use of two parameters for describing intra particle mass transfer is substantiated by the experimental work.

Acknowledgements

The Aprotinin was kindly provided by Ole Schou, *Protein Purification*, Novo Nordisk A/S, Denmark.

Symbols

A	Equilibrium ratio	
B	Lumped equilibrium parameter	M^v
c_s	Salt ion concentration	M

D	Diffusion coefficient in free solution	cm^2/s
D_p	Pore diffusion coefficient	cm^2/s
D_q	Solid diffusion coefficient	cm^2/s
K	Equilibrium constant	
k'	Retention factor	
K_d	Steric exclusion factor	
k_f	External mass transfer coefficient	cm/s
K_m	Over-all mass transfer coefficient	cm/s
k_p	Pore mass transfer coefficient	cm/s
k_q	Solid mass transfer coefficient	cm/s
p	Constant, $\epsilon/(1-\epsilon)K_d\epsilon_p$	
v	Interstitial velocity	cm/s
v_0	Superficial velocity	cm/s
V_R	Retention volume	mL
V_{NR}	Retention volume at non-retained conditions (A=0)	mL

Greek letters

α	External mass transfer parameter	cm/s
β	Velocity exponent	
ϵ	Bed porosity	
ϵ_p	Particle porosity	
Λ	Capacity	M
λ	Axial dispersion parameter	
ν	Charge ratio	

References

[1] D.C. Nash and H.A. Chase, J. Chromatogr. A 807 (1998) 185.

[2] A.E. Rodrigues, C. Chenou and M.R. de la Vega, Chem. Eng. Jou. 61 (1996) 191

[3] J. Horvarth, E. Boschetti, L. Guerrier and N. Cooke, J. Chromatogr. A 679 (1994) 11.

[4] J.J. van Deemter, F.J. Zuiderweg and A. Klinkenberg, Chem. Eng. Sci. 5 (1956) 271.

[5] R.H. Perry and D.W. Green, Perrys Chemical Engineers' Handbook, 7th ed., ch. 16, McGraw-Hill, New York, 1997.

[6] M.E. Young, P.A. Carroad and R.L. Bell, Biotechnol. Bioeng. 12 (1980) 947.

[7] P.W. Atkins, Physical Chemistry, 4th ed., Oxford University Press, 1990.

[8] T. Kataoka, H. Yoshida and K. Ueyama, J. Chem. Eng. Japan 38 (1972) 132.

[9] E.J. Wilson and C.J. Geankoplis, Ind. Eng. Chem. Fundamen. 5 (1966) 9.

[10] M.S. Saunders, J.B. Vierow and G. Carta, AIChE J. 35 (1989) 53.

[11] I.L. Jones and G. Carta, Ind. Eng. Chem. Res. 32 (1993) 117.

Table 1: Parameters and experimental conditions

		Tyrosine		Aprotinin	
Buffer		none		50 mM NaAc	
pH		11 (NaOH)		5 (HCl)	
c_{feed}	(g/L)	0.3		1	
$D \times 10^6$	(cm^2/s)	10		1.3	
Resin		**Resource 15Q**	**Q HyperD 20**	**Resource 15S**	**S HyperD 20**
V_{col}	(mL)	6	1.7	1&6	1.7
d_p	(μm)	15	20	15	20
ϵ		0.48	0.37	0.48	0.37
ϵ_p		0.51	0.54	0.51	0.54
v_0	(cm/s)	0.05-0.2	0.1-0.5	0.008-0.2	0.1-0.3
c_{salt}	(M)	0.02-1	0.02-0.3	0.15-2.05	0.25-1.05
K_d		1	1	1	0.74
B	(M^ν)	0.16	0.13	0.01	0.13
ν		1.86	1.87	5.52	4.34
λ		1.9	1.2	1.9	1.2
$\alpha \times 10^3$	(cm/s)	55	13	9.4	2.2
β		1/3	1/3	1/3	1/3
$k_p \times 10^3$	(cm/s)	11	11	3.2	0.36
$k_q \times 10^3$	(cm/s)	2.2	1.4	0.58	0.15
$D_p \times 10^6$	(cm^2/s)	1.7	2.2	0.48	0.073
$D_q \times 10^6$	(cm^2/s)	0.33	0.28	0.087	0.031